NASA CONTRACTOR REPORT

NASA CR-2210

NASA CR-2210

POGO SUPPRESSION ON SPACE SHUTTLE - EARLY STUDIES

by S. Rubin, R. G. Wagner, and J. G. Payne

Prepared by
THE AEROSPACE CORPORATION
El Segundo, Calif.
for Langley Research Center

NATIONAL AERONAUTICS AND SPACE ADMINISTRATION • WASHINGTON, D. C. • MARCH 1973

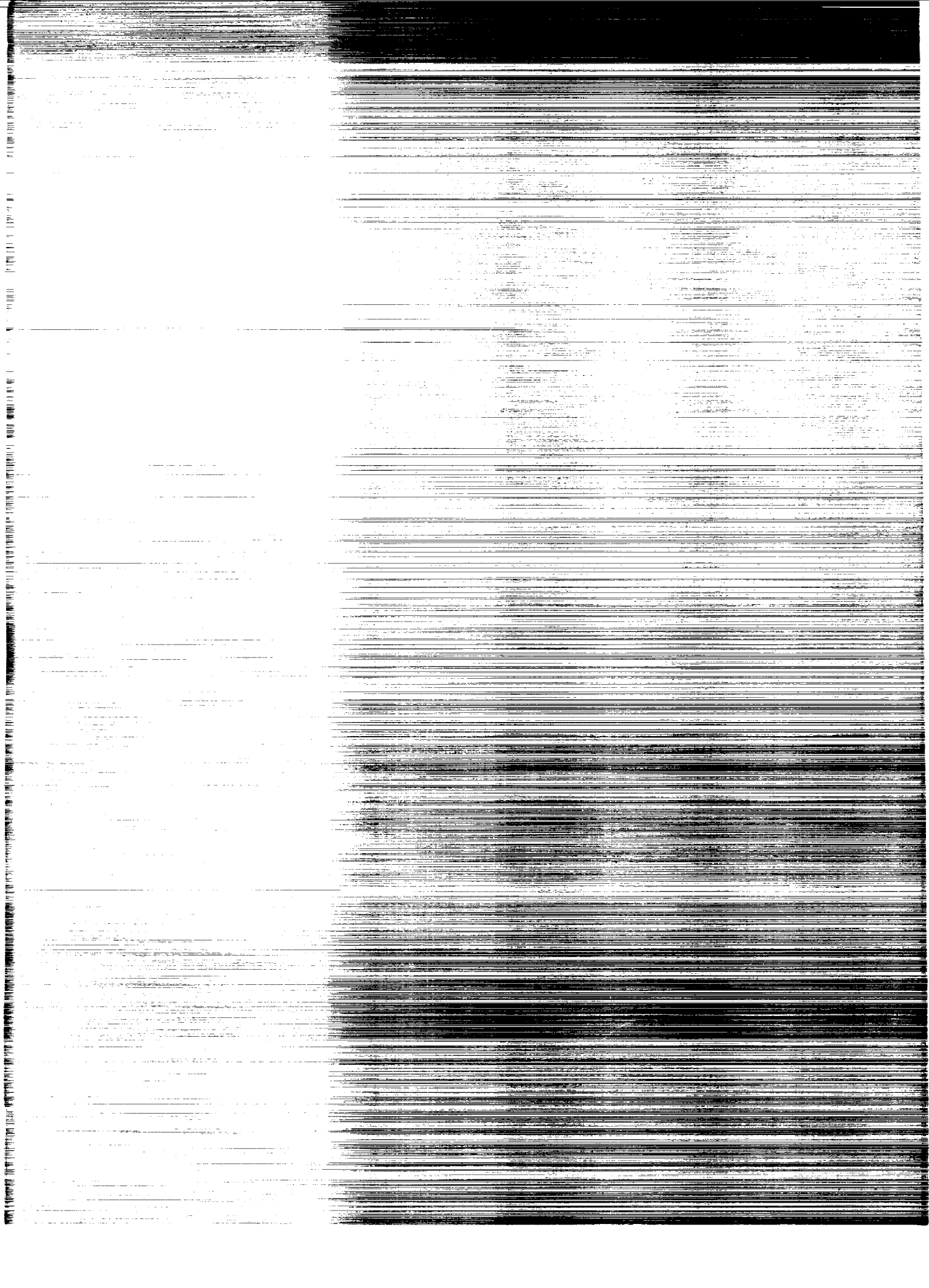

1. Report No.	2. Government Accession No.	3. Recipient's Catalog No.
NASA CR-2210		

4. Title and Subtitle	5. Report Date
POGO SUPPRESSION ON SPACE SHUTTLE - EARLY STUDIES	March 1973
	6. Performing Organization Code
7. Author(s)	8. Performing Organization Report No.
S. Rubin, R. G. Wagner and J. G. Payne	
9. Performing Organization Name and Address	10. Work Unit No.
The Aerospace Corporation El Segundo, Calif.	502-32-02-01
	11. Contract or Grant No. NAS1-10631
12. Sponsoring Agency Name and Address	13. Type of Report and Period Covered
National Aeronautics and Space Administration Washington, D.C. 20546	Contractor Report
	14. Sponsoring Agency Code

15. Supplementary Notes

16. Abstract

Preliminary studies for pogo prevention on the Shuttle vehicle are reported. The importance of the effect of oscillatory outflow from a hydroelastic tank is displayed in terms of excitation of normal modes for a structure containing that tank assuming its outlet is closed. Evaluation of an approximate propulsion frequency response at undamped feedline resonances reveals the conditions for which the contribution of tank outflow is destabilizing and also provides a criterion for identifying those structural modes which are of potential significance for system stability. Various finite-element and normal-mode models for hydraulic feedlines are evaluated relative to accuracy of admittances of a long line. A procedure is recommended for modeling a feed system to minimize the required number of second-order equations. Specific recommendations are made for the analytical estimation of pump cavitation compliance and a first estimate for the shuttle pumps is given. Weakness in past practices of pump testing are identified and a new three-phase program is proposed. Finally, results of numerical studies on the early vehicle configuration are presented. It is concluded that an accumulator between the boost and main pump offers promise of higher effectiveness than one at the engine inlet.

17. Key Words (Suggested by Author(s))	18. Distribution Statement
Pogo; Shuttle; Stability; Vibration; Hydroelastic Tanks; Structural Dynamics, Propulsion Dynamics; Propulsion Testing, Cavitation; Hydraulic Line Modeling	Unclassified-Unlimited

19. Security Classif. (of this report)	20. Security Classif. (of this page)	21. No. of Pages	22. Price*
Unclassified	Unclassified	130	$3.00

*For sale by the National Technical Information Service, Springfield, Virginia 22151

CONTENTS

CONTENTS (Continued)

TABLES

FIGURES

POGO SUPPRESSION ON SPACE SHUTTLE - EARLY STUDIES

By S. Rubin, R. G. Wagner and J. G. Payne
The Aerospace Corporation

SUMMARY

Preliminary studies for pogo prevention on the Shuttle vehicle are reported. Section 1 on "Coupling of Hydroelastic Tank to Feedline" displays the importance of the effect of oscillatory outflow from a hydroelastic tank in terms of normal modes of vibration for a structure containing a closed-bottom tank. The primary influence of the tank outflow is shown to be a new generalized force on the structural modes which equals the product of the modal pressure at the tank bottom and the volumetric outflow. The equations derived should be employed for future mathematical models.

Section 2 on "Method of Approximate Stability Analysis" describes a generalization of a previously developed method so as to account for such additional matters as tank outflow, the presence of two separate pumps for a propellant, and the presence of an accumulator at the inlet of either pump. Propulsion-feedback frequency response is derived in closed form for a system containing one engine, one propellant, and one structural mode. Evaluation at undamped feedline resonances reveals the conditions for which the contribution of tank outflow is stabilizing or destabilizing. The results are then employed to develop a criterion for identifying those structural modes which are of potential significance for system stability. Use of this method is recommended for preliminary evaluation of pogo stability, including the evaluation of accumulators.

In Section 3 on "Feedline Modeling" various finite-element and normal-mode models for uniform hydraulic feedlines are evaluated with the objective of minimizing the required number of second-order equations. A criterion of accuracy is based on a 5-percent tolerance on frequency and amplitude for the four admittance functions which relate flow and pressure at the two ends of a long line. The result is a procedure for optimum modeling a complex feedsystem using a building-block approach. A criterion is given for selecting either a particular finite-element approach or open-open modes for each section of the feedsystem.

Section 4 on "Engine Analysis and Testing" makes specific recommendations for the analytical estimation of pump cavitation compliance and dynamic gain. It also identifies weakness in thepast practices of pump testing and proposes a three-phase program of turbopump dynamic testing involving: (a) computer simulation studies of test practices, (b) comprehensive dynamic tests of available subscale pumps using water, and (c) verification tests on full-scale turbopumps using propellant. The development of a flowmeter for dynamic flow measurement is recommended.

The last section on "Vehicle Studies" relates the results of numerical studies on the booster lox system of the preliminary vehicle configuration based on the approximation method described in section 2. It is concluded that an accumulator between the boost and main pump offers promise of higher effectiveness than one at the engine inlet. It is also concluded that the small distributed resistance of feedlines can be important for high-frequency peaks in propulsion frequency response. A first estimate of the cavitation compliance of the Shuttle pumps is given.

INTRODUCTION

The effort to achieve pogo stability on the Space Shuttle vehicle system is complicated by the unusual degree of complexity and variability in the system dynamics. Complexities of the liquid propulsion system are introduced by the multiple organ-pipe modes of the long oxidizer feedline in the frequency range of the active structural modes and by the intricate nature of the high-chamber-pressure engine, particularly the presence of multiple pumps for each propellant. Structural complexity results from the multibody configuration which gives rise to strong coupling of longitudinal to other motions. Variability is contributed to the structural dynamics by the wide range of payloads and to the propulsion dynamics by the thrust-control feature of the engine. Pogo suppression, therefore, is made more demanding by the fact that stability must be established over a much wider range of system variables than has heretofore been required. As a consequence, additional burdens are placed on the mathematical modeling, on the experimental programs, and on the analysis techniques to assure that stability can be achieved. The studies reported deal with various elements of the task of preventing pogo on the Space Shuttle in consonance with the criteria and recommended practices provided by reference 1.

Studies began with an assessment of the interaction of the booster lox system with the structural system. This study paralleled similarly directed studies of the early configuration by vehicle contractors and by NASA. Of particular concern to us was the stability at coincidences of higher modes of the oxidizer feedsystem with structural modes. So, while other studies of accumulators were limited to a location at the engine inlet as used on past vehicles, our studies dealt with the additional possibility of an accumulator between the boost and main pumps. The concept of an interpump accumulator is to introduce damping at feedline resonances by the action of the resistance of the boost pump upstream of the accumulator. Engine contractors were contacted about the practical feasibility of an interpump accumulator and the response was favorable. It was then learned that one engine contractor was considering an accumulator downstream of the first-stage of the main lox pump to reduce high-frequency peaks in propulsion frequency response. This location was then added to our studies.

The approximate method of analysis, previously developed during studies of Titan pogo stability and later employed for Saturn V S-IC studies, was extended to deal with the presence of two pumps, multiple accumulator locations, and distributed feedline resistance. It was felt that the latter might be significant for the engine-inlet accumulator, since the small feedline resistance is the only means for dissipation upstream of the accumulator. The approximate method was particularly valuable for identifying the most critical stability conditions. In particular, the most critical tuning of the higher feedline modes with structural modes was readily accomplished.

Results of a numerical study for one of the proposed vehicle feedline configurations showed a superiority for the interpump location. These results are described in section 5. Subsequent analyses for another feedline configuration produced a condition of instability that was clearly incorrect in that the system was behaving in an essentially passive manner (that is, with negligible thrust

oscillation). The suspected difficulty was the lack of account for the influence of oscillatory flow out of the vehicle tank on the forces exerted on the tank walls. Based on the work of reference 2, such an effect was identified in reference 1 as a lack in the state of the art of structural modeling for pogo. A thorough analytical study of outflow was conducted and the result was the formal derivation of the appropriate equations appearing in Appendix A and the interpretive discussion in section 1. Section 2 shows the effect of the outflow on the propulsion-feedback transfer function, and then the importance of outflow under certain restricted conditions is evaluated. On the basis of these results, the criterion given in the Appendix of reference 1 for selecting the significant structural modes for pogo stability was revised.

Another major study was directed toward an evaluation of approaches to the mathematical modeling of feedlines. The requirements for such modeling were more severe for the Shuttle than on past vehicles because of the desire to maintain accuracy over a number of organ-pipe modes and to account for resistance. A variety of approaches to feedline modeling have been employed over the years for pogo studies. The need for Shuttle was for a consistent and comprehensive evaluation of promising alternative approaches. Included was the need for an accuracy criterion that was based on the role of the feedline in the frequency response of the propulsion system. The study described in section 3 is our contribution in this area.

Still another study was directed toward improving the experimental determination of the dynamic behavior of turbopumps. As pointed out in reference 1, experience has shown that such tests are difficult to perform and have produced questionable results. Some of the difficulties with past test practices are identified in section 4. A new approach is discussed and our proposed three-step program for Shuttle pump testing is outlined.

SYMBOLS

Units: M (mass), F (force), L (length), T (time)

a	acoustic velocity, $[LT^{-1}]$
A	area $[L^2]$
A_T	throat area of combustion chamber, $[L^2]$
b_n	a ratio of pressures, defined after eq. (2-13)
B	see eq. (2-18)
C	compliance, $[F^{-1}\ L^5]$
C_f	Thrust coefficient, [–]
C^*	characteristic velocity of combustion chamber, $[\ L\ T^{-1}]$
D	ratio of engine-inlet force to thrust, defined after eq. (2-13), sometimes $1/D$ or $1/D_R$ is called "engine gain," [–]
F	force, [F]
g	standard acceleration of gravity, $[L\ T^{-2}]$
G_e	structural gain for engine motion, $\phi^2(e)/M$, $[M^{-1}]$
h_t	height of propellant in tank, [L]
h_ℓ	height of tank-to-engine feedline, [L]
$H(s)$	propulsion-feedback transfer function, see eq. (2-13), $[FL^{-1}\ T^2]$
$\overline{H}$	value of $H(i\omega)$ at ω_n, $[FL^{-1}\ T^2]$
i	imaginary unit, $\sqrt{-1}$
I	variational integral
J	factor defined after eq. (2-13), [–]
K	stiffness, $[F\ L^{-1}]$
ℓ	line length, [L]
L	inertance, $[FL^{-5}\ T^2$ or $ML^{-4}]$
$\mathscr{L}$	Lagrangian

$m + 1$	pump dynamic gain, [–]
M	mass
M_n	generalized mass of nth structural mode, [M]
N	number of segments
$\mathscr{P}_n$	modal tank-bottom pressure per unit acceleration of generalized coordinate, $[FL^{-3}\ T^2]$
P	oscillatory pressure, $[F\ L^{-2}]$
q_n	generalized displacement of nth structural mode
Q	volumetric flow, $[L^3T^{-1}]$
R	Resistance, $[FL^{-5}\ T]$
s	Laplace variable used to denote the complex frequency $\sigma + i\omega$, $[T^{-1}]$
t	time, [T]
T	thrust, [F]; kinetic energy, [FL]
T'	effective thrust, [F]
T_o	thrust per unit mass flow into chamber, $[M^{-1}F\ T]$
V	potential energy, [FL]
x	structural displacement, [L]
x_f	fluid displacement, [L]
y_{ij}	element of admittance matrix, $[F^{-1}L^5T^{-1}]$
Y	flow admittance, $[F^{-1}L^5T^{-1}]$
Z	flow impedance, $[F\ L^{-5}T]$
a_{ij}	element of a transmission matrix, various units
β	wave number (angular frequency divided by acoustic velocity), $[L^{-1}]$
δF	variation of F
ζ	fraction-of-critical damping for structural mode, [–]
ζ_N	structural damping required for neutral system stability, [–]

η	parameter describing effect of outflow excitation, see eq. (2-18), [–]
θ	complex propagation angle
ρ	propellant mass density, $[M\ L^{-3}]$
σ	real part of complex frequency, $[T^{-1}]$
τ	travel time in a hydraulic line, $\sqrt{LC}$ or ℓ/a, [T]
τ_d	vaporization time delay, [T]
τ_r	chamber residence time, [T]
ϕ_n	modal displacement, [–]
Φ	velocity potential function
ω	angular frequency, $[T^{-1}]$
ω_n	natural frequency of structural mode, $[T^{-1}]$
ω^*	feedline natural frequency, $[T^{-1}]$
ω_o	quarter-wave organ-pipe frequency of feedline, $[T^{-1}]$

Subscripts

a	accumulator
b	bubble
d	discharge
e	engine
f	fluid
I	imaginary part
k	index for structural-system modes
ℓ	feedline
n	nth structural-system mode
p	pump
R	real part; relative

s	suction
t	tank

Other

| |	determinant
(tb)	at tank bottom
(e)	at engine
(f)	fluid
∇	mathematical operator del

1. COUPLING OF HYDROELASTIC TANK TO FEEDLINE

1.1 Introduction

In liquid-propellant missile systems the pogo vibrational stability problem is a result of coupling between the vehicle structural dynamics and the dynamics of the propulsion system. In formulating a linear mathematical model of the phenomenon a modal representation is employed for the structural system. The model is generally defined so that the active stage includes only the propellant in the tanks, with the tanks usually treated as if closed-off at the tank/feedline interface. The propellant feedsystem is then analytically coupled to this constrained structural system.

In the usual approach the change in tank pressures resulting from dynamic flow out of the tanks (termed "outflow") is neglected when coupling the feedline to the tank. The rationale is simply that because of the smallness of the line area relative to the tank cross-sectional area, this flow should have a negligible influence on fluid pressures within the tank, and therefore the effect on the structural system should also be negligible. Reference 2 correctly concluded that this assumption is invalid. It was shown that the integrated effect of the small change in the tank-interior pressures can easily produce a generalized force on the structural modes which is of the same order of significance as one of the basic propulsion system forces, the engine-inlet force. This result has been ignored until recently. Unfortunately, although the correct conclusions were reached in reference 2, the derivation contained a minor error and was limited to a very elementary model of the tank. Since the results are therefore not directly applicable to current structural models which employ quite detailed descriptions of the propellant/tank systems, a more general derivation of the outflow equations was necessary.

Reexamination of the outflow problem during this study was motivated by an anomalous result found in the course of analysis of the early Shuttle configuration during an investigation of various accumulator placements. Applying the usual approach of neglecting outflow effects, an instability was predicted in a particular circumstance when it was clear that the system should not have been unstable. (The system parameters were such that no significant thrust resulted for frequencies in the vicinity of the predicted "instability," so the system was essentially behaving in a passive manner.) Subsequent analyses indeed showed that the anomalous behavior was the result of not properly accounting for the outflow effects.

General dynamical equations have therefore been derived, accounting for the effects of tank outflow when the feedlines are coupled to the tanks. It is shown that the assumption of negligible influence is in general invalid and that the resulting forces applied to the structural system are significant when compared with other propulsion-system forces. Consistent with the usual formulation of the pogo model a modal representation of the structure is employed.

1.2 Method of Analysis

A derivation of the equations for coupling the feedline to a tank is presented in Appendix A. Only the case of a single propellant tank is considered since incorporation of multiple tanks is an obvious generalization. As shown schematically in the free-body diagrams of figure 1, the structural/propulsion system is separated into a structural system with fluid in the tanks (fig. 1b), and a feedline-engine or propulsion system (fig. 1c). Outflow from the tanks is a permissible fluid motion of the structural system. The forces $\hat{F}_i$ (i = 1, 2) are a symbolic representation of the usual propulsion-system forces, such as thrust, engine-inlet force, and reaction forces at feedline supports (ref. 1). These are of no concern for the present analysis and are carried along for the sake of completeness only. The equations of motion, defining structural-system response to the indicated "external" forces generated by the propulsion system, are derived using Hamilton's principle (ref. 3 or 4). The approach employed is to describe fluid motion within the tank in terms of two velocity potential functions, one representing motion consistent with the modal analysis of the structural system, the second representing the additional motion required to remove any fluid constraints introduced for convenience in the modal analysis. (For example, in the case of a closed-bottom-tank modal analysis, the second potential function represents a flow across the tank-bottom/feedline interface). The sum of the two potential functions fully represents fluid motions of the coupled structural/propulsion system. Equations are derived corresponding to different approaches to the structural-mode analyses, based on assuming different fluid boundary conditions at the tank/feedline interface. Fluid compressibility, surface waves (sloshing), and ullage-gas dynamic effects are neglected.

As a matter of definition, use of the phrase "tank bottom" refers to the tank-bottom/feedline-fluid interface. Because of the smallness of the feedline area compared to the tank area, the variation of parameters across the feedline area is neglected.

1.3 Feedline Within Structural System

The equations in Appendix A were derived for the case in which the feedline is represented as an entity separate from the structural system. Another approach is to make the feedline an integral part of the structural system. A suitably accurate definition of the feedline stiffness characteristics requires accounting for compressibility of the liquid in the line, whereas the Appendix A analysis assumes an incompressible fluid. However, since the line is typically treated as a one-dimensional system, the liquid compressibility can be viewed as additional flexibility in the line structure itself. The analysis of Appendix A and the results for the three boundary conditions at the tank/feedline interface considered are therefore applicable for like boundary conditions at the termination of the portion of feedline contained within the structural system.

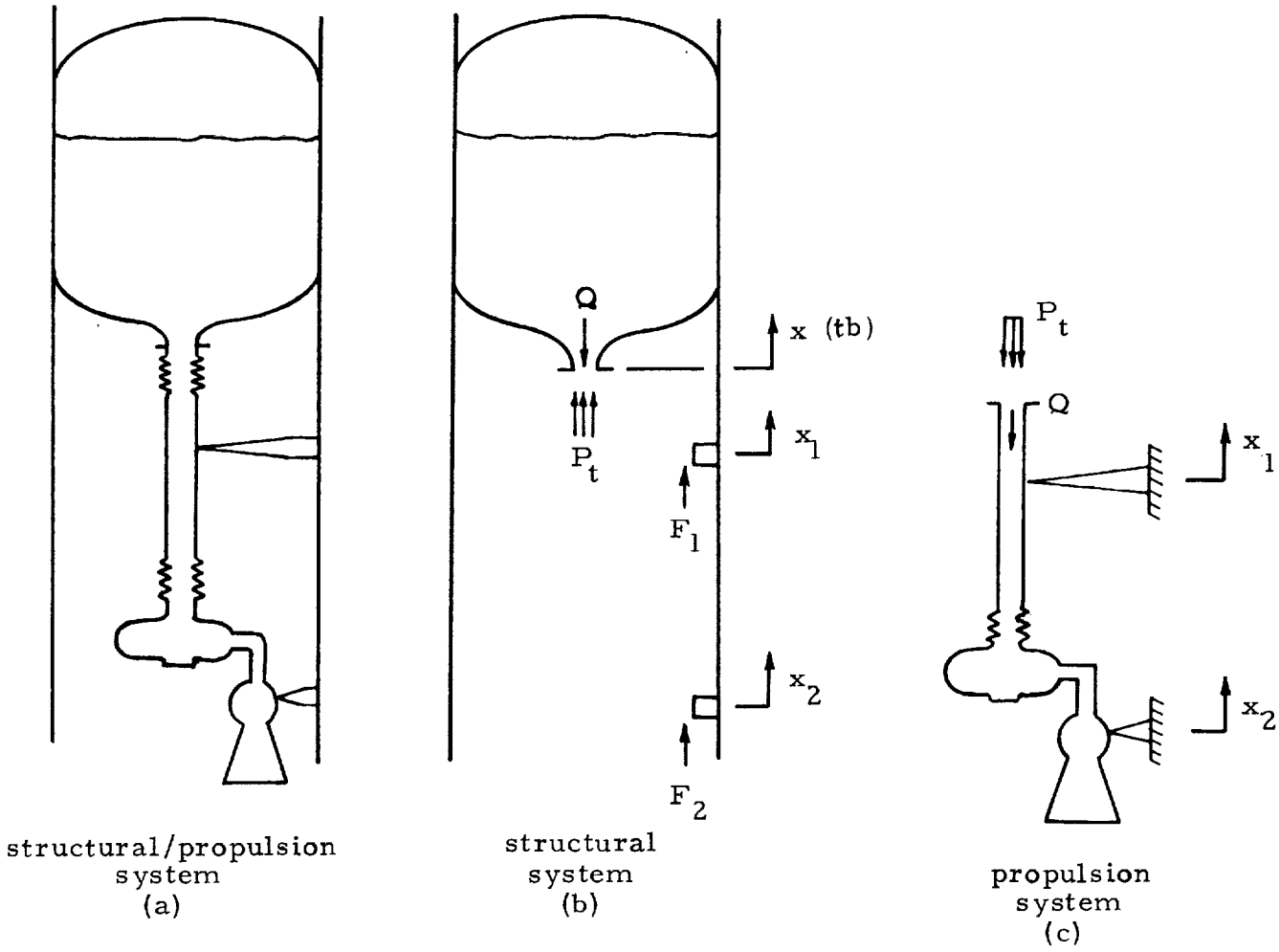

Figure 1. Schematic representation of systems.

1.4 Discussion of Closed-Tank Results

In the most typical formulation of the pogo model the structural system is defined with closed-bottom tanks. For this case (adding modal damping ζ_n for completeness), equation (A-20) of Appendix A gives the governing coupling equations as follows:

$$\left.\begin{aligned} M_n\,(\ddot{q}_n + 2\zeta_n\,\omega_n\dot{q}_n + \omega_n^2\,q_n) \\ = \mathscr{P}_{ln}(tb)\;\dot{Q}_R + P_t\,A_\ell\;\phi_n(tb) + \sum_i \vec{F}_i\cdot\vec{\phi}_{ni} \\ P_t = \sum_k \mathscr{P}_{lk}(tb)\;\ddot{q}_k - L_t\dot{Q}_R \end{aligned}\right\} \qquad (1\text{-}1)$$

The upper equation is the equation of motion for the nth mode of the structure with closed-bottom tanks. The first of the generalized force terms at the right represents the work done by the modal tank-bottom pressure $\mathscr{P}_{ln}(tb)$, acting through the fluid displacement relative to the tank bottom (expressed by the outflow $\dot{Q}_R$). The second generalized force represents the work done by the applied "external" pressure P_t acting through the modal displacement of the fluid (which is constrained to be the same as the structural displacement at the tank bottom; see fig. 1b). The third term at the right of the upper equation represents the work done by the "usual" propulsion-system forces mentioned earlier. The lower equation simply states that the tank-bottom pressure is the sum of the pressures in each of the structural modes, augmented by the second term which is the pressure due to outflow Q_R from a rigid tank.

For practical reasons structural dynamicists often prefer a formulation of dynamical problems in symmetrical forms and in terms of absolute rather than relative coordinates. Introducing the absolute volumetric flow Q,

$$Q = Q_R - A_\ell\;\dot{x}(tb) = Q_R - A_\ell\sum_n \phi_n(tb)\;\dot{q}_n \qquad (1\text{-}2)$$

where x(tb) is the structural motion at the tank bottom, yields equation (A-21) which can then be written in a symmetrical form simply by using the second equation to eliminate P_t in the first. The result for the nth mode (after adding modal damping) is

$$\begin{aligned} &M_n(\ddot{q}_n + 2\zeta_n\,\omega_n\dot{q}_n + \omega_n^2 q_n) - \left[\mathscr{P}_n(tb) - A_\ell\,L_t\,\phi_n(tb)\right]\dot{Q} \\ &- A_\ell\sum_k\left[\mathscr{P}_{ln}(tb)\;\phi_k(tb) + \mathscr{P}_{lk}(tb)\;\phi_n(tb) - A_\ell\,L_t\,\phi_n(tb)\;\phi_k(tb)\right]\ddot{q}_k = \sum_i \vec{F}_i\cdot\vec{\phi}_{ni} \end{aligned} \qquad (1\text{-}3a)$$

$$-\sum_k \left[\mathscr{P}_{lk}(tb) - A_\ell L_t \phi_k(tb)\right] \ddot{q}_k + L_t \dot{Q} = -P_t \tag{1-3b}$$

The minus sign on P_t is a result of choosing positive Q downward and positive structural displacements upward; see figure 1. Transforming to the Laplace variable s, a display of this result in matrix form, using the displacement variables $q_1, \ldots q_k, \ldots -Q/s$, is as follows:

$$\begin{bmatrix} D_{11}(s) + (\delta M_{11})s^2 & \cdots & (\delta M_{1k})s^2 & \cdots & d_1(s) \\ \vdots & & \vdots & & \vdots \\ (\delta M_{1k})s^2 & \cdots & D_{kk}(s) + (\delta M_{kk})s^2 & \cdots & d_k(s) \\ \vdots & & \vdots & & \vdots \\ d_1(s) & \cdots & d_k(s) & \cdots & L_t s^2 \end{bmatrix} \begin{Bmatrix} q_1 \\ \vdots \\ q_k \\ \vdots \\ -Q/s \end{Bmatrix} = \begin{Bmatrix} \sum_i \vec{F}_i \cdot \vec{\phi}_{1i} \\ \vdots \\ \sum_i \vec{F}_i \cdot \vec{\phi}_{ki} \\ \vdots \\ P_t \end{Bmatrix} \tag{1-4}$$

where

$$D_{kk}(s) = M_k(s^2 + 2\zeta_k \omega_k s + \omega_k^2)$$

$$\delta M_{nk} = \delta M_{kn} = \left[\mathscr{P}_{ln}(tb)\, \phi_k(tb) + \mathscr{P}_{lk}(tb)\, \phi_n(tb) - A_\ell L_t \phi_n(tb)\, \phi_k(tb)\right]$$

$$d_k(s) = \left[\mathscr{P}_{lk}(tb) - A_\ell L_t \phi_k(tb)\right] s^2$$

1.5 Importance of Outflow

This section shows that outflow can provide a significant excitation to the structural system. This is accomplished using a one degree-of-freedom representation of the fluid/tank system in which the entire body of fluid is assumed to move with displacement x_f, and the tank flexibility is represented by a single spring supporting the fluid mass. With this model we examine the relative importance of the terms associated with outflow using the form given by equations (1-3). All but one of the outflow terms is shown to be negligible relative

to other terms of comparable form. That term is $\mathscr{P}_{ln}(tb)\,\dot{Q}$ in the first line of equation (1-3), shown to have the same order of significance as does the engine-inlet (or suction-pressure feedback) force.

For the simplified model, fluid displacement can be expressed in terms of the structural-mode generalized coordinates by

$$x_f = \sum_n \phi_n(f)\, q_n$$

tank-bottom pressure in the nth mode by

$$\mathscr{P}_{ln}(tb) = \rho h_t \phi_n(f)$$

and the contribution of fluid motion to the nth generalized mass by

$$M_{nf} = \rho h_t A_t \phi_n^2(f)$$

where h_t is fluid height in the tank and A_t is tank area. If the tank inertance L_t given by

$$L_t = \rho h_t / A_t$$

is used, and the above relations are substituted into equations (1-3), the change in the generalized force on the nth mode arising from outflow can be written as

$$\delta F_n = \mathscr{P}_{ln}(tb)\left[1 - \frac{A_\ell}{A_t}\,\frac{\phi_n(tb)}{\phi_n(f)}\right]\dot{Q} + \sum_k \delta M_{nk}\,\ddot{q}_k \qquad (1\text{-}5)$$

where δM_{nk} has now taken the form:

$$\delta M_{nk} = \frac{A_\ell}{A_t} M_{nf}\left[\frac{\phi_k(tb)}{\phi_n(f)} + \frac{\phi_k(f)\,\phi_n(tb)}{\phi_n^2(f)} - \frac{A_\ell}{A_t}\,\frac{\phi_n(tb)\,\phi_k(tb)}{\phi_n^2(f)}\right] \qquad (1\text{-}5a)$$

The two terms within the brackets of equations (1-5) and (1-5a), which contain the ratio of line to tank area A_ℓ / A_t, can be neglected relative to other term(s) within the brackets since in practice $A_\ell << A_t$. These two terms result from those in equation (1-3) which contain the tank intertance L_t. The negligibility of L_t results from its inverse proportionality to the tank area A_t; on this

basis set $L_t = 0$ in section 3 in order to obtain a simplified approximate frequency response for the propulsion system.

The negligibility of the entire quantity δM_{nk} in equation (1-5a) can be demonstrated by means of the following argument. The quantity δM_{nk} is of the order of magnitude of $(A_\ell/A_t)M_{nf}$, where M_{nf} is the fluid's contribution to the total generalized mass M_n. Thus, since $M_{nf} < M_n$, δM_{nk} is at most of the order of $(A_\ell/A_t)M_n$. It can be seen from equation (1-4) that the matrix of the δM_{nk} terms is additive to the diagonal matrix formed by the M_k terms contained within the $D_{kk}(s)$. But, since $A_\ell/A_t << 1$, this addition is a small perturbation on the matrix of the D_{kk}, and thus on the structural system's modal frequencies and mode shapes (see section 6.12 of ref. 5). It can therefore be concluded that the δM_{nk} terms are negligible.

In view of the terms disposed of in equation (1-5), the expression for the change in generalized force has been reduced to

$$\delta F_n \approx \mathscr{P}_{ln}(tb)\,\dot{Q} \tag{1-6}$$

Again, a comparative term is required, which in this case is best provided by the engine-inlet force contained in the $\vec{F}_i$ force terms of equation (1-3). This force, $P_s A_\ell$, produces the generalized force, F_{ns}, given by

$$F_{ns} = P_s A_\ell\, \phi_n(e) \tag{1-7}$$

and the ratio is formed

$$\frac{\delta F_n}{F_{ns}} \approx \frac{\mathscr{P}_{ln}(tb)\,\dot{Q}}{P_s A_\ell \phi_n(e)} = \frac{\rho h_t}{A_\ell}\,\frac{\phi_n(f)}{\phi_n(e)}\,\frac{\dot{Q}}{P_s} \tag{1-8}$$

For a resistanceless, compressible line, the transmission-line equation (see sec. 3) can be used to define the absolute flow Q in terms of the pressures P_t, P_s:

$$Q = -\left(P_s - P_t \cos \omega\tau\right) \Big/ \frac{\rho h_\ell}{A_\ell}\,\frac{\sin \omega\tau}{P_s} \tag{1-9}$$

where τ is the acoustic travel time for the line length h_ℓ. Therefore

$$\frac{\delta F_n}{F_{ns}} \approx -\frac{h_t}{h_\ell}\,\frac{\phi_n(f)}{\phi_n(e)}\,\frac{\omega\tau}{\sin \omega\tau}\,\frac{P_s - P_t \cos \omega\tau}{P_s} \tag{1-10}$$

Based on past experience with typical systems it is often true that P_s is considerably larger than P_t, so that the last of the four factors in equation (1-10) can be of order 1. Noting that the first three factors can also be of order 1, it is finally concluded that δF_n can be of the same order of magnitude as F_{ns}. That is, the effect of outflow can be as significant as the suction-pressure feedback force and should therefore be properly accounted for in pogo modeling. Note that this is true even for the case of an incompressible line ($\tau = 0$). Amplification of this argument is provided in section 2, where it is shown that the effect of outflow on tank pressures can be viewed as a modification of the suction-pressure feedback force and that this modification can be large.

1.6 Conclusions

1. Appropriate account for the tank outflow can be derived by using Hamilton's principle and the superposition of two velocity potential functions for the incompressible fluid. One function describes the fluid motion consistent with the constraint boundary condition at the tank outlet assumed for the determination of structural modes. The second function represents the additional fluid motion required to remove the constraint imposed on the fluid.

2. The resulting equation for each mode of a closed-tank structural system, equation (1-1), shows two additional generalized force terms due to the outflow. The first term represents the work done by the modal tank-bottom pressure acting through the fluid relative displacement out of the tank. The second term represents the work done by the total tank-bottom pressure acting on the modal displacement of the tank-bottom structure. Equation (1-1) also states that the total tank-bottom pressure is the sum of the modal pressures plus a pressure arising from the outflow from a rigid tank. These results can be put into the symmetrical form of equation (1-3), if desired.

3. An assessment of the importance of the various terms has been made using a simplified model of the fluid/tank system. The primary influence of the tank outflow is embodied in the first of the generalized force terms identified in (2) above. This term was compared to the generalized force due to suction-pressure feedback and it is concluded that they can be of comparable magnitude.

4. In view of (3), dynamic flow out of a tank during oscillation of the coupled structural/propulsion system produces an excitation of modes of the closed-tank structural system which cannot in general be ignored.

5. The results are equally applicable to the case when the tank extends into a feedline and the closed-type of boundary condition for determination of structural modes is applied at the bottom of the feedline. This is based on the fact that compressibility of the fluid in the line can be accounted for by additional structural flexibility in the wall of the feedline.

6. Other boundary constraints on the fluid at the tank outlet in the structural system can also be treated. Such results are given in Appendix A.

1.7 Recommendations

For Shuttle pogo modeling, coupling equations (1-1) or (1-3) should be employed to account for tank outflow when closed tanks or closed feedlines are assumed for the determination of structural modes. If fixed or free boundary conditions on the fluid are desired for the structural analysis, the appropriate equations are (A-18) and (A-24), respectively.

2. METHOD OF APPROXIMATE STABILITY ANALYSIS

2.1 Introduction

The mathematical model for pogo stability analysis of a vehicle involves so many interactions of the coupled system that the analyst has difficulty in achieving a thorough understanding. This is especially true for the complex Shuttle vehicle. It is therefore useful to have an approximate method to serve as a tool to gain insight into the importance of the system parameters and also to conduct preliminary qualitative analyses. Such an approach was developed in reference 6 by first simplifying the system to one involving one engine, one propellant, and one structural mode. Next an expression was derived in closed form for the net propulsion-system frequency response, $H(\omega)$, which expresses the generalized force per unit reference acceleration. As a final step, an approximation for the structural damping required for neutral stability (ζ_N) was obtained, namely*

$$\zeta_N \simeq - \frac{\overline{H}_I G_p}{2} \tag{2-1}$$

where $\overline{H}_I$ is the imaginary part of the propulsion-system frequency response evaluated at the natural frequency of the structural mode, and G_p is the structural gain (square of the modal displacement divided by generalized mass) for the reference position on the vehicle.

For purposes of analysis of the Shuttle vehicle, the system used in reference 6 is generalized somewhat by incorporating the following additions:

1. Structural-mode excitation from tank outflow
2. The presence of two pumps within the engine (representing the boost pump and the first stage of the main pump)
3. The presence of an accumulator at the inlet of either pump
4. Distributed resistance of the tank-to-engine feedline
5. More refined treatment of combustion dynamics

A revision of the criterion for assessing the significance of structural modes given in the Appendix of reference 1 will then be derived.

In section 5 of the report, the approximate method is employed for stability evaluations of the early Shuttle configuration.

---

*Equation (2-1) is based on eq. (36) to (39) of ref. 6 (note that eq. (39) of ref. 6 has a minus sign missing).

2.2 System Model and Governing Equations

A schematic representation of the system to be analyzed is shown in figure 2. This simplified system is believed to display the major characteristics of an actual vehicle system. Discussion of the linearized mathematical model for the various elements follows. The state variables for the fluid are pressure P and volumetric flow Q; thus impedance quantities have the same units as does the ratio P/Q (as opposed to ref. 6 where the flow quantity is weight flow).

2.2.1 Feedline. - Assume that the steady velocity in the feedline is low compared to the acoustic speed, so that Mach-number effects are negligible. The line can then be treated as a simple uniform transmission line. Its properties are fluid mass density ρ, length ℓ, flow area A_ℓ, total inertance $L_\ell = \rho\ell/A_\ell$, total resistance R_ℓ due to wall friction, and acoustic travel time $\tau = \ell/a$. The acoustic speed "a" accounts for wall radial flexibility as well as fluid compressibility. The wall moves with velocity $\dot{x}_\ell$ in the direction opposing the flow. The complex propagation angle θ satisfies the relationship:

$$\theta^2 = s^2\tau^2 (1 + R_\ell / s\, L_\ell) \tag{2-2}$$

where s is the Laplace variable. The transmission equations can be written in the form:

$$P_1 = a_{11}P_t + a_{12}Q_t + a_{13}\dot{x}_\ell \tag{2-3a}$$

$$Q_1 = a_{21}P_t + a_{22}Q_t + a_{23}x_\ell \tag{2-3b}$$

where

$$a_{11} = a_{22} = \cosh\theta$$

$$a_{12} = -Z_\ell \frac{\sinh\theta}{\theta},\quad a_{21} = -\frac{1}{Z_\ell}\theta\sinh\theta$$

$$a_{13} = -A_\ell R_\ell \frac{\sinh\theta}{\theta},\quad a_{23} = -\frac{A_\ell R_\ell}{Z_\ell}(1 - \cosh\theta)$$

$$Z_\ell = R_\ell + sL_\ell$$

2.2.2 Pump-inlet admittance. - A pump-inlet admittance Y(s) is used to describe the combined effect of an accumulator and pump-inlet cavitation. If an accumulator is represented by compliance C_a, inertance L_a, and resistance R_a, and the cavitation bubble compliance is C_b, then

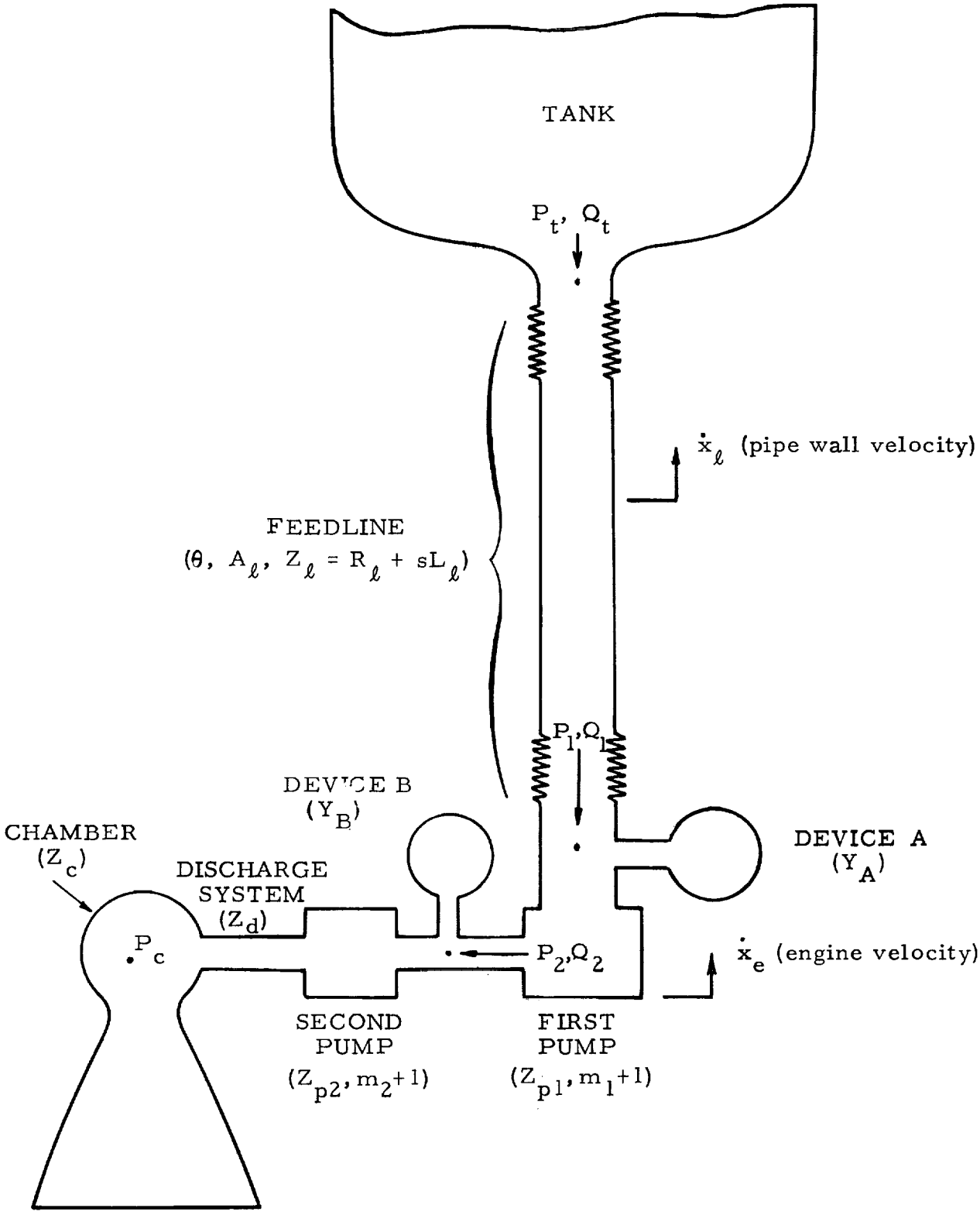

Figure 2. Propulsion system for approximate transfer function.

$$Y(s) = sC_b + \left(\frac{1}{sC_a} + sL_a + R_a\right)^{-1} \tag{2-4}$$

If the accumulator is a purely compliant device, it is simply

$$Y(s) = s\left(C_a + C_b\right) \tag{2-4a}$$

2.2.3 Engine elements. - The engine elements are modeled in the same fashion as was done in reference 6. Each pump (minus cavitation) is modeled by

$$P_d = (m + 1)P_s - Z_p Q'_d$$

$$Q'_d = Q'_s \tag{2-5}$$

where P_s and P_d are suction and discharge pressures, Q'_s and Q'_d are suction and discharge volumetric flows relative to the pump, $m + 1$ is the pump dynamic gain, and Z_p is the flow impedance of the pump.

If incompressible flow is assumed, the combination of the main pump, discharge line, injector, and combustion chamber satisfy the two relations

$$P_c/P_2 = (m_2 + 1)\, Z_c/Z', \quad P_c/Q_2 = Z_c \tag{2-6}$$

The combustion impedance Z_c is given by

$$Z_c = \frac{\rho C^*}{A_T} \frac{e^{-\tau_d s}}{1 + \tau_r s} \tag{2-7}$$

where C^* is an effective characteristic velocity for perturbations in propellant flow (account is taken of the slope of the curve of C^* versus mixture ratio; see ref. 6), τ_d is the time delay accounting for the average time the individual propellant spends in the chamber prior to vaporization, and τ_r is the gas residence time accounting for the mixing and reaction time common to both propellants (ref. 7). (When the effect of two propellants is considered, C^* and τ_d for one propellant will have different values, in general, than those for the other propellant.) The total impedance downstream of the boost pump is Z' (sum of the flow impedance and the combustion impedance):

$$Z' = Z_{p2} + Z_d + Z_c \tag{2-8}$$

where Z_d is the impedance of the discharge line and injector.

2.2.4 Structural mode. - The structural modes are derived for close-bottom tanks as given in the previous section. For a single mode, the engine acceleration $\ddot{x}_e$ can be written (as in eq. 2 of ref. 6) in terms of an effective thrust T':

$$\ddot{x}_e = \frac{s^2 G_e}{s^2 + 2\zeta\omega_n s + \omega_n^2} T' \tag{2-9}$$

where $\phi_n(e)T'$ is the total generalized force acting on the mode, $G_e = \phi_n^2(e)/M$ is the structural gain for engine motion, ω_n is the natural frequency, ζ is the fraction-of-critical damping, M is the generalized mass, and $\phi_n(e)$ is the modal displacement of the engine. If the fluid frictional forces acting on the feedline pipe are neglected, then from equations (1-1) and (1-2) can be obtained:

$$T' = A_T C_f P_c - A_\ell P_1 + \frac{\mathscr{P}_n}{\phi_n(e)} \left[\dot{Q}_t + A_1 \frac{\phi_n(tb)}{\phi_n(e)} \ddot{x}_e \right] + A_\ell \phi_n(tb) P_t \tag{2-10}$$

where Q_t is the absolute flow out of the tank, $\mathscr{P}_n$ is the modal tank-bottom pressure (pressure per unit acceleration of the generalized coordinate) and $\phi_n(tb)$ is the modal displacement of the tank-bottom structure. Also, the tank-bottom pressure with outflow is

$$P_t = \frac{\mathscr{P}_n}{\phi_n(e)} \ddot{x}_e - L_t \left[\dot{Q}_t + A_\ell \frac{\phi_n(tb)}{\phi_n(e)} \ddot{x}_e \right] \tag{2-11}$$

where L_t is the inertance of the propellant in the tank. On the basis of the discussion of equation (1-5) in section 1.5, the second term at the right of equation (2-10) can be neglected because of the presence of the relatively small tank inertance L_t. Thus, to a first approximation, tank outflow does not affect tank-bottom pressure, and it follows that it does not affect any pressure or flow in the propulsion system. Therefore the only effect of the tank outflow is on the effective thrust, which can now be written as

$$T' \doteq A_t C_f P_c - A_\ell P_1 + \frac{\mathscr{P}_n}{\phi_n(e)} \dot{Q}_t + 2 \frac{\mathscr{P}_n}{\phi_n(e)} A_\ell \frac{\phi_n(tb)}{\phi_n(e)} \ddot{x}_e \tag{2-12}$$

2.3 Transfer Function for Propulsion Feedback

Now consider the effective thrust per unit engine acceleration to represent the feedback transfer function for the propulsion system. Assembling the results of section 2.2 and omitting all the algebra results in the following form:

$$H(s) = \frac{T'}{\ddot{x}_e} = \frac{(m_1 + 1)(m_2 + 1)(A_\ell Z'_\ell / s)\rho T_o J (1 - DJ)}{\left(Z + Z' Z_{p1} Y_B\right)\left(\frac{\theta}{\tanh\theta} + Y_A Z_\ell\right) + (m_1 + 1)(m_2 + 1 + ZY_A) Z_\ell}$$

$$+ \left(\frac{\mathscr{P}_n}{\phi_n(e)}\right)^2 \frac{s}{Z_\ell} \frac{\theta}{\tanh\theta} + A_\ell \frac{\phi_n(tb)}{\phi_n(e)} \frac{\mathscr{P}_n}{\phi_n(e)} \left[2 - \frac{R_\ell}{Z_\ell} \frac{\phi_n(\ell)}{\phi_n(tb)}\right] \qquad (2\text{-}13)$$

where

$Z'_\ell = Z_\ell \left[1 - \frac{R_\ell}{Z_\ell} \frac{\phi_n(\ell)}{\phi_n(e)}\right]$ (a modification of the feedline series impedance due to the action of pipe motion on the liquid)

$T_o = A_t C_f Z_c / \rho$ (thrust per unit mass flow into the chamber)

$J = 1 + b_n \frac{\theta}{\sinh\theta}$ (a factor which accounts for the relative influence of tank-bottom pressure)

$b_n = \frac{\mathscr{P}_n s}{A_\ell Z'_\ell \phi_n(e)}$ (modal tank-bottom pressure divided by the engine-inlet pressure for an incompressible liquid in the feedline moving with the engine)

$D = \frac{A_\ell (Z + Z' Z_{p1} Y_B)}{(m_1+1)(m_2+1) A_T C_f Z_c}$ (ratio of engine-inlet force $P_1 A_\ell$ to thrust; 1/D is sometimes called "engine gain;" note that in ref. 6 D is the real part of this ratio of forces)

$Z_e = Z' + (m_2+1) Z_{p1}$ (total series impedance of the engine; Z_{p1} for first pump and Z' for the remainder including the combustion impedance)

With the exception of the structural excitation due to tank outflow, equation (2-13) is identical to the results of equations (15-19) of reference 6 under the following limiting conditions (stated in the notation of ref. 6):

a. The feedline is resistanceless ($R_\ell \to 0$, Z'_ℓ and $Z_\ell \to s L_1$, $\theta \to i\beta h$)

b. All the propellant in the tank is assumed to move with a modal displacement $\phi_n(t)$ and $\mathscr{P}_n \to \rho h_t \phi_n(t)$

c. There is no device or cavitation internal to the engine ($Y_B \to 0$)

d. There is no second pump ($Z_{p2} \to 0$, $m_2 + 1 \to 1$)

e. There is a pure compliance at the engine inlet ($Y_A = s / L_1 \omega_b^2$, where $\omega_b^2 C_A L_\ell = 1$)

f. The chamber dynamics are described by an equivalent time lag ($\tau_d \to 0$, $\tau_r \to \tau_c$).

In equation (2-13) the effect of structural excitation due to tank dynamic outflow manifests itself by the presence of the second and third terms and, most importantly, by the presence of J in the 1-DJ factor in the numerator of the first term. Without the outflow effect, the factor would be 1-D, where D accounts for the "suction-pressure feedback" (that is, the subtractive effect from the thrust of the pressure-times-area force at the engine inlet). Therefore the major effect of the outflow can be viewed as a modification of the suction-pressure-feedback force, with $|J| > 1$ increasing the magnitude of the feedback force and with $|J| < 1$ decreasing the magnitude of the feedback force. A more detailed evaluation of the effect of outflow is discussed next.

2.4 Effect of Outflow Without Feedline Resistance

An evaluation of the effect of tank dynamic outflow on the propulsion-feedback transfer function will now be made with the following simplifying conditions:

1. No feedline resistance ($R_\ell \to 0$, Z_ℓ and $Z'_\ell \to sL_\ell$, $\theta \to s\tau$, J real)
2. No admittance internal to the engine ($Y_B = 0$)
3. Pure compliance at inlet of first pump ($Y_A = sC_A$, $\omega_b^2 = 1/L_\ell C_A$)
4. Negligible delay and residence times in chamber (T_o real)

As a consequence of the introduction of the above simplifications into equation (2-13), the imaginary part of the feedback frequency response becomes

$$H_I(i\omega) = \text{Imag.}\ \frac{(m_1 + 1)(m_2 + 1) A_\ell L_\ell \rho T_o J(1 - DK)}{Z\left(\frac{\omega\tau}{\tan \omega\tau} - \frac{\omega^2}{\omega_b^2}\right) + i (m_1 + 1)(m_2 + 1) L_\ell \omega} \qquad (2\text{-}14)$$

where K = J when outflow excitation of the structure is included and K = 1 when outflow excitation is neglected. Note that the second and third terms at the right of equation (2-13) contribute nothing since, for the assumptions made, they are real.

2.4.1 At feedline resonances. - At a feedline resonance frequency ω^*, which is a solution of

$$\frac{\omega^*\tau}{\tan \omega^*\tau} - \frac{\omega^{*2}}{\omega_b^2} = 0 \qquad (2\text{-}15)$$

we find by using equation (2-14) that

$$H_I(i\omega^*) = -\frac{\rho A_\ell T_o}{\omega} J\,(1 - D_R K) \tag{2-16}$$

where D_R is the real part of D, the ratio of engine-inlet force to thrust; both $1/D$ and $1/D_R$ are sometimes called the "engine gain." Thus, by virtue of equation (2-1), the structural damping required for neutral stability is proportional to $J(1 - D_R K)$ at a resonance of a resistanceless feedline. Plots of $J(1 - D_R K)$ versus J for various values of D_R are shown in figure 3. If it is recalled that $K = J$ when outflow excitation is present (heavy curves) and $K = 1$ when outflow excitation is absent (light lines), it can be observed that instability is promoted by the outflow effect in the regions for which $0 < J < 1$, since for each D_R in this region a higher ordinate occurs when the outflow effect is present (except for the trivial case $D_R = 0$ when outflow has no influence). For $J > 1$, outflow lessens the possibility of an instability; for $J < 0$, the propulsion feedback is stabilizing without the outflow effect and even more stabilizing with the outflow effect.

As seen in figure 3, a higher D_R (lower "engine gain") tends to be helpful for achieving stability. Estimates during studies of the early Shuttle configuration yielded values of D_R between 0.3 and 2.8 (corresponding to "engine gains" between 3 and 0.4) depending on the values assumed for pump dynamic gain (pump gain is discussed in section 4.2). A desire has been expressed by some that the engine be designed to insure that the "gain" does not exceed unity (i.e., $D_R > 1$). In the absence of outflow excitation, a unity gain ($D_R = 1$) does produce zero feedback as shown in figure 3; however, outflow excitation will produce a positive feedback for $0 < J < 1$. Thus, even if the engine design had such a low "gain," there is no guarantee that instability will not occur in view of excitation of the structure by the tank outflow.

Further discussion of the significance of the results on figure 3 requires some discussion of the meaning of the parameter J, defined after equation (2-13). Suppose that the fluid at the engine-inlet moves with the engine (that is, $Q_1 = -A_\ell \dot{x}_e$). If Q_t is then eliminated from equations (2-3a, b), the following expression for pressure at the bottom of the feedline can be obtained.

$$P_1 = A_\ell Z'_\ell \frac{\tanh\theta}{\theta} \dot{x}_e \left(1 + \frac{1}{A_\ell Z_\ell} \frac{\theta}{\sinh\theta} \frac{P_t}{\dot{x}_e}\right) \tag{2-17}$$

If it is recognized that the tank-bottom pressure P_t and the engine velocity $\dot{x}_e$ are related via the structural mode-shape parameters [that is, $P_t/\dot{x}_e = \mathscr{P}_n \ddot{q}_n/\phi_n(e)\dot{q}_n = \mathscr{P}_n s/\phi_n(e)$], then it can be seen that the parenthetical expression in equation (2-17) is exactly the parameter J. The expression ahead of the parentheses in equation (2-17) gives the feedline-bottom pressure when the fluid at the feedline bottom moves with the engine, in the absence of pressure at the top. Then J is a multiplicative factor which accounts for the contribution to the feedline-bottom pressure due to the presence of a pressure at the top. So if $J > 1$, tank pressure P_t serves to increase the engine-inlet pressure P_1; if

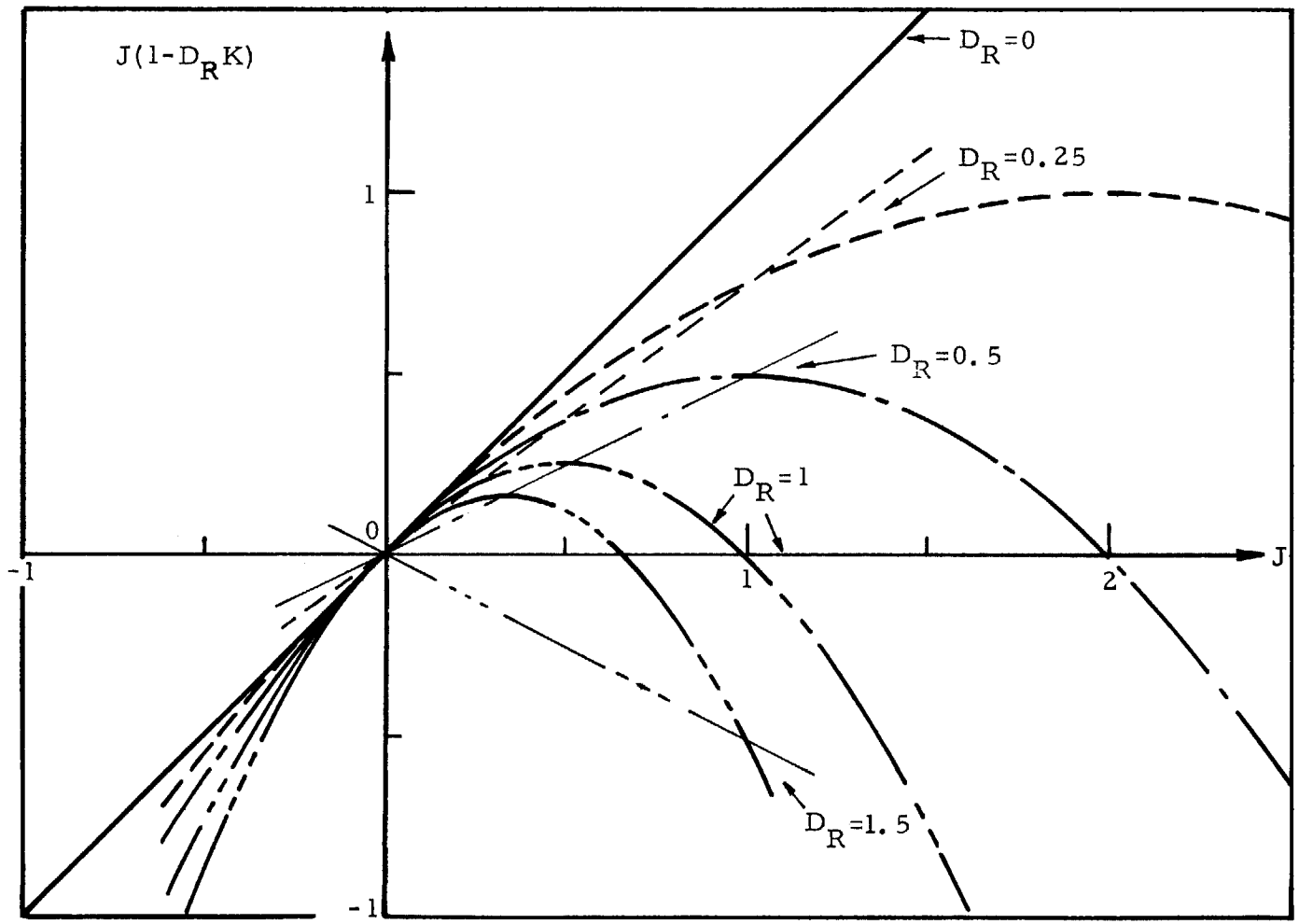

Figure 3. Propulsion-feedback factor with and without outflow.

$0 < J < 1$, P_t reduces P_1 but does not change its sign; if $J < 0$, P_t reverses the phase of P_1. Further, when $J = 1$ (P_s due only to $\dot{x}_e$) or $J = 0$ (P_t and $\dot{x}_e$ nullify each other to produce $P_s = 0$) we see from figure 3 that outflow has no effect; these are physically reasonable results.

We return now to figure 3 and our observation that outflow promotes instability at undamped feedline resonances only for $0 < J < 1$. Physically, then, outflow enhances instability at such resonances only when tank pressure is serving to detract partially from engine-inlet pressure. When outflow serves to magnify engine-inlet pressure ($J > 1$), the outflow is stabilizing and can, in fact, cause a reversal from destabilization due to propulsion feedback (positive ordinate) to stabilization due to the feedback (negative ordinate). This latter situation is typical of the critical conditions for stability identified during the early studies as discussed in section 5.2.2. Thus, unless the nature of the effect of outflow excitation is altered by the presence of the feedline resistance, outflow will be stabilizing at those conditions where the most severe tendency toward instability would exist in the absence of outflow excitation.

2.4.2 At arbitrary frequency. - Let η be the ratio of the value of H_I with outflow excitation to the value of H_I without outflow excitation. Manipulation of equation (2-14) produces the expression

$$\eta = \frac{B - DJ}{B - D} \tag{2-18}$$

where

$$B = 1 + \frac{L_e\left(\frac{\omega\tau}{\tan \omega\tau} - \frac{\omega^2}{\omega_b^2}\right)}{(m_1 + 1)(m_2 + 1) L_\ell}$$

and the total engine impedance is given by

$$Z_e = R_e + i\omega L_e$$

Note that at a feedline resonance, or if the total engine impedance is real (i.e., $L_e = 0$), $B \to 1$ and $D \to D_R$, therefore $\eta \to (1 - D_R J)/(1 - D_R)$ and the effect of outflow is the same as that discussed in the previous section.

Equation (2-18) can be quite helpful in estimating the effect of outflow. As a trial of its accuracy, a complete stability analysis was performed for a Titan Centaur vehicle at a time of minimum stability, both with and without outflow. The results showed that the outflow produced an η value of 0.7 (outflow stabilizing by 3 dB). The use of equation (2-18) for the dominant propellant and the dominant structural mode gave very close to the same result. In this case the assumptions leading to the derivation of equation (2-18) were well satisfied.

2.5 Criterion for Significance of Structural Modes

The Appendix of reference 1 provides a criterion for identifying those structural modes which are of potential significance for pogo stability. It is assumed that a coincidence of any structural mode with a feedline mode is possible. Two additional assumptions made for that analysis were: (1) no suction-pressure feedback (D = 0) and (2) the gross motion of the propellant in the tank equals that of the engine ($P_t = \rho h_t \ddot{x}_e$). Thus, the results fall within the framework of section 2.4.1, where K = 1 and $J = 1 + h_t/h_\ell$. In this case, the factor $J(1-D_R)$ appearing in equation (2-16) is $1 + h_t/h_\ell$.

A revised criterion based on the presence of outflow excitation is now sought. If the actual value of D_R is used, it is assumed that the value of J can have the worst possible value for stability. This means that $J(1 - D_R J)$ is assumed to be the value at the maximum of the curve for the particular value of D_R (see fig. 3); this maximum value is $1/4D_R$ and occurs when $J = 1/2D_R$. If equation (2-16) is used it is found that

$$H_I(i\omega^*) = -\frac{\rho A_\ell T_o}{4\omega^* D_R} = -\frac{(m_1 + 1)(m_2 + 1)(\rho T_o)^2}{4\omega^* R_e} \tag{2-19}$$

Based on equation (2-1), a criterion for structural-mode selection can be written as

$$\frac{\sum_j G_p}{f_n} \geq \frac{16\pi}{3}\frac{D_R \zeta_N}{\rho T_o A_\ell} = \frac{16\pi}{3}\frac{R_e \zeta_N}{(m_1 + 1)(m_2 + 1)(\rho T_o)^2} \tag{2-20}$$

where the summation denotes the sum of the structural gains over the j engines, and the structural natural frequency $\omega_n = 2\pi f_n$ equals the feedline resonant frequency ω^*. The factor of 3 in the denominator provides that the mode will only be significant if its damping is greater than 1/3 that required for neutral stability, in the case that all the worst-case assumptions are valid. The information needed to employ equation (2-20) to select the significant structural modes is (1) the desired value of structural damping required for neutral stability (ζ_N) for each mode, (2) the engine gain ($1/D_R$), and (3) the thrust per unit propellant velocity into the engine ($\rho T_o A_\ell$).

Figure 4 shows a comparison between the numerator factor $J(1 - D_R K)$ appearing in equation (2-16) as employed in reference 1, namely $1 + h_t/h_\ell$, and the one employed for equation (2-19), namely $1/4D_R$. If as anticipated for the Shuttle $D_R < 1/4\ (1 + h_t/h_\ell)$, the current criterion may reject some modes which would be accepted as significant by the criterion in reference 1.

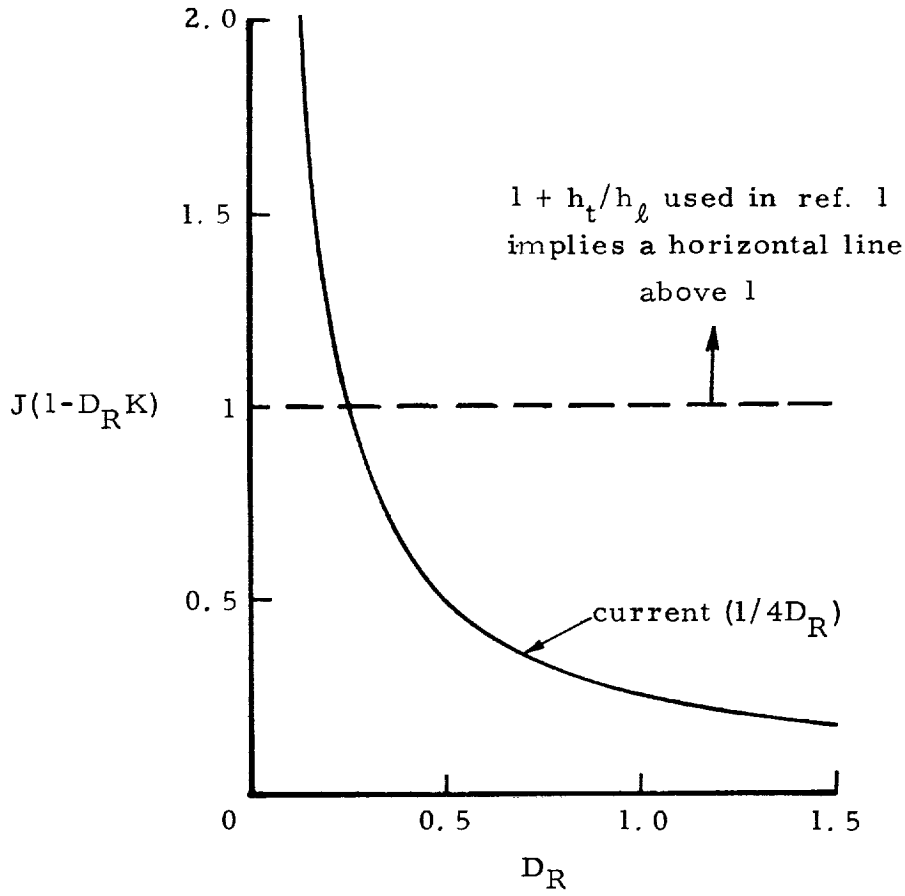

Figure 4. Factor used for assessing significance of structural modes.

2.6 Conclusions

1. The method of approximate stability analysis developed in reference 6 can be extended without undue complexity to account for (a) excitation of the structural mode by dynamic outflow from a vehicle tank, (b) the presence of two pumps with an accumulator at the inlet of each, (c) distributed resistance in the tank-to-engine feedline.

2. The major effect of the outflow excitation is to modify the suction-pressure feedback force by a multiplicative factor J. This factor accounts for the contribution of tank pressure to engine-inlet pressure.

3. When the feedline is resistanceless and a lumped compliance is present only at the engine-inlet, stability at feedline resonances is simply proportional to $J(1 - D_R J)$ where D_R is the real part of the ratio of engine-inlet force and thrust (the reciprocal of D_R is sometimes called "engine gain"). Outflow is destabilizing only for $0 < J < 1$, that is when tank pressure reduces the magnitude of engine-inlet pressure without reversing its phase. When tank pressure increases engine-inlet pressure ($J > 1$) as was typical of the worst stability cases in studies of the early Shuttle configuration (section 5.2.2), the outflow effect is increasingly stabilizing as J increases. A lowering of engine gain is stabilizing, but cannot guarantee stability.

4. The effect of outflow at any frequency can be determined by use of the simple expression in equation (2-18) when resistance of the feedline is neglected and lumped compliance is present only at the engine inlet.

5. Equation (2-20) provides a useful criterion for identifying those structural modes which are of potential significance for system stability. This criterion may reject modes for the Shuttle vehicle which would have been accepted by the criterion in reference 1, which was developed without an account for tank outflow.

2.7 Recommendations

1. The method of approximate stability analysis given here should be employed for initial analytical studies of stability on the Shuttle.

2. When more refined analytical studies are warranted, the approximate method should still be employed as an aid for guiding the studies and for interpreting results.

3. The criterion given by equation (2-20) should be employed to identify those structural modes worthy of inclusion in a comprehensive mathematical model of stability for the Shuttle vehicle.

4. A simplification of the imaginary part of the propulsion frequency response in equation (2-14) should be sought which is valid under less restrictive conditions than are equations (2-16) and (2-18); for example, when distributed feedline resistance is included.

3. FEEDLINE MODELING

3.1 Introduction

In developing a mathematical model for pogo stability, one of the most important aspects is the representation of the distributed properties of the vehicle feedlines. In general the feedline model must provide an accurate representation of all possible interrelationships between pressure and flow at the vehicle-tank and engine-inlet ends of the feedline. When outflow was neglected, flow at the tank end of the feedline did not couple the propulsion and structural systems. Thus the requirements for feedline modeling are now more stringent because of the account for outflow. The accuracy of the modeling must extend from zero frequency up to some upperbound frequency established by considerations of the stability of the overall coupled system. The number of equations required to accurately model the feedlines can represent a significant portion of the total number required for the mathematical model. For the Shuttle vehicle, rough estimates indicate that the number of equations may be of the order of 200. Thus, considerations of computer storage capability and computational time requirements indicate that attention be paid to the efficiency of the feedline modeling.

Most computer programs cannot handle an exact representation because of the involvement of transcendental functions [see eq. (2-3)]; thus, practically, one must resort to an approximation. The most widely employed technique for approximation is the finite-element approach wherein a line is subdivided into segments. Bases for the finite elements used in pogo models have been lumped parameters (e.g., refs. 8 and 9), power-series expansion (e.g., ref. 10), and product-series expansion (e.g., ref. 11). An approach using normal modes also has been employed (e.g., ref. 12). Another approach is the use of product-series expansions of the transfer functions for the overall line (refs. 10 and 13). A possibility which has not to our knowledge been employed for pogo models is an energy-minimization procedure to represent the line by a number of discrete displacement coordinates.

Our investigation concentrates on finite elements for uniform lines because they possess so much generality. Such finite elements can be employed directly for a piecewise uniform modeling of feedlines within the mathematical model of the overall coupled system, or they can be employed to develop a model of the feedlines alone as a basis for the determination of normal modes. A shortcoming of the normal-mode approach for an overall feedline network is its basic inability to handle an arbitrary distribution of damping (ref. 14), although normal modes can still be used for individual portions of line which are completely uniform. The product-series expansion has generally been considered only for uniform lines, being based on the well known open-open and open-closed natural frequencies; an application to nonuniform lines would require that the associated natural frequencies be obtained first. In summary, the finite-element method is fundamental to all approaches except (1) an energy-minimization method, or (2) a normal-mode or product-series method for uniform sections of line. An investigation of the normal-mode and collocation approaches is discussed in a later portion of this section of the report.

Finite-element approximations can have physical or mathematical bases (ref. 15). Physical models involve the use of lumped parameters (that is, masses, springs, and dashpots), while mathematical models can be based on various low-frequency approximations for the mathematically exact behavior. For purposes of an initial study, three limitations on the models were imposed in order to keep the number of possibilities reasonably finite: (1) the equations are expressible in second-order polynomial form, (2) dissipation is not considered, and (3) the model must be well behaved in the limiting case of an incompressible line. The first limitation is based on the fact that most of the other portions of the overall structure/propulsion system are naturally of second-order form, and it is expected that computational inefficiency would result if only a minor number of elements of the overall system have a higher order form. The limitation to the dissipationless line is based on the belief that the consideration of the small distributed dissipation, which is characteristic of feedlines, would not be likely to alter the relative merits of various models. The final limitation is quite an arbitrary one since the use of a special model for an incompressible line would really pose no difficulty. What this limitation actually does is to remove the possibility of an impedance form for the finite-element model since the coefficients in this form become infinite for an incompressible line. Transmission and admittance forms for the equations are not ruled out. Impedance and admittance forms are essentially duals of one another, and so no significant loss is expected from the lack of consideration of the impedance form. The three basic matrix forms (admittance, impedance, transmission) and their interrelationships are discussed in reference 16.

3.2 Finite-Element Transmission Models

Various transmission models whose accuracy is to be studied are presented in this section. The exact transmission-matrix description of the one-dimensional dissipationless feedline shown in figure 5 can be written as

$$\begin{Bmatrix} P_s \\ \dot{Q}_s \end{Bmatrix} = \begin{bmatrix} \cos \omega\tau & -L \dfrac{\sin \omega\tau}{\omega\tau} \\ \dfrac{1}{L} \omega\tau \sin \omega\tau & \cos \omega\tau \end{bmatrix} \begin{Bmatrix} P_t \\ \dot{Q}_t \end{Bmatrix} \tag{3-1}$$

where $L = \ell/Ag$ is the line inertance, $\tau = \sqrt{LC}$ is the travel time, and C is the line compliance.

3.2.1 Lumped-parameter model. - Three lumped-parameter representations are in common use: spring-mass, mass-spring-mass (or Rayleigh), and spring-mass-spring (or Duncan). Reference 15 shows the latter two to be equivalent in terms of modal frequency errors, both being superior to the simple spring-mass model. Hence the Rayleigh model was chosen for investigation. The transmission matrix for a symmetrical mass-spring-mass system, as shown in figure 6, is

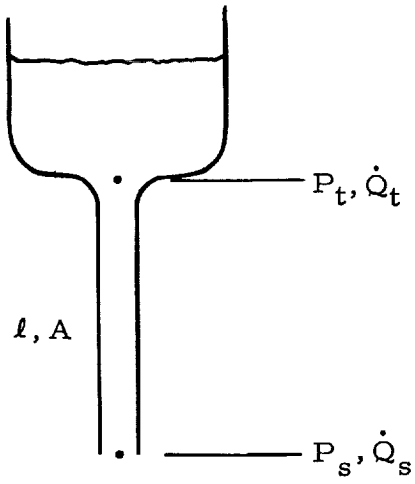

Figure 5. Feedline schematic.

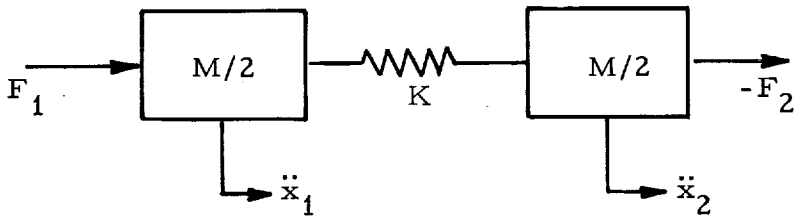

Figure 6. Lumped-parameter model.

$$\begin{Bmatrix} F_2 \\ \ddot{x}_2 \end{Bmatrix} = \begin{bmatrix} \left(1 - \frac{M\omega^2}{2K}\right) & -M\left(1 - \frac{M\omega^2}{4K}\right) \\ \frac{\omega^2}{K} & \left(1 - \frac{M\omega^2}{2K}\right) \end{bmatrix} \begin{Bmatrix} F_1 \\ \ddot{x}_1 \end{Bmatrix} \tag{3-2}$$

Converting this result to a hydraulic system [$(F, \ddot{x}) \rightarrow (P, \dot{Q})$; and $(M, 1/K) \rightarrow (L, \tau^2/L)$] yields

$$\begin{Bmatrix} P_2 \\ \dot{Q}_2 \end{Bmatrix} = \begin{bmatrix} 1 - \frac{(\omega\tau)^2}{2} & -L\left(1 - \frac{(\omega\tau)^2}{4}\right) \\ \frac{1}{L}(\omega\tau)^2 & 1 - \frac{(\omega\tau)^2}{2} \end{bmatrix} \begin{Bmatrix} P_1 \\ \dot{Q}_1 \end{Bmatrix} \tag{3-3}$$

This result is in a form directly comparable to the exact solution in equation (3-1).

3.2.2 Maclaurin-series model. - Expanding equation (3-1) in a Maclaurin series and retaining no powers of ω higher than two yields our first mathematical approximation:

$$\begin{Bmatrix} P_2 \\ \dot{Q}_2 \end{Bmatrix} = \begin{bmatrix} 1 - \frac{(\omega\tau)^2}{2} & -L\left(1 - \frac{(\omega\tau)^2}{6}\right) \\ \frac{1}{L}(\omega\tau)^2 & 1 - \frac{(\omega\tau)^2}{2} \end{bmatrix} \begin{Bmatrix} P_1 \\ \dot{Q}_1 \end{Bmatrix} \tag{3-4}$$

3.2.3 Product-series model. - Expanding equation (3-1) in a one-term product series yields

$$\begin{Bmatrix} P_2 \\ \dot{Q}_2 \end{Bmatrix} = \begin{bmatrix} 1 - \frac{4(\omega\tau)^2}{\pi^2} & -L\left(1 - \frac{(\omega\tau)^2}{\pi^2}\right) \\ \frac{1}{L}(\omega\tau)^2 & 1 - \frac{4(\omega\tau)^2}{\pi^2} \end{bmatrix} \begin{Bmatrix} P_1 \\ \dot{Q}_1 \end{Bmatrix} \tag{3-5}$$

This is a form equivalent to the one suggested in section 2.3.2 of reference 11.

3.2.4 Series-exact-at-specified-frequency model. - A second-order Maclaurin series expansion has the form:

$$f(x) = f(0) + f'(0)x + \frac{f''(0)}{2} x^2$$

Consider altering this series by adding an ϵx^2 term such that the series is exact at $x = x_\ell$, thus

$$\epsilon x_\ell^2 = f(x_\ell) - f(0) - f'(0)x_\ell - \frac{f''(0)}{2} x_\ell^2$$

and

$$f(x) = f(0) + f'(0)\, x\, \ell + \frac{f(x_\ell) - f(0) - f'(0)x_\ell}{x_\ell^2} x^2 \tag{3-6}$$

Using equation (3-6) to force an exact result at a frequency ω_o yields

$$\begin{Bmatrix} P_2 \\ \dot{Q}_2 \end{Bmatrix} = \begin{bmatrix} 1 - a(\omega\tau)^2 & -L\left(1 - b(\omega\tau)^2\right) \\ \frac{1}{L}(\omega\tau)^2 & 1 - a(\omega\tau)^2 \end{bmatrix} \begin{Bmatrix} P_1 \\ \dot{Q}_1 \end{Bmatrix} \tag{3-7}$$

where

$$a = \frac{1 - \cos \omega_o \tau}{(\omega_o \tau)^2} \qquad \text{and} \qquad b = \frac{1}{(\omega_o \tau)^2} \left[1 - \frac{\sin \omega_o \tau}{\omega_o \tau}\right]$$

3.2.5 Minimum-frequency-error models. - Two models were derived to minimize errors in the modal frequencies. The derivation of the two models is presented in Appendix B and follows the work of reference 15. Appendix B shows that the transmission matrix

$$[\alpha] = \begin{bmatrix} 1 - \frac{(\omega\tau)^2}{2} & -L\left(1 - \frac{(\omega\tau)^2}{3}\right) \\ \frac{1}{L}(\omega\tau)^2 & 1 - \frac{(\omega\tau)^2}{2} \end{bmatrix} \tag{3-8}$$

will have a modal-frequency error proportional to $1/N^4$ where N is the number of segments, and the matrix

$$[\alpha] = \begin{bmatrix} 1 - 0.4746(\omega\tau)^2 & -L\left(1 - 0.2312(\omega\tau)^2\right) \\ \frac{1}{L}(\omega\tau)^2 & 1 - 0.4726(\omega\tau)^2 \end{bmatrix} \tag{3-9}$$

will have a modal-frequency error proportional to $1/N^6$.

3.3 Finite-Element Admittance Models

The exact equations for the line shown in figure 5 can be cast into the following admittance form:

$$\begin{Bmatrix} \dot{Q}_t \\ -\dot{Q}_s \end{Bmatrix} = \frac{1}{L}\begin{bmatrix} \omega\tau/\tan\omega\tau & -\omega\tau/\sin\omega\tau \\ -\omega\tau/\sin\omega\tau & \omega\tau/\tan\omega\tau \end{bmatrix}\begin{Bmatrix} P_t \\ P_s \end{Bmatrix} = \begin{bmatrix} y_{11} & y_{12} \\ y_{21} & y_{22} \end{bmatrix}\begin{Bmatrix} P_t \\ P_s \end{Bmatrix} \tag{3-10}$$

It is possible to approximate this expression in the same mathematical ways used to approximate the transmission matrix.

3.3.1 Maclaurin-series model. - A Maclaurin-series expansion of equation (3-10), retaining powers of ω no higher than the second, is

$$[Y] = \frac{1}{L}\begin{bmatrix} 1 - \frac{(\omega\tau)^2}{3} & -1 - \frac{(\omega\tau)^2}{6} \\ -1 - \frac{(\omega\tau)^2}{6} & 1 - \frac{(\omega\tau)^2}{3} \end{bmatrix} \tag{3-11}$$

3.3.2 Product-series model. - A one-term product-series expansion of equation (3-10) is

$$[Y] = \frac{1}{L}\begin{bmatrix} 1 - \frac{4(\omega\tau)^2}{\pi^2} & -1 - \frac{(\omega\tau)^2}{\pi^2} \\ -1 - \frac{(\omega\tau)^2}{\pi^2} & 1 - \frac{4(\omega\tau)^2}{\pi^2} \end{bmatrix} \tag{3-12}$$

3.3.3 Series-exact-at-specified-frequency model. - Following the procedures of section 3.2.4, one can force second-order series expansions of cot $\omega\tau$ and csc $\omega\tau$ to be exact at a frequency ω_o, yielding

$$[Y] = \frac{1}{L}\begin{bmatrix} 1 - c(\omega\tau)^2 & -1 - d(\omega\tau)^2 \\ -1 - d(\omega\tau)^2 & 1 - c(\omega\tau)^2 \end{bmatrix} \tag{3-13}$$

where

$$c = \frac{1 - (\omega_o\tau)\cot\omega_o\tau}{(\omega_o\tau)^2} \qquad \text{and} \qquad d = \frac{(\omega_o\tau)\csc\omega_o\tau - 1}{(\omega_o\tau)^2}$$

3.3.4 Minimum-frequency-error model. - Starting from the form of the admittance matrix in equation (3-13), it is possible to determine coefficients c and d such that the error in modal frequencies is proportional to $1/N^4$. An initial step is to transform equation (3-13) into the rearward-transmission-matrix formulation:

$$\begin{Bmatrix} P_2 \\ \dot{Q}_2 \end{Bmatrix} = \frac{1}{1 + d(\omega\tau)^2}\begin{bmatrix} 1 - c(\omega\tau)^2 & -L \\ \frac{1}{L}\left[\left(1 + d(\omega\tau)^2\right) - \left(1 - c(\omega\tau)^2\right)\right] & 1 - c(\omega\tau)^2 \end{bmatrix}\begin{Bmatrix} P_2 \\ \dot{Q}_2 \end{Bmatrix} \tag{3-14}$$

Following the procedures discussed in Appendix B, we obtain $c = 5/12$ and $d = 1/12$ to product a natural-frequency error proportional to $1/N^4$. Thus the desired matrix is

$$[Y] = \frac{1}{L}\begin{bmatrix} 1 - \frac{5(\omega\tau)^2}{12} & -1 - \frac{(\omega\tau)^2}{12} \\ -1 - \frac{(\omega\tau)^2}{12} & 1 - \frac{5(\omega\tau)^2}{12} \end{bmatrix} \tag{3-15}$$

It is not possible, starting from equation (3-13), to find c and d such that the natural-frequency error is proportional to $1/N^6$, as was possible for the transmission-matrix form.

3.4 Normal-Mode and Collocation Models

Flexibility and ease of application make finite-element approaches quite attractive. Analysis of large systems, however, often requires the use of more efficient techniques in order to minimize the number of equations required to accurately represent the system. Limited examination of two particularly effective methods for doing this have been included in this study, namely, the use of normal-mode representations and the application of a collocation method.

The normal-mode approach is well known and represents a powerful tool in performing dynamic analyses of large and complex systems. However, the most efficient use of this approach is not obvious when applied to components of a large system; this is clear from the many papers appearing in the literature on component-mode-synthesis techniques. The present study was limited to use of the open-open and open-closed modes of a uniform line.

The collocation approach, in which a discrete set of physical variables is retained, as opposed to the generalized variables of the modal approach, is much less widely used. Yet in its most refined form it is approximately as powerful a method for reducing problem size as the normal-mode approach (ref. 17). The collocation method presented here is essentially a Rayleigh-Ritz approach using a set of polynomials as interpolation functions for system displacement variables. An advantage of the approach over a modal approach is that physical variables are retained, thus allowing greater flexibility. (Parametric studies, for example, could be more readily performed).

The equations of motion are developed by employing a standard formulation (ref. 18). For the case of a resistanceless, one-dimensional line element, the system dynamics can be described in terms of a displacement variable u(x, t) as indicated in figure 7.

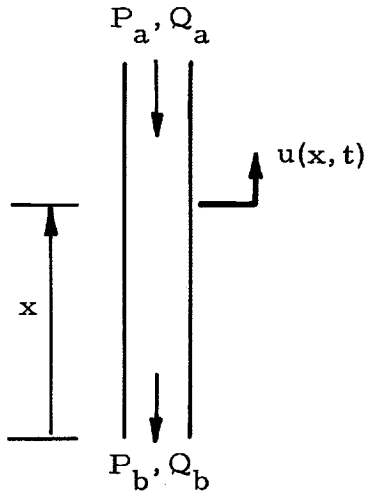

Figure 7. One-dimensional line segment.

For a line of length ℓ, area A, inertance L, and acoustic velocity a, the system Lagrangian $\mathscr{L}$ can be written as

$$\mathscr{L} = \frac{LA^2}{2\ell}\int_0^{\ell}\left[\left(\frac{\partial u}{\partial t}\right)^2 - a^2\left(\frac{\partial u}{\partial x}\right)^2\right]dx \tag{3-16}$$

Assuming the existence of generalized coordinates q_n and associated shape functions $f_n(x)$, such that

$$u(x,t) = \sum_n f_n(x)q_n(t) \tag{3-17}$$

the Lagrangian becomes

$$\mathscr{L} = \frac{LA^2}{2}\sum_n\sum_k b_{kn}\dot{q}_k\dot{q}_n - c_{kn}q_kq_n \tag{3-18a}$$

where

$$b_{nk} = \frac{1}{\ell}\int_0^{\ell} f_n(x)f_k(x)dx \tag{3-18b}$$

$$c_{nk} = \frac{\ell}{\tau^2}\int_0^{\ell} f_n'(x)f_k'(x)dx \tag{3-18c}$$

where $f_n'(x)$ is the derivative with respect to x of $f_n(x)$ and where the travel time $\tau = \ell/a$ has been introduced. Application of Lagrange's equations yields the equations of motion in the form

$$\sum_k b_{nk}\ddot{q}_k + \sum_k c_{nk}q_k = \left[-P_a f_n(\ell) + P_b f_n(0)\right]\Big/LA \qquad n=1,2,\ldots \tag{3-19}$$

The corresponding flow at any point along the line, Q(x), is given by

$$Q(x) = -\sum_n A f_n(x)\, \dot{q}_n(t) \tag{3-20}$$

The equations for the modal approach can now be written down directly. In the case of open-open modes,

$$u(x,t) = \sum_n \cos \frac{n\pi x}{\ell}\, q_n(t) \tag{3-21a}$$

$$\ddot{q}_n + \omega_n^2 q_n = \begin{cases} 2\left[P_b - P_a(-1)^n\right]/LA & (n \neq 0) \\ (P_b - P_a)/LA & (n = 0) \end{cases} \tag{3-21b}$$

where

$$\omega_n^2 = \left(\frac{n\pi}{\tau}\right)^2$$

$$Q(x,t) = -\sum_{n=0}^{\infty} A \cos \frac{n\pi x}{\ell}\, \dot{q}_n(t) \tag{3-21c}$$

In the case of open-closed modes,

$$u(x,t) = q_o(t) + \sum_{n=1}^{\infty} \sin \frac{(2n-1)\pi x}{2\ell}\, q_n(t) \tag{3-22a}$$

Noting that $\ddot{q}_o(t) = \ddot{u}(0,t) = -\dot{Q}_b(t)/A$, equations (3-19, 20) become

$$\left.\begin{aligned} \dot{Q}_b/A - \sum_{n=1}^{\infty} \frac{2}{\pi(2n-1)}\, \ddot{q}_n &= \frac{-P_b + P_a}{LA} \\ \ddot{q}_n + \omega_n^2 q_n - \frac{4}{\pi(2n-1)}\, \frac{\dot{Q}_b}{A} &= \frac{+2(-1)^n P_a}{LA} \end{aligned}\right\} \tag{3-22b}$$

where

$$\omega_n^2 = \left[\frac{(2n - 1)\pi}{2\tau}\right]^2$$

and finally,

$$Q(x,t) = Q_b(t) - \sum_{n=1}^{\infty} A \sin \frac{(2n - 1)\pi x}{2\ell} \dot{q}_n(t) \qquad (3\text{-}22c)$$

As noted previously, collocation procedures (which characteristically retain the physical variables) can be refined to produce results nearly comparable to those of a modal approach (ref. 17). To assess the potential advantages of such a method, one of the simplest forms was investigated in which $u(x,t)$ is defined in terms of the deflections $u_n(t) = u(x_n, t)$ at a discrete set of points x_n along the line, and in terms of polynomial interpolation functions. Since the equations of motion are derived via the Lagrangian, the method is equivalent to a Rayleigh-Ritz energy approach. The deflection $u(x,t)$ can be expressed as a linear combination of a set of N linearly independent functions $g_n(x)$ as

$$u(x,t) = \sum_{n=1}^{N} g_n(x) C_n(t) \qquad (3\text{-}23)$$

where the $C_n(t)$ are a corresponding set of coefficients. The $C_n(t)$ are defined so that the deflections $u(x_n, t)$ at a set of N points are exact. Then, $u(x,t)$ can be written in matrix format as

$$u(x,t) = \left| g_1(x), \ldots, g_N(x) \right| \left[A \right]^{-1} \begin{Bmatrix} u_1(t) \\ \vdots \\ u_N(t) \end{Bmatrix} \equiv \sum_{n=1}^{N} f_n(x) u_n(t) \qquad (3\text{-}24)$$

where elements of the matrix [A] are given by

$$A_{nk} = g_k(x_n) \qquad k, n = 1, 2, \ldots N$$

and where the $C_n(t)$ have been replaced by

$$\begin{Bmatrix} C_1(t) \\ \vdots \\ C_N(t) \end{Bmatrix} = \begin{bmatrix} A \end{bmatrix}^{-1} \begin{Bmatrix} u_1(t) \\ \vdots \\ u_N(t) \end{Bmatrix}$$

The functions $f_n(x)$, which are linear combinations of the functions $g_n(x)$, are known as Lagrangian interpolation functions. Since this is in the form of equations (3-17), with deflections at the N points u_k acting as the generalized variables, the resulting equations of motion, equations (3-19), can be written in matrix form as

$$[M] \left|\ddot{u}\right| + [K] \left|u\right| = \left|F\right| \tag{3-25}$$

where

$$\left|F\right| = \left|P_a A,\ 0,\ \ldots, 0,\ P_b A\right|$$

and, from equations (3-18b) and (3-18c),

$$\left.\begin{aligned} M_{nk} &= (LA^2)\, b_{nk} \\ K_{nk} &= (LA^2)\, c_{nk} \end{aligned}\right\}$$

The case considered in this study assumed a polynomial form for the functions $g_k(x)$; that is

$$g_k(x) = x^{k-1} \tag{3-26}$$

Equations (3-21), (3-22), (3-25), and (3-26) provide the basis for the evaluation of line modeling via the two modal and one collocation methods considered.

3.5 Accuracy Criteria

As previously mentioned, the feedline model must accurately represent the interrelationships between pressures and flows at the end of the feedlines. The admittance form of the feedline equations can be written as

$$\begin{Bmatrix} Q_t \\ -\dot{Q}_s \end{Bmatrix} = \frac{1}{L}\begin{bmatrix} \omega\tau/\tan\omega\tau & -\omega\tau/\sin\omega\tau \\ -\omega\tau/\sin\omega\tau & \omega\tau/\tan\omega\tau \end{bmatrix}\begin{Bmatrix} P_t \\ P_s \end{Bmatrix} \tag{3-27}$$

The function $\omega\tau/\tan\omega\tau$ can be viewed as defining the suction (tank) flow per unit suction (tank) pressure, while the function $\omega\tau/\sin\omega\tau$ defines the suction (tank) flow per unit tank (suction) pressure. Note that these two functions appear in the propulsion frequency-response relationship given by equation (2-13); $\omega\tau/\tan\omega\tau$ appears in the characteristic equation for the propulsion system while $\omega\tau/\sin\omega\tau$ is important for the tank pressure influence.

While the exact admittance matrix is both reciprocal (the suction flow rate per unit tank pressure equals the tank flow rate per unit suction pressure) and symmetric (tank flow per unit tank pressure equals the suction flow per unit suction pressure), the admittance matrices implied by some approximate models do not necessarily have both of these properties. Consider the general transmission matrix:

$$\begin{Bmatrix} P_t \\ \dot{Q}_t \end{Bmatrix} = \begin{bmatrix} \alpha_{11} & \alpha_{12} \\ \alpha_{21} & \alpha_{22} \end{bmatrix}\begin{Bmatrix} P_s \\ \dot{Q}_s \end{Bmatrix} \tag{3-28}$$

Converting this to an admittance description yields

$$\begin{Bmatrix} \dot{Q}_t \\ -\dot{Q}_s \end{Bmatrix} = \begin{bmatrix} y_{11} & y_{12} \\ y_{21} & y_{22} \end{bmatrix}\begin{Bmatrix} P_t \\ P_s \end{Bmatrix} = \begin{bmatrix} \dfrac{\alpha_{22}}{\alpha_{12}} & \dfrac{-|\alpha|}{\alpha_{12}} \\ \dfrac{-1}{\alpha_{12}} & \dfrac{\alpha_{11}}{\alpha_{12}} \end{bmatrix}\begin{Bmatrix} P_t \\ P_s \end{Bmatrix} \tag{3-29}$$

Except for the Rayleigh model, the transmission models developed in section 3.2 have $|\alpha| \neq 1$, which implies a lack of reciprocity (ref. 16); that is y_{12} and y_{21} are not equal, and hence both must be compared to $\omega\tau/\sin\omega\tau$. However, $\alpha_{11} = \alpha_{22}$ for all the transmission models, so that $y_{11} = y_{22}$, indicating that symmetry is maintained. In the case of the open-closed modal system of section 3.4, truncation of the modes produces an unsymmetric representation such that $y_{11} \neq y_{22}$. Thus, for this model, both y_{11} and y_{22} must be evaluated relative to $\omega\tau/\tan\omega\tau$.

In the past, when outflow effects were neglected at the tank/feedline interface, the critical parameters were suction flow due to tank and suction pressures, and satisfaction of neither the reciprocity nor symmetry relations was required. Now, however, outflow effects have been found significant and care

must be taken to insure that approximations introduced in the line modeling are valid for all four of the possible admittance functions.

Permissible bounds on the exact functions $\omega\tau/\tan\omega\tau$ and $\omega\tau/\sin\omega\tau$ are based on a 5-percent amplitude error and a 5-percent frequency shift at each point along a function. The outermost of these two bounds provides the allowable error band. The results are shown in figures 8 and 9. The various models are to be evaluated in terms of the frequency range over which the appropriate y_{ij} fall within these error bounds.

3.6 Evaluation of Finite-Element Models

As discussed in section 3.5, the various functions $y_{11}(\omega\tau)$, $-y_{12}(\omega\tau)$ and $-y_{21}(\omega\tau)$ were used to evaluate the models developed in sections 3.2 and 3.3. In order to evaluate the admittance models, they were first cast into the transmission formulation making no approximations. Then the transmission matrix for a line divided into N segments was found by raising the transmission matrix for each segment to the Nth power:

$$[\alpha(\omega\tau)] = \begin{bmatrix} \alpha_{11}(\omega\tau/N) & -\frac{L}{N}\alpha_{12}(\omega\tau/N) \\ \frac{N}{L}\alpha_{21}(\omega\tau/N) & \alpha_{22}(\omega\tau/N) \end{bmatrix}^N \tag{3-30}$$

Then the resulting $[\alpha]$ was used to compute the functions $y_{11}(\omega\tau)$, $-y_{12}(\omega\tau)$, $-y_{21}(\omega\tau)$ for comparison with the error bounds on these functions. Note that the Rayleigh transmission and all of the admittance models give identical results for y_{12} and y_{21}, whereas the other models do not behave in reciprocal fashion. Values of N = 1, 3, 5 and 10 were employed and computations were made for values of $\omega\tau/N$ ranging from 0 to π. For N = 1, all models were evaluated; the exact-at-specified-frequency transmission and admittance matrices were evaluated for $\omega_o\tau = \pi/4$, $\pi/3$, $\pi/2$, and $3\pi/4$. It was apparent that several of the candidate models were not promising, and so for N = 3, and N = 5, several were discarded. Finally, for N = 10, several more models were discarded. Figures 10 through 13 show y_{11} and y_{12} versus $\omega\tau$ for two of the models: the lumped (Rayleigh) transmission and admittance-series exact at $\omega_o\tau = \pi/3$.

The results of the computations are summarized in Table I, where the maximum value of $\omega\tau/2\pi N$ (fractional part of a wave length per element) for which the functions remain within the ±5-percent amplitude and frequency bands are shown, as well as some selected results for y_{12} using a 10-percent amplitude band.

Several aspects of Table I should be noted. The admittance Maclaurin series forced to be exact at $\omega_o\tau = \pi/3$ appears to be the best of these models in terms of the matching of both y_{11} and y_{12}, as well as uniformity of convergence. Several other models, particularly the product-series transmission model,

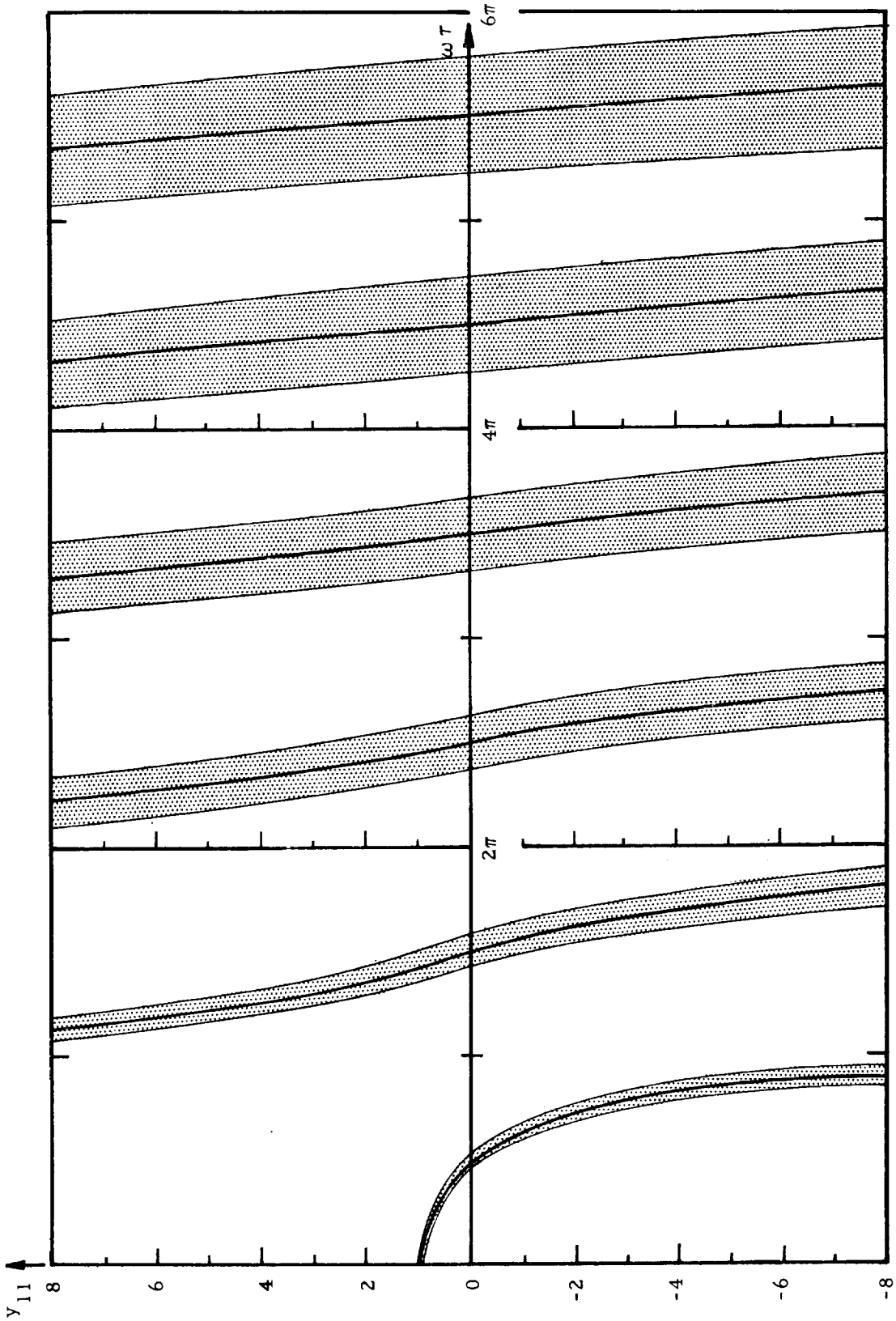

Figure 8. Exact function y_{11} ($= \omega\tau/\tan\omega\tau$) vs. $\omega\tau$.

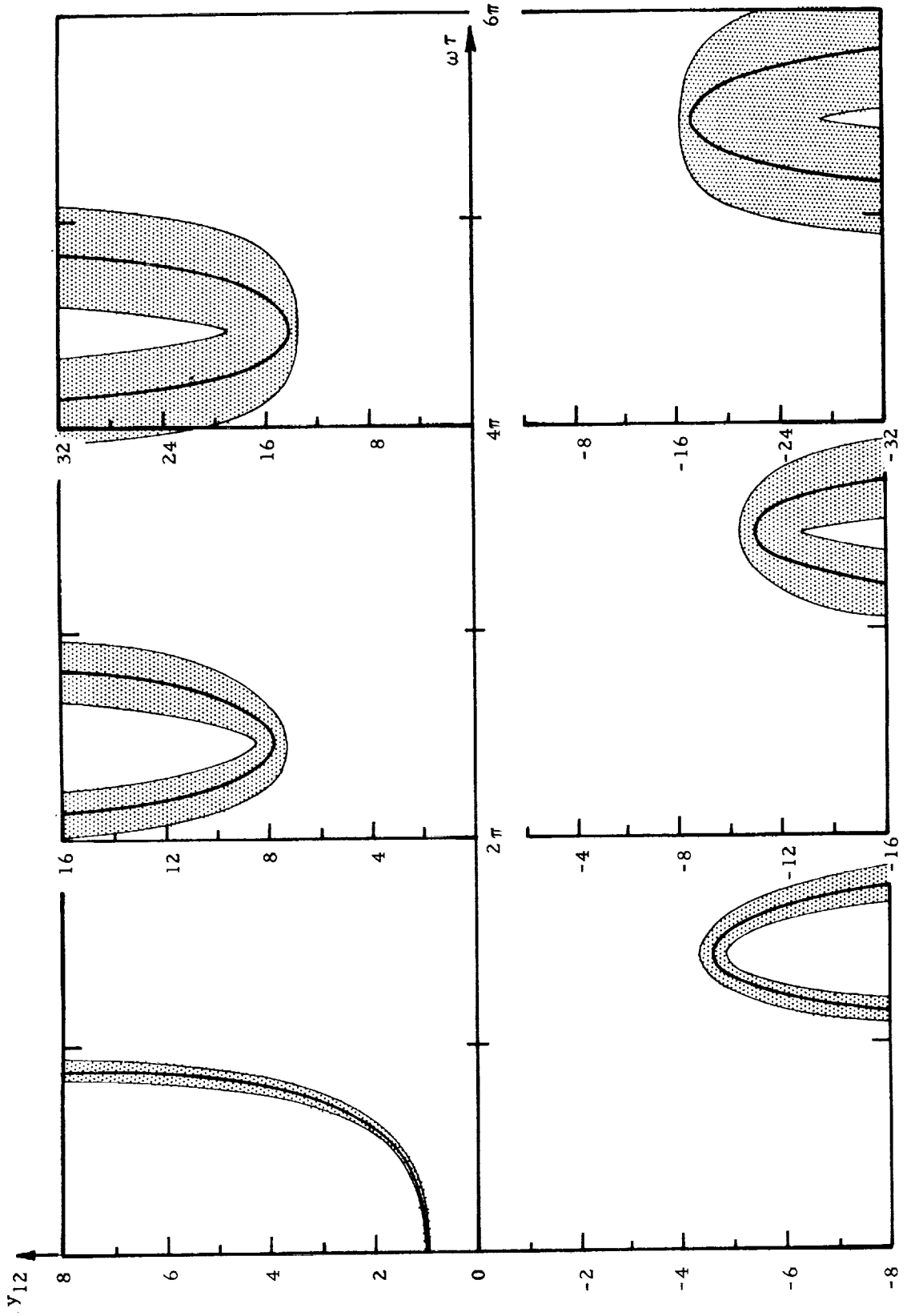

Figure 9. Exact function y_{12} ($= \omega\tau/\sin\omega\tau$) vs. $\omega\tau$.

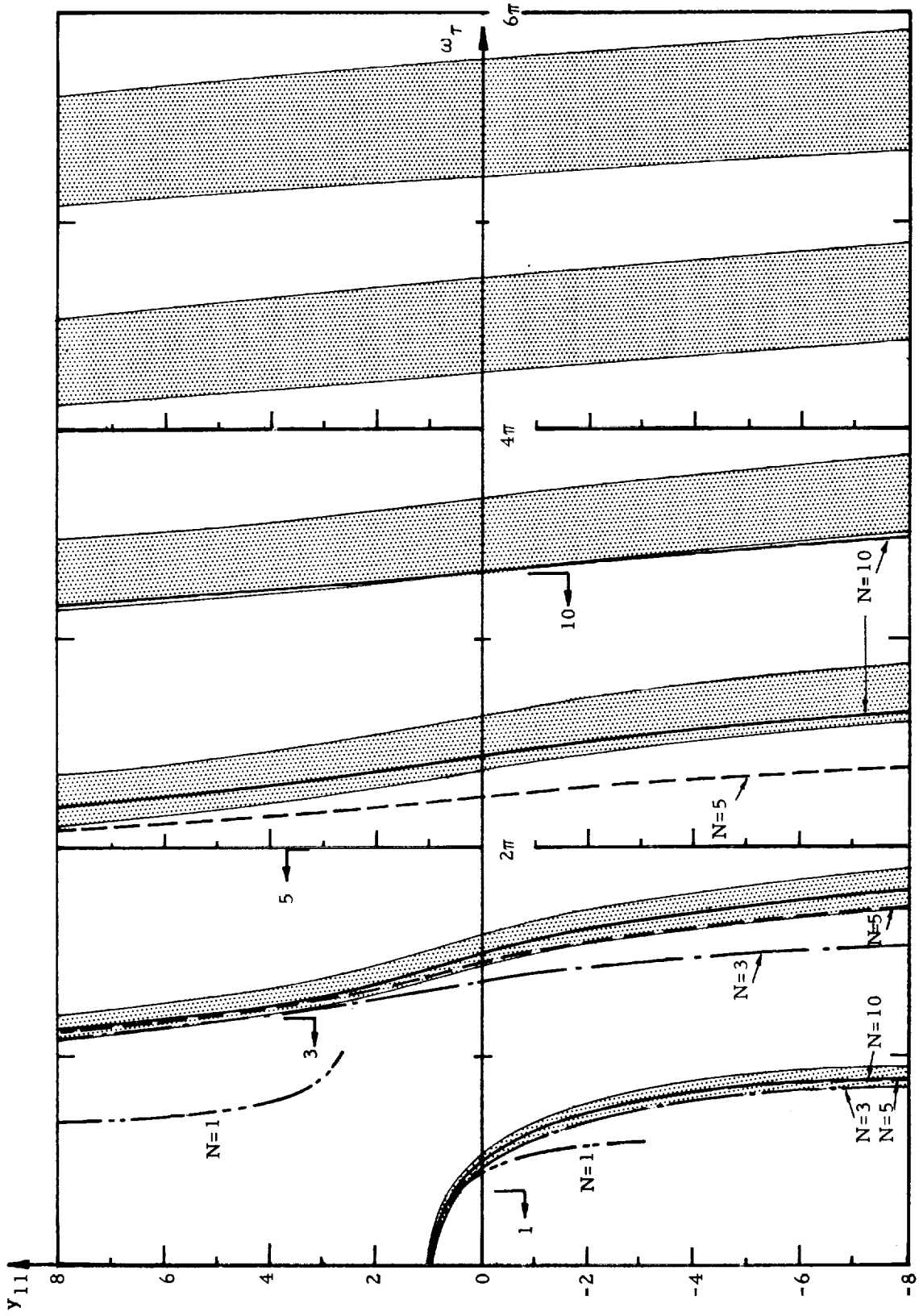

Figure 10. Function y_{11} vs. $\omega\tau$ for lumped-transmission model.

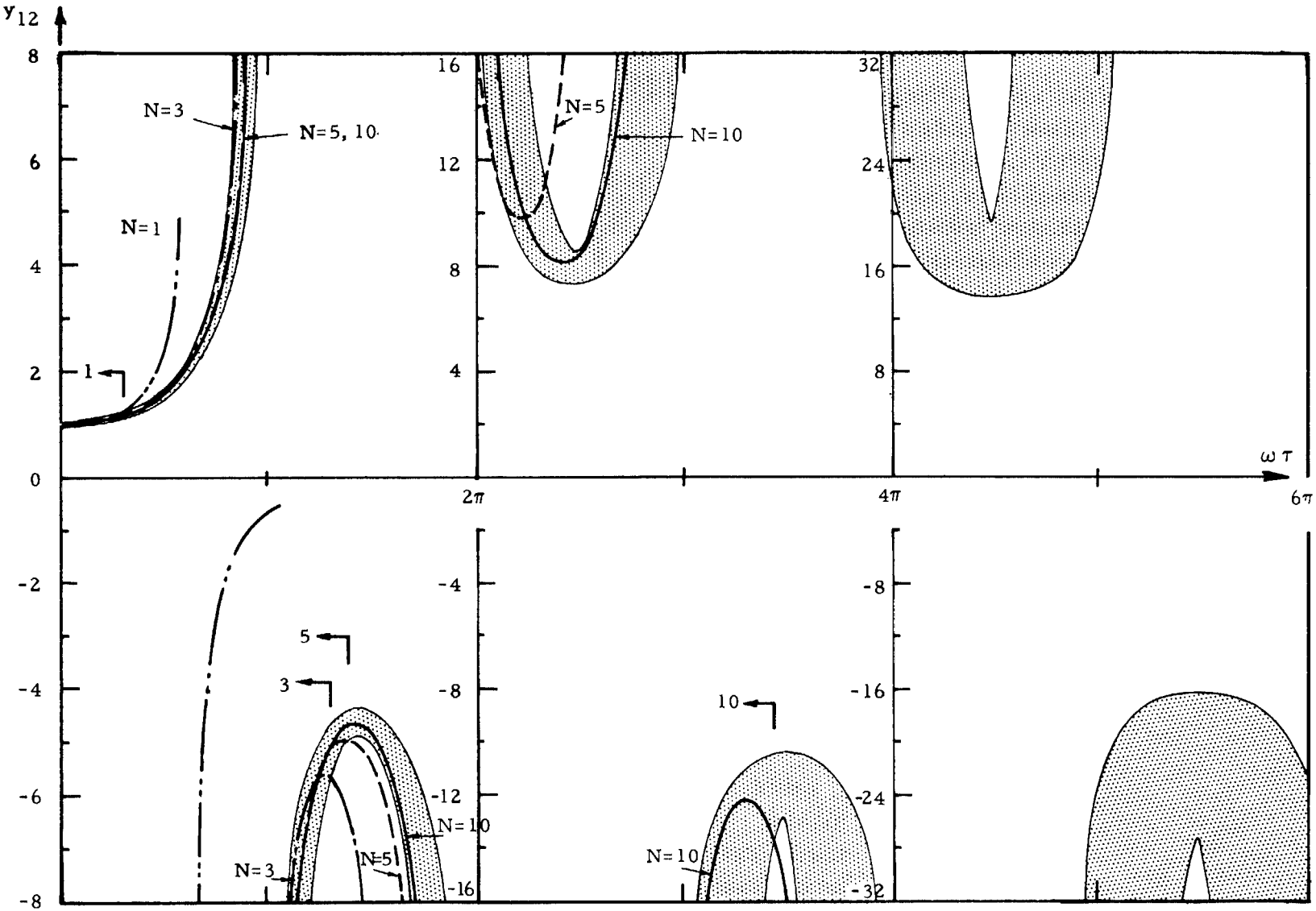

Figure 11. Function y_{12} vs. $\omega\tau$ for lumped-transmission model.

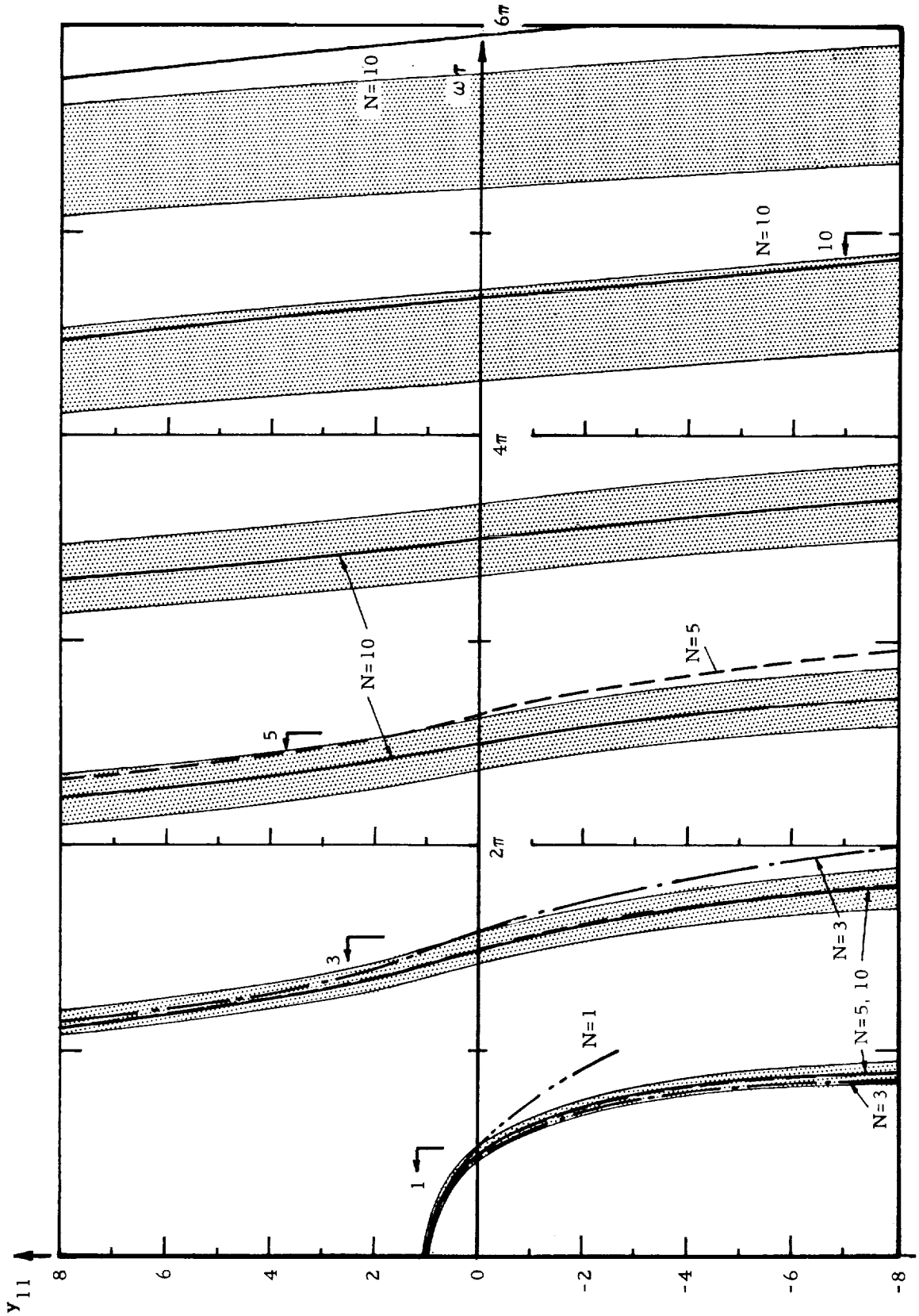

Figure 12. Function y_{11} vs. $\omega\tau$ for series-exact-at-$\pi/3$ admittance model.

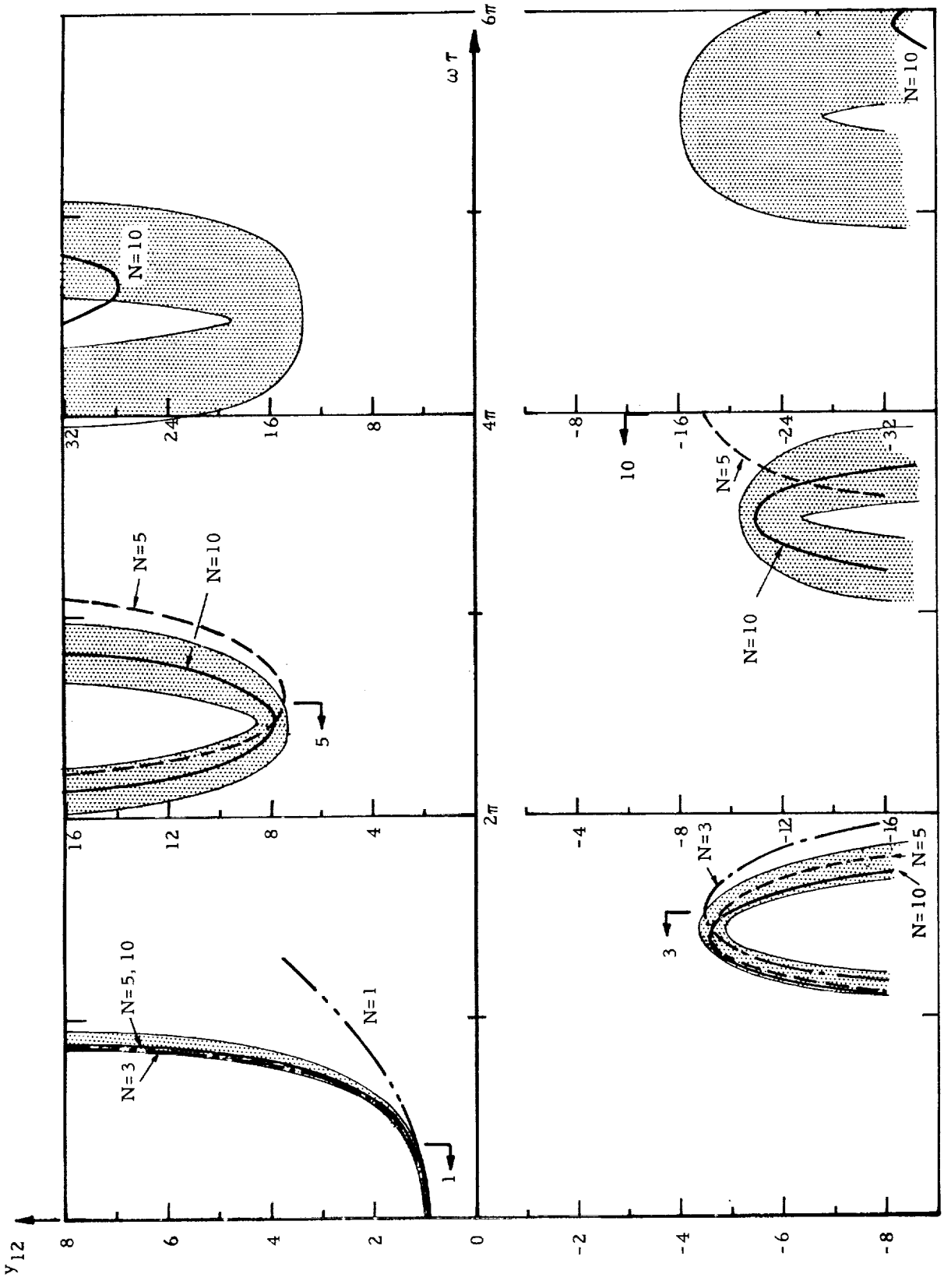

Figure 13. Function y_{12} vs. $\omega\tau$ for series-exact-at-$\pi/3$ admittance model.

Table I. Range of accuracy of finite-element models.

Tabulations are maximum values of $\omega\tau/2\pi N$ (fractional part of a full-wave frequency per element) for which functions remain within the error bounds.

TRANSMISSION MODELS:	y_{11} N= 1	3	5	10	y_{12} 1	y_{12}; y_{21}; (y_{12})[1] 3	y_{12}; (y_{12}) 5	y_{12}; y_{21} 10
Lumped	0.20	0.20	0.16	0.17	0.13	0.22; 0.22; 0.22	0.14; 0.14	0.17; 0.17
Maclaurin Series	0.18	0.17	0.13	0.13	0.13	0.13; 0.17; 0.13	0.13; 0.14	0.12; 0.11
Product Series	0.50	0.33	0.40	0.30	0.13	0.06; 0.07; 0.08	0.12; –	0.13; 0.06
Series exact at $\pi/4$	0.20				0.13			
Series exact at $\pi/3$	0.23	0.23	0.23		0.10	0.17; 0.17; 0.17	0.13; –	
Series exact at $\pi/2$	0.30	0.33	0.38		0.10	0.06; 0.07; 0.09	0.12; –	
Series exact at $\pi/4$	0.13				0.08			
$1/N^4$ frequencies error	0.10				0.08			
$1/N^6$ frequency error	0.22	0.23	0.17		0.08	0.21; 0.23; 0.23	0.13; –	

ADMITTANCE MODELS:[2]	y_{11} N= 1	3	5	10	y_{12} 1	y_{12}; (y_{12}) 3	y_{12}; (y_{12}) 5	y_{12} 10
Maclaurin Series	0.20	0.17	0.18	0.18	0.20	0.17; –	0.18; –	0.18
Product Series	0.13	0.33	0.36		0.30	0.21; –	0.14; 0.23	
Series exact at $\pi/4$	0.20				0.22			
Series exact at $\pi/3$	0.27	0.25	0.26	0.25	0.24	0.25; 0.26	0.26; 0.26	0.23
Series exact at $\pi/2$	0.31	0.04	0.03		0.15	0.05; 0.08	0.04; 0.05	
Series exact at $3\pi/4$	0.08				0.05			
$1/N^4$ frequency error	0.13	0.19	0.30		0.33	0.20; –	0.13; 0.22	

Notes: (1) (y_{12}) indicates for y_{12} a 10% amplitude band and 5% frequency band; all others are 5% on both bands.

(2) $y_{12} = y_{21}$ for admittance models

match y_{11} better, but are relatively poor for y_{12} and y_{21}. Other models exhibit poor convergence. For example, the product admittance model for N = 1 does well with y_{12}, but poorly with y_{11}; the situation is reversed for N = 3. Increasing the amplitude band to ±10-percent did not significantly alter the range of accuracy except for two of the admittance models for N = 5.

3.7 Evaluation of Normal-Mode and Collocation Models

As in the case of the finite-element models, evaluation of the normal-mode and collocation models is accomplished by determining the accuracy with which the models match the four exact admittance functions of a uniform one-dimensional feedline. The required admittance functions y_{11}, y_{12}, y_{21}, y_{22} are defined by equations (3-10) (note the correspondence between P_t, P_s and P_a, P_b in figures 5 and 7). For both the normal-mode and collocation models, reciprocity holds (i.e., $y_{12} = y_{21}$) so that only y_{11}, y_{22} and y_{12} need be examined. These are determined from frequency-response functions obtained using the equations of motion developed in section 3.4.

For the normal-mode models, an Nth-order model is defined to include the set of the first N non-zero-frequency (i.e., flexible) modes. A zero-frequency (i.e., rigid-body) mode representing translation of the entire fluid line is added to produce a system with N + 1 degrees of freedom. (Number-of-degrees-of-freedom is defined to be the minimum number of independent variables necessary to completely define an arbitrary motion of the system.) This corresponds to truncating the series in equations (3-21) and (3-22) at n = N. For the open-open modes, n = 0 in equation (3-21) corresponds to the rigid-body mode. The models were then evaluated for values of N ranging from 1 to 10.

For the collocation approach, the number N + 1 defines the number of collocation points along the line, including end points, and is therefore also a system with N + 1 degrees of freedom. The points were chosen at equal intervals. In the collocation case considered, N also represented the highest order of the polynomial interpolation functions. Only values of N = 1, 2, and 5 were investigated.

3.7.1 Model using open-open modes. - In addition to being reciprocal, each open-open mode is also symmetric, so that $y_{11} = y_{22}$. It is therefore only necessary to determine the accuracy of the two functions y_{22} and y_{21} when using open-open modes. Figures 14 and 15 are plots of y_{22} and y_{21} for the case N = 5. Since open-open modes are employed, the infinities of the function are constrained to occur at the correct frequency. Deviations of the open-closed modal frequencies, which are given by the zeros at y_{22} and which fall in between the open-open frequencies, would be expected to produce a reasonably accurate measure of the accuracy of the system in terms of frequency error (see fig. 14). Therefore, open-closed modal frequencies were computed using N + 1 open-open modes (including the rigid-body mode) and the resulting errors determined for N = 1 to 10. The open-closed modes are found from the eigenproblem set up from equations (3-21b) by setting $P_a = P_b = 0$ and using equation (3-21a), to constrain the end of the line to have zero motion; i.e., let

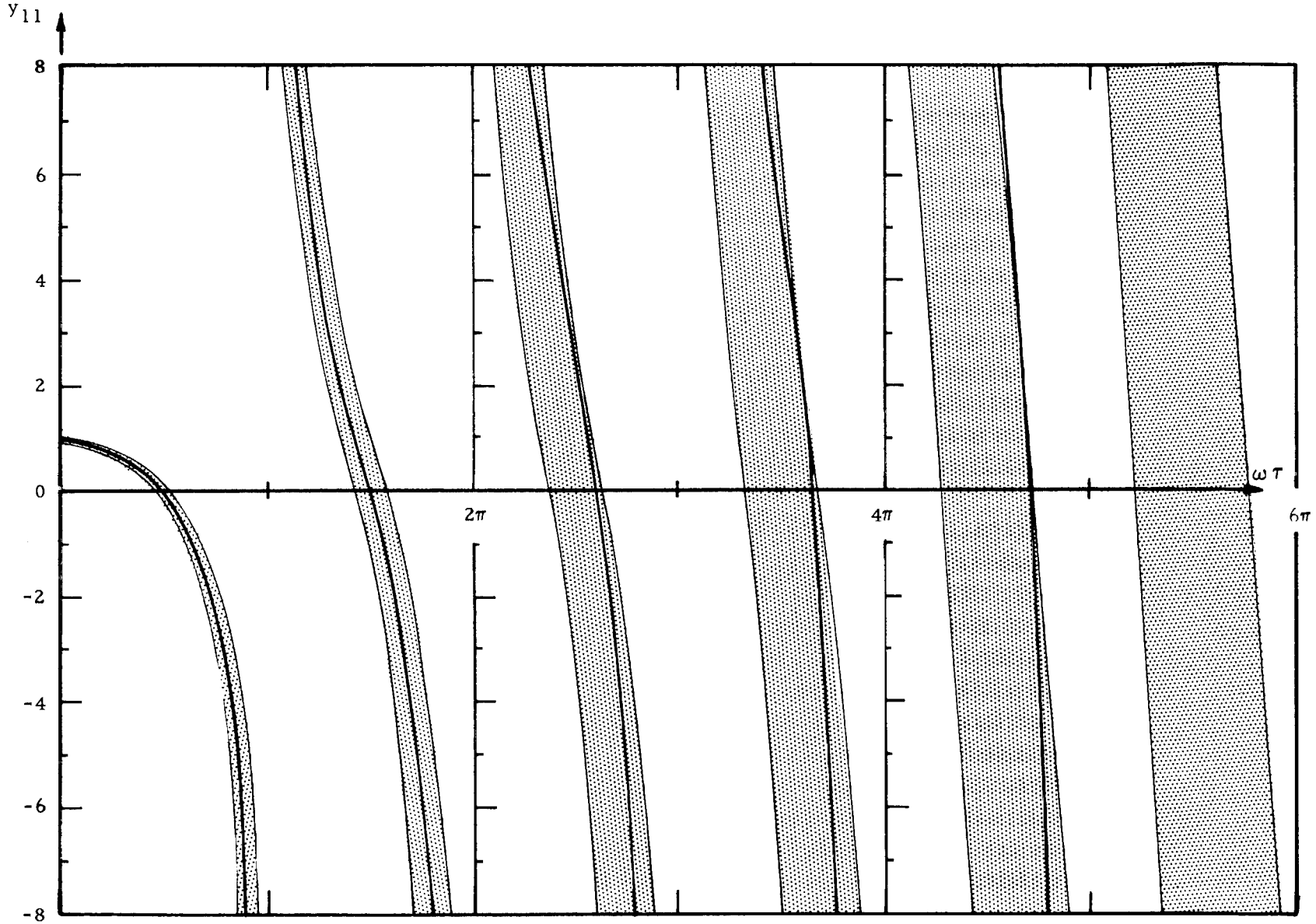

Figure 14. Function y_{22} vs. $\omega\tau$ for the open-open modal model, N = 5

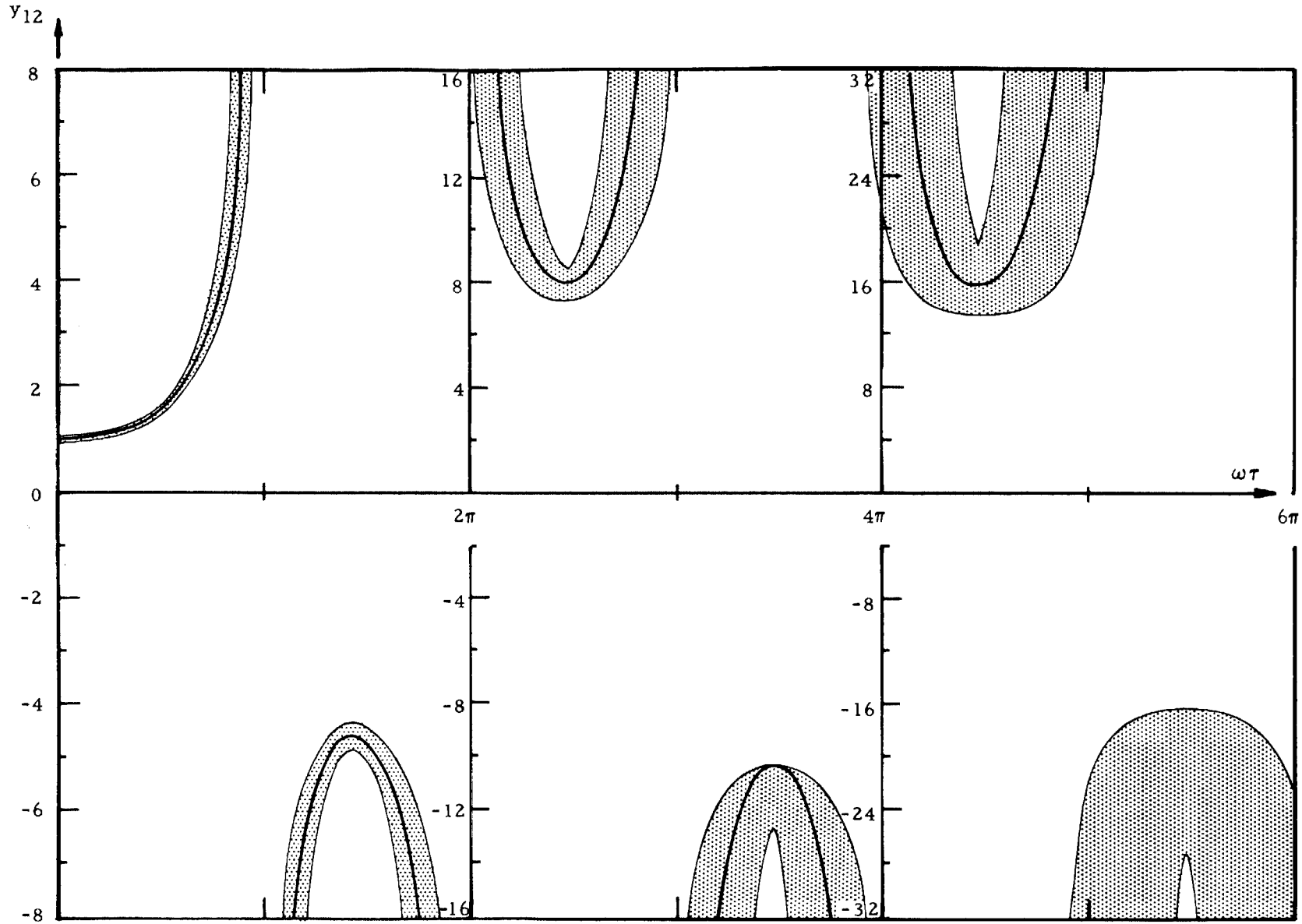

Figure 15. Function y_{21} vs. $\omega\tau$ for the open-open modal model, N = 5

$$u(0,t) = \sum_{n=0}^{N} q_n(t) = 0$$

The results are shown graphically in figure 16, where the percent error in each modal frequency is plotted vs N. For any N the error progressively increases with increasing mode number. Note that the error in modal frequency tends to fall within a relatively narrow band; that is, the frequency error is basically dependent only on the number of modes used and is relatively independent of the frequency range of interest, at least up to the last open-open mode used. Two envelopes are shown in figure 16, the lower envelope shows the number of open-open modes, N, required to limit the error in the first open-closed mode (i.e., $\omega_n\tau = \pi/2$) to a specified accuracy. The upper envelope shows the number of modes necessary to maintain a given degree of accuracy up to the Nth mode, the highest mode calculated. The curves are applicable only at odd multiples of $\pi/2$. Furthermore, if N is selected to yield suitable accuracy up to the nth mode at $\omega\tau = (2n-1)\pi/2$ (n not necessarily equal to N), then the range of accuracy can be extended upward an additional $\pi/2$ to $\omega\tau = n\pi$, the next highest open-open mode.

Turn now to the function y_{21}, and note from figure 15 that the maximum error is one of amplitude and occurs at or near the open-closed modal frequencies. The function y_{21} was therefore evaluated for a series of values of N at each of the exact open-closed modal frequencies, and the amplitude error determined. The results are shown in figure 17. Given a specified degree of allowable amplitude error, this plot can be used to determine the required number of open-open modes need. In this case, also, the curves are to be read at odd multiples of $\pi/2$ and the frequency range of applicability $\omega\tau$ extended upward by $\pi/2$.

In summary, for open-open modes: (1) the error in y_{22} is approximately the error in the open-closed modal frequencies, (2) the error in y_{21} is approximately the amplitude error at the exact open-closed modal frequencies. Figures 16 and 17 provide the means for determining the required number of modes to remain within specified amplitude and frequency error bands. The curves are valid only at odd multiples of $\pi/2$; the range of applicability, expressed by $\omega\tau$, may be extended upwards by $\pi/2$ once N has been determined.

3.7.2 Model using open-closed modes. - Unlike the open-open modes, a truncated set of open-closed modes leads to the unsymmetric behavior $y_{11} \neq y_{22}$. This point will be seen to be critical to a total assessment of the accuracy of the open-closed mode representation. (Note that y_{22} represents flow at the closed end due to a pressure at the closed end.) For the case N = 5, the functions y_{22} and y_{21} are shown in figures 18 and 19. One characteristic of these results is that both functions are exact at the open-closed modal frequencies. Both functions remain well within error bands up to the last open-closed mode frequency, rapidly diverging beyond. A good description of the accuracy of y_{22} and y_{21} is given by the frequency error of the infinities of the function (occurring at open-open modes of the system). Equations (3-22b) were used for $n = 1, 2, \ldots N$, and the open-open modes were computed by setting the pressures

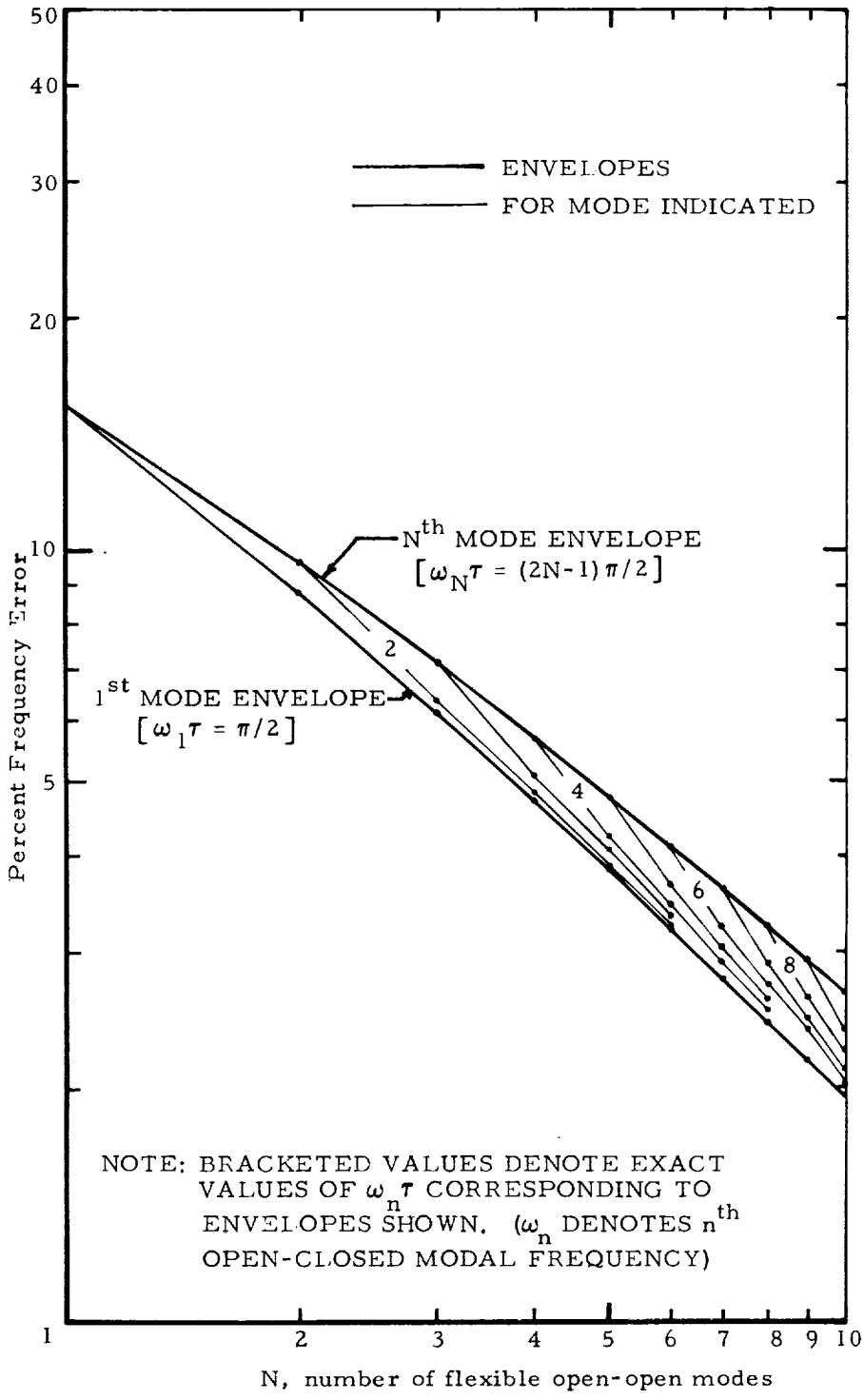

Figure 16. Frequency error in y_{22} (y_{11}) for the open-open modal model.

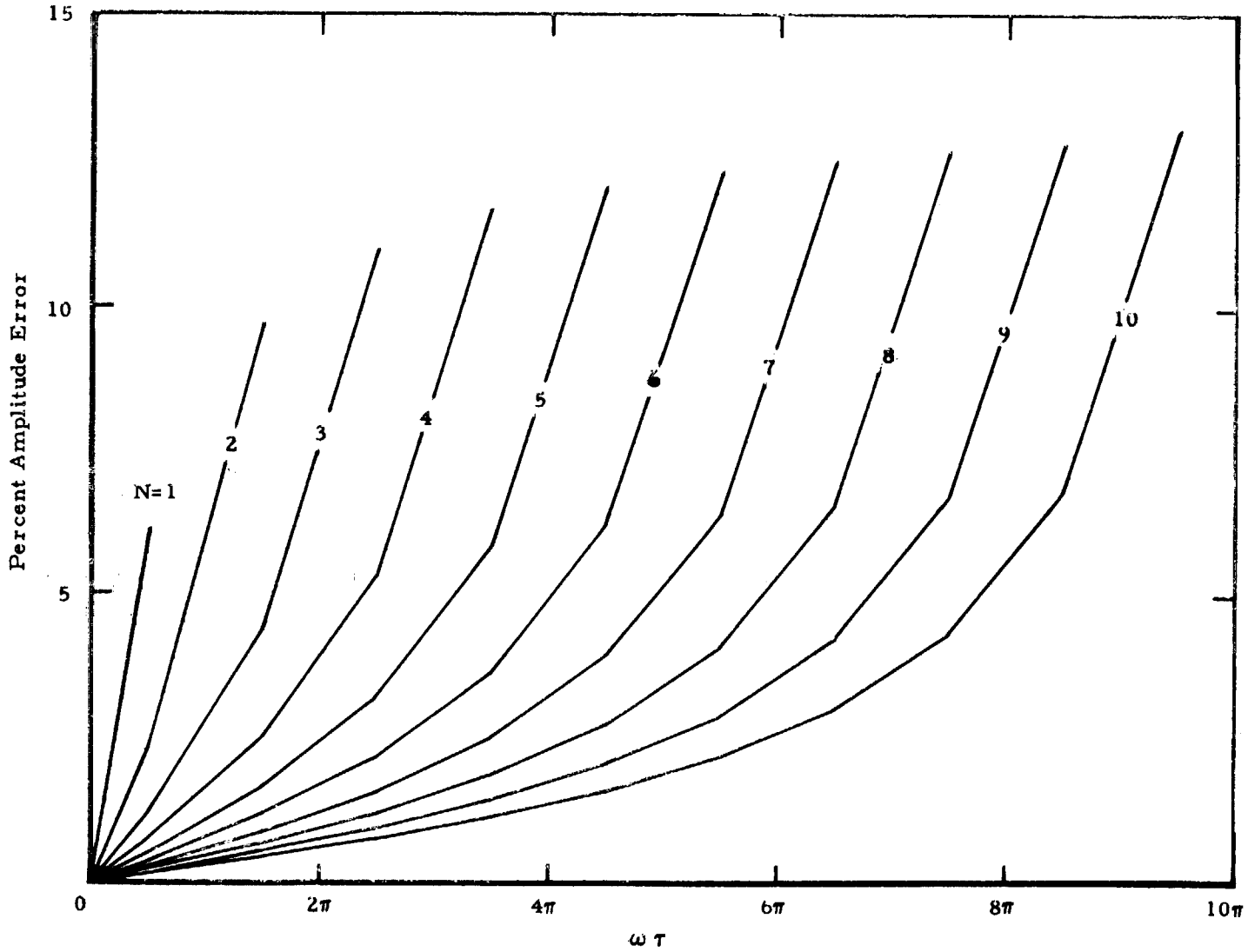

Figure 17. Amplitude error in y_{21} (y_{12}) vs. $\omega\tau$ for the open-open modal model.

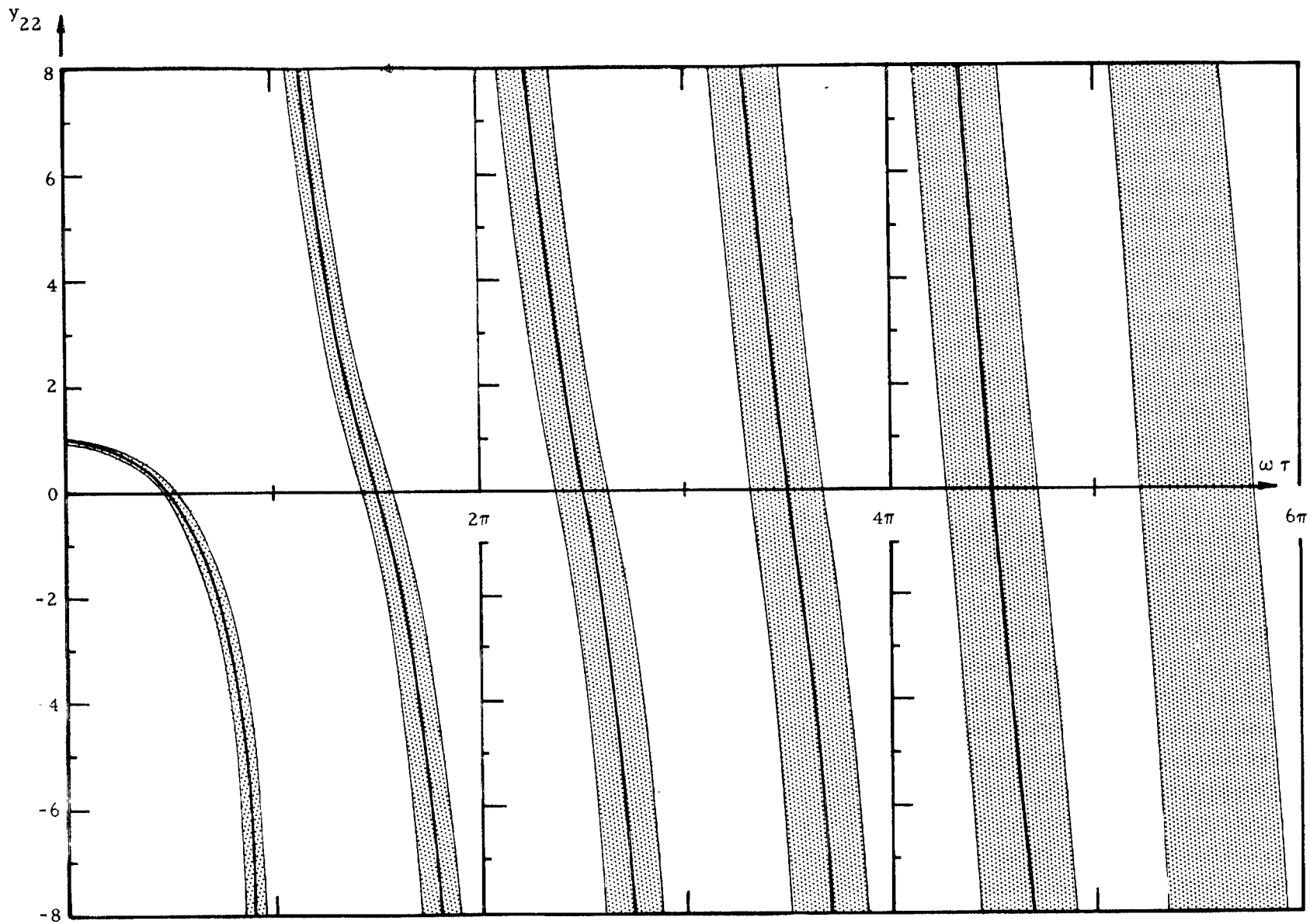

Figure 18. Function y_{22} vs. $\omega\tau$ for the open-closed modal model, N = 5.

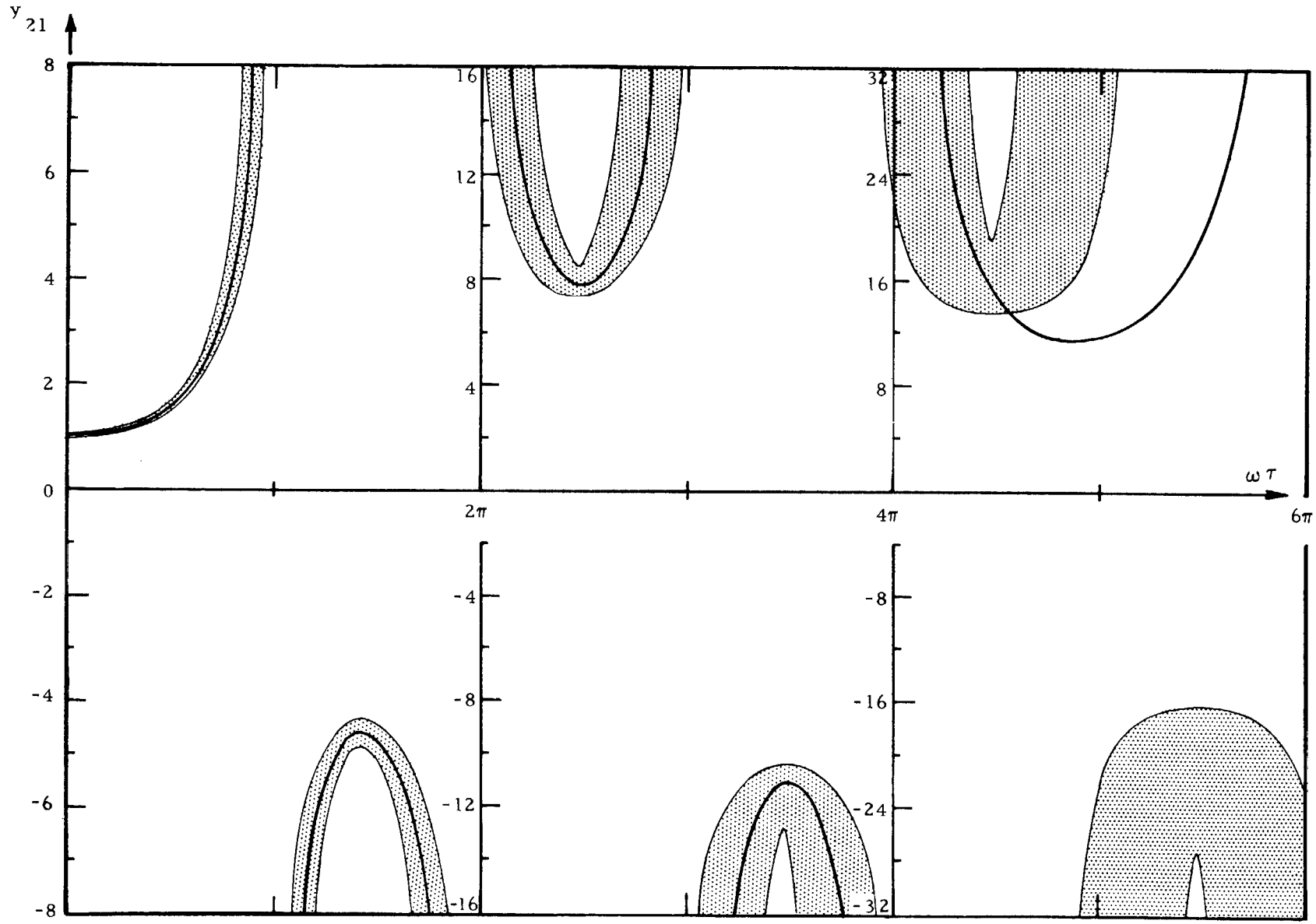

Figure 19. Function y_{21} vs. $\omega\tau$ for the open-closed modal model, N = 5.

P_a, P_b equal to zero and solving the resulting eigenvalue problem. This was done for all N from 1 to 10. It was determined that the Nth mode was quite inaccurate, the error varying from about 15-percent at N = 1 to about 20-percent at N = 10. This is not unexpected since this mode is above the last open-closed mode used. For the remaining modes it was found that the values were quite accurate within 1.5-percent of the exact values. On the basis of these results it was concluded that, in general, the functions y_{22}, y_{21} are satisfactorily accurate up to the last open-closed mode used.

This highly favorable view of the open-closed modal model, unfortunately, fails to hold when the function y_{11} is considered. (Recall that y_{11} represents flow at the top of the line due to pressure at the top of the line.) Refer to figures 20 and 21, where y_{11} is plotted for N = 5 and N = 1, 2, 4, 8, respectively, and note that the accuracy of y_{11} is approximately given by the error of the frequency of zero crossings. (A similar result was obtained above for the open-open modes.) Note further that the modal functions being employed here are for an open condition at point a, and a closed condition at b (see fig. 7); the zero crossings of the function y_{11} represent modes open at b, closed at a. A plot of frequency error similar to that of figure 16 can be determined, and is shown in figure 22. In this case the error does not steadily increase with higher mode number; results are tabulated in Table II. Excluding the results shown for the Nth mode, a relatively narrow error band again results, slightly higher than that of y_{22} in the open-open mode case. This again indicates the error is roughly independent of the frequency range, with the range of accuracy extending up to the frequency of the next-to-highest open-closed mode used [i.e., $\omega\tau = (2N-3)\pi/2$].

3.7.3 Comparison of modal models. - Results are summarized in figure 23, where the two modal approaches are compared on the basis of the number of equations (number of flexible modes N, plus one) required to achieve the allowable 5-percent amplitude and frequency error. Results from figures 16, 17, 20 and 21 were employed. The results indicate that a distinct advantage exists for using open-closed modes in the "low" frequency range ($\omega\tau < 2.5\pi$) only if the accuracy limitation is ignored for the function y_{11}. (The function y_{11} is the flow at the top of the line due to a pressure at the top.) For larger values of $\omega\tau$, even this does not result in a large saving in required equations. Neglect of the accuracy of y_{11}, however, is not in general acceptable in light of the importance of tank dynamic outflow as discussed in sections 1.5 and 2.4. When y_{11} errors are also considered one finds that a lower bound exists on the number of equations (and hence modes) required to attain the 5-percent accuracy; a minimum of five modes or six equations is required for either the open-open or open-closed modal system. It therefore appears that modal representations are relatively inefficient for low frequencies (i.e., values of $\omega\tau < 2.5\pi$).

3.7.4 Collocation model. - The last approach considered in section 3.4 was a collocation one, in which a set of interpolation functions was defined as a polynomial function of distance x along the line; the physical coordinates u_k at a discrete set of points x_k were retained. This provides some additional flexibility not available in the modal approach in that physical variables are retained. This leads to both symmetric and reciprocal results so that $y_{11} = y_{22}$ and $y_{21} = y_{12}$. Only a single case is presented (N = 5) as an indication of the method's potential usefulness. The functions y_{22} and y_{21} are plotted in

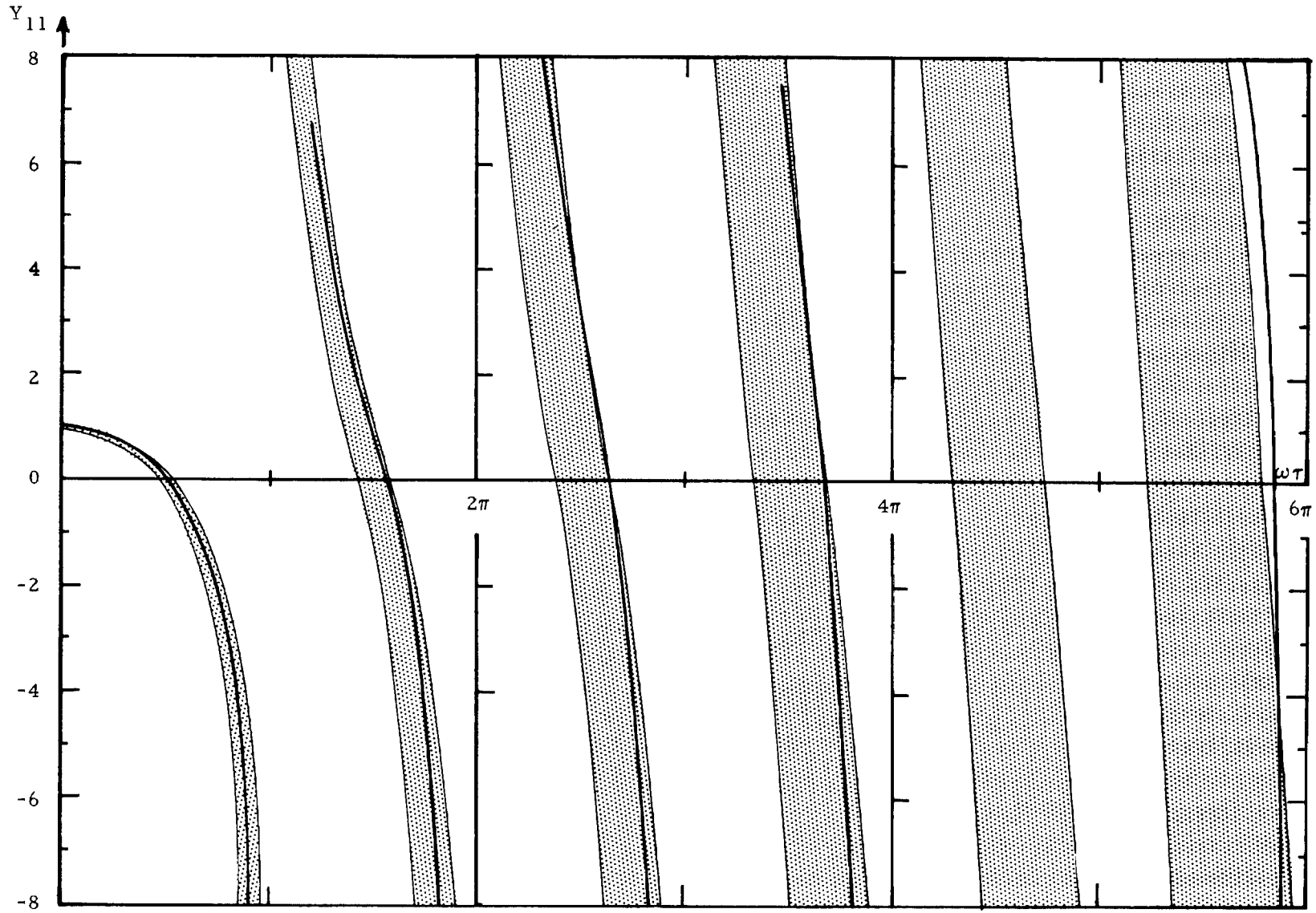

Figure 20. Function y_{11} vs. $\omega\tau$ for the open-closed modal model, N = 5.

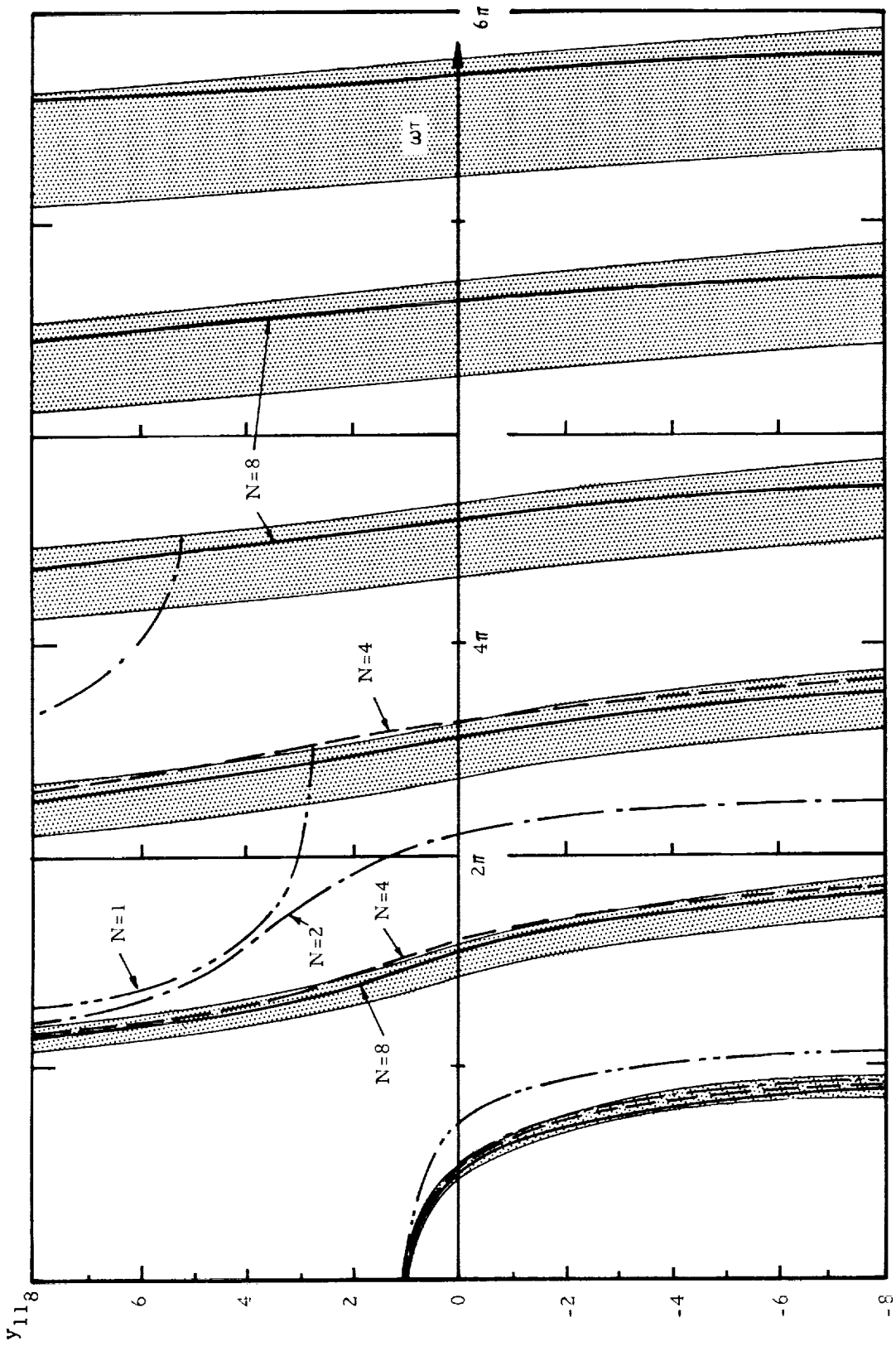

Figure 21. Function y_{11} vs. $\omega\tau$ for the open-closed modal model, N = 1, 2, 4, 8.

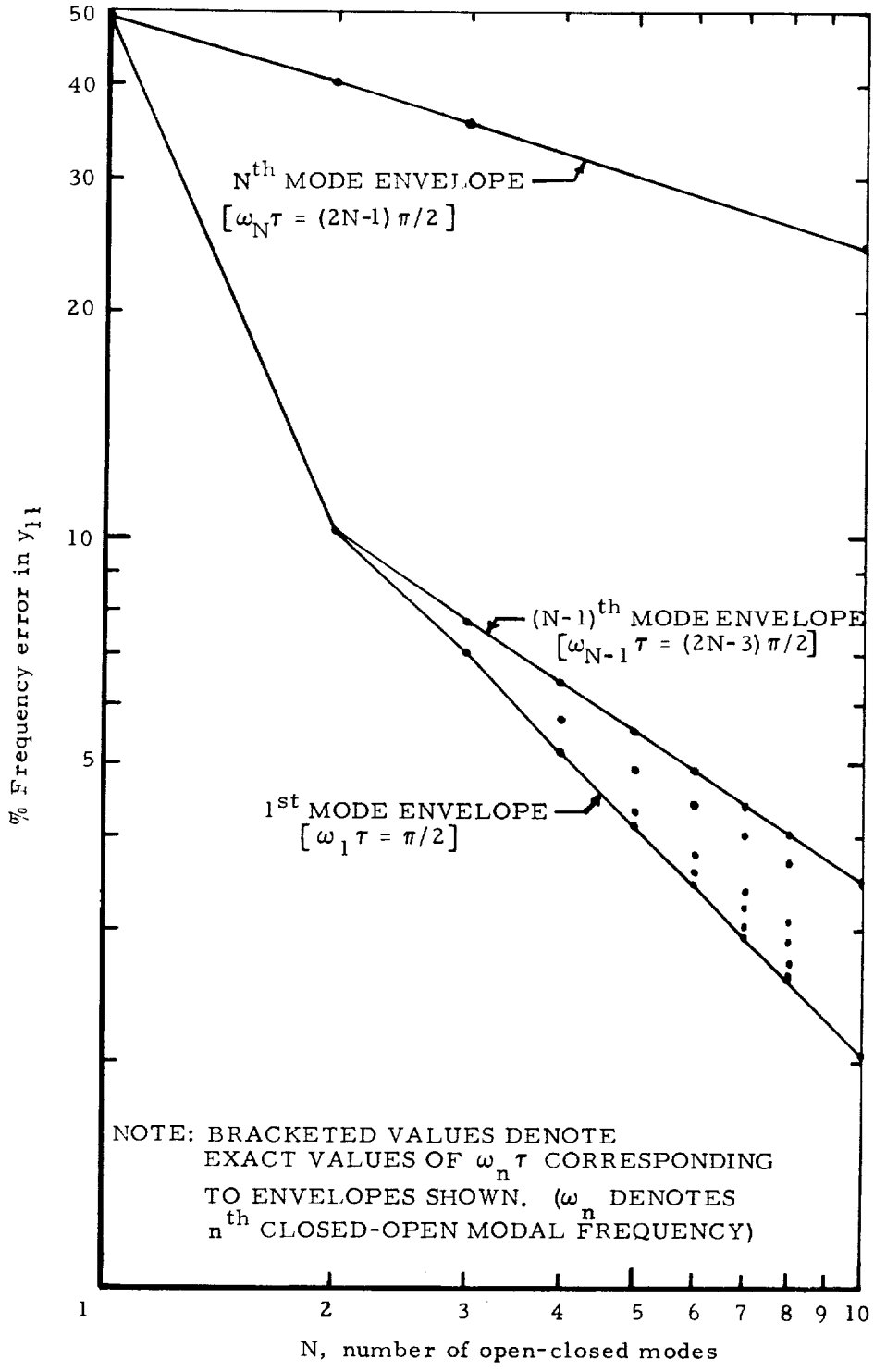

Figure 22. Frequency error in y_{11} for the open-closed modal model.

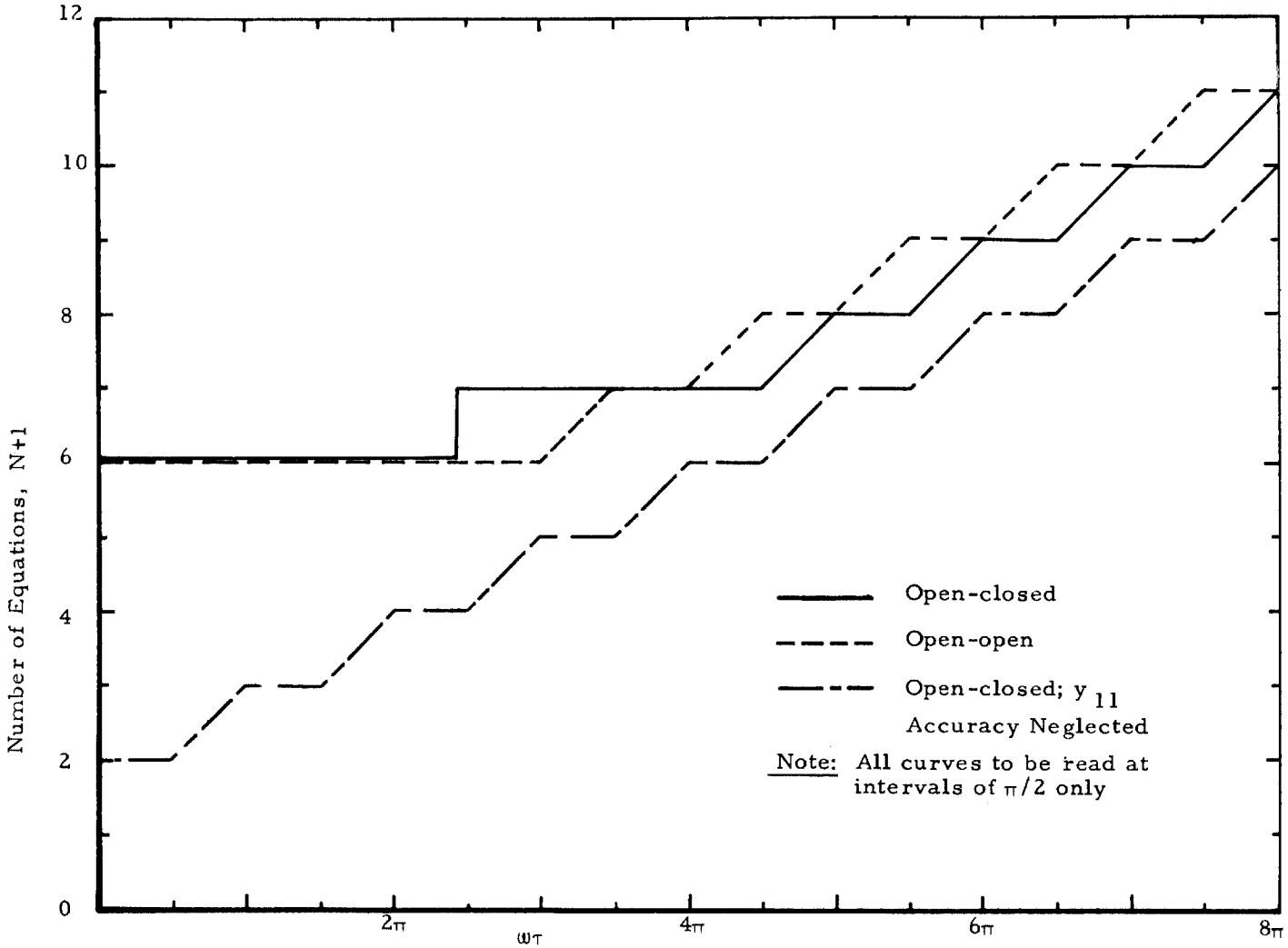

Figure 23. Number of equations vs. $\omega\tau$ for the modal models.

Table II. Percent error in closed-open modal frequencies obtained from open-closed modes.

N	MODE 1 ($\omega\tau=\pi/2$)	MODE 2 ($\omega\tau=3\pi/2$)	MODE 3 ($\omega\tau=5\pi/2$)	MODE 4 ($\omega\tau=7\pi/2$)	MODE 5 ($\omega\tau=9\pi/2$)	MODE 6 ($\omega\tau=11\pi/2$)	MODE 7 ($\omega\tau=13\pi/2$)
1							
2	10.1						
3	7.72	7.00					
4	5.18	6.40	5.73				
5	4.32	4.17	5.53	4.97			
6	3.45	3.78	3.59	4.90	4.40		
7	3.01	2.95	3.39	3.21	4.42	4.05	
8	2.58	2.71	2.64	3.09	2.92	4.04	3.73

Notes: ( ) denotes exact frequencies.

Only N-1 modes shown, error for Nth mode large.

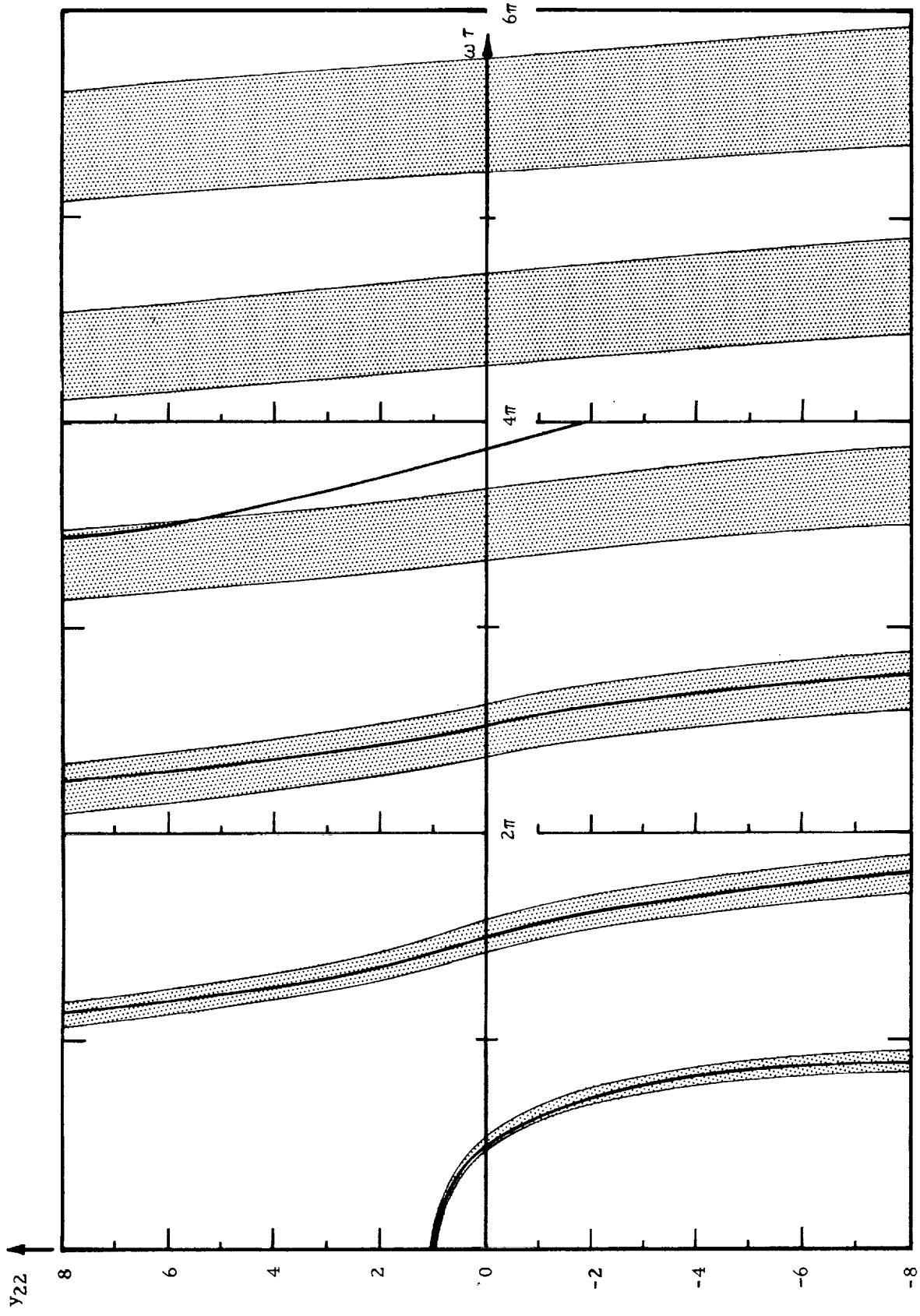

Figure 24. Function y_{22} vs. $\omega\tau$ for the collocation model, N = 5.

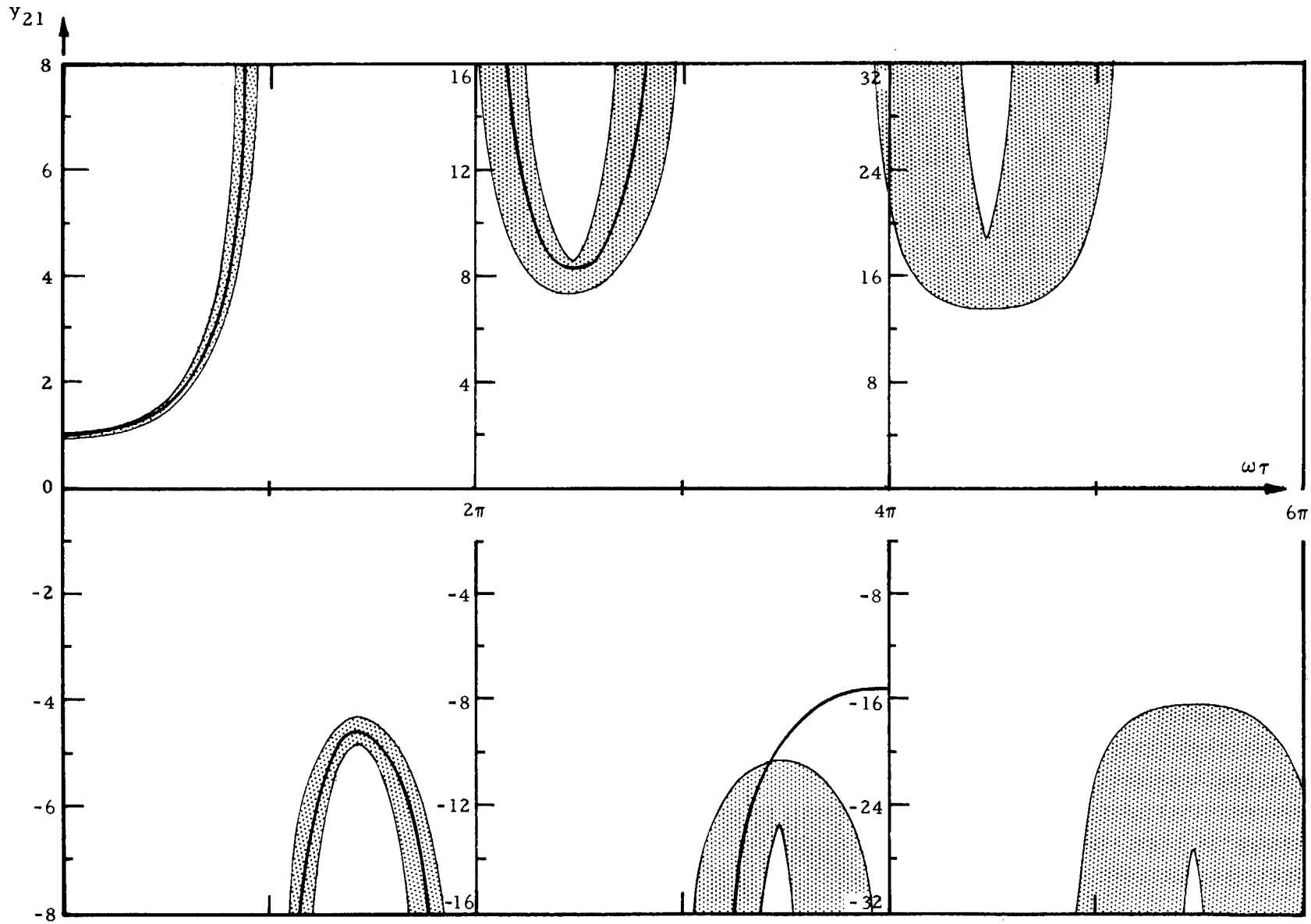

Figure 25. Function y_{21} vs. $\omega\tau$ for the collocation model, N = 5.

figures 24 and 25, respectively. Relative to the 5-percent error criterion, the results are found to be within bounds up to a value $\omega\tau = 3.4\pi$.

Figure 23 can be used to determine the range of accuracy $\omega\tau$ for the modal methods for N = 5. Comparison with the value $\omega\tau = 3.4\pi$ indicates the collocation method is approximately equivalent to the modal methods.

3.8 Minimizing the Number of Equations for Finite Elements

In this section we turn our attention to procedures for minimizing the number of equations required for a finite-element modeling of a feedline. Effectively this would reduce correspondingly the order of the matrix eigenvalue problem required to perform closed-loop stability analyses. As will be observed, the matrix size reduction is achieved at the expense of reduced sparsity of the matrix. Computer programs for the general eigenvalue problem, however, tend not to attempt to take advantage of sparsity. The result is that both the computing time and the storage requirements are lessened by the reduction in matrix order.

Consider two segments of a line as shown in figure 26. First let us suppose that the two segments are described by admittance matrices $[y_a]$, and $[y_b]$, so that we have

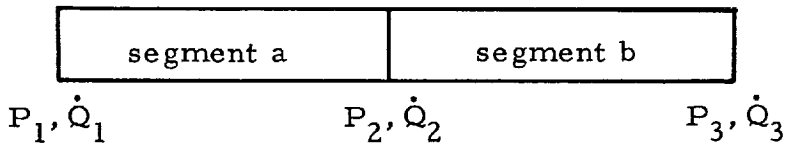

Figure 26. Two-segment line.

$$\begin{Bmatrix} \dot{Q}_1 \\ \dot{Q}_2 \end{Bmatrix} = \begin{bmatrix} y_{a11} & y_{a12} \\ y_{a21} & y_{a22} \end{bmatrix} \begin{Bmatrix} P_1 \\ P_2 \end{Bmatrix}$$

$$\begin{Bmatrix} \dot{Q}_2 \\ \dot{Q}_3 \end{Bmatrix} = \begin{bmatrix} y_{b11} & y_{b12} \\ y_{b21} & y_{b22} \end{bmatrix} \begin{Bmatrix} P_2 \\ P_3 \end{Bmatrix}$$

If one equates the two equations for $\dot{Q}_2$ given by the second and third equations, the following three equations are obtained:

$$\dot{Q}_1 = y_{a11} P_1 + y_{a12} P_2$$

$$y_{a21} P_1 + y_{a22} P_2 = y_{b11} P_2 + y_{b12} P_3 \tag{3-31}$$

$$\dot{Q}_3 = y_{b21} P_2 + y_{b22} P_3$$

Notice that there is no change in the order (that is, the highest power of s) of the equations by this elimination. This procedure could be systematically followed to eliminate all the internal flow variables within an N segment line. The result is a reduction from 2N transmission equations involving the N + 1 pressures and N + 1 flows, to N + 1 equations involving the N + 1 pressures and the two end flows for a total of N + 3 variables.

In parallel fashion, it would be possible for an impedance formulation to achieve the same reduction in the number of equations and variables by eliminating all the internal pressure variables.

The Rayleigh lumped-parameter model is a special one in the transmission category because it can also be put into a second-order impedance form. Namely,

$$-\omega^2 \begin{Bmatrix} P_1 \\ P_2 \end{Bmatrix} = \frac{L}{\tau^2} \begin{bmatrix} 1 - \frac{(\omega\tau)^2}{2} & -1 \\ -1 & 1 - \frac{(\omega\tau)^2}{2} \end{bmatrix} \begin{Bmatrix} \dot{Q}_1 \\ \dot{Q}_2 \end{Bmatrix} \tag{3-32}$$

or for a spring-mass analogous system

$$\begin{Bmatrix} F_1 \\ F_2 \end{Bmatrix} = K \begin{bmatrix} 1 - \frac{(M\omega)^2}{2K} & -1 \\ -1 & 1 - \frac{(M\omega)^2}{2K} \end{bmatrix} \begin{Bmatrix} x_2 \\ x_2 \end{Bmatrix} \tag{3-32a}$$

The elimination of the internal pressure variables produces the usual form of the equations of motion for a lumped-parameter system. For the spring-mass

system in figure 27 made up of two Rayleigh segments, the result of the elimination of the internal force F_2 is the familiar form:

$$
\begin{aligned}
-\frac{M\omega^2}{2}x_1 + K(x_1 - x_2) &= F_1 \\
-M\omega^2 x_2 + K(2x_2 - x_1 - x_3) &= 0 \\
-\frac{M\omega^2}{2}x_3 + K(x_3 - x_2) &= F_3
\end{aligned}
\tag{3-33}
$$

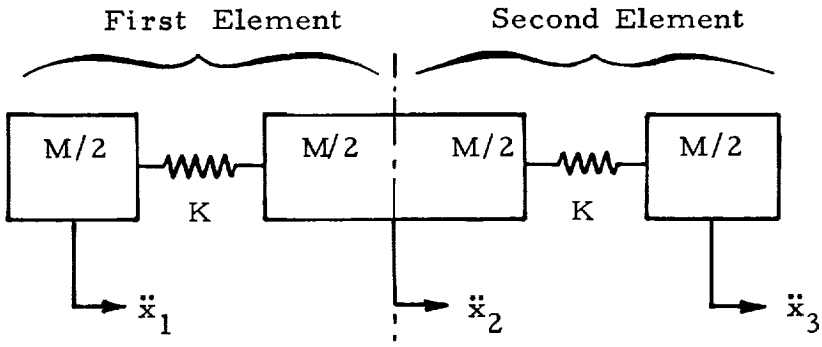

Figure 27. Two-segment Rayleigh mechanical model.

In addition to this type of reduction, the Rayleigh element can be reduced in another way which is common to any transmission form as discussed next.

Suppose segment a in figure 26 is represented by a rearward transmission matrix and segment b by a forward transmission matrix:

$$
\begin{Bmatrix} P_2 \\ \dot{Q}_2 \end{Bmatrix} = [a_a]_r \begin{Bmatrix} P_1 \\ \dot{Q}_1 \end{Bmatrix} \tag{3-34a}
$$

$$
\begin{Bmatrix} P_2 \\ \dot{Q}_2 \end{Bmatrix} = [a_b]_f \begin{Bmatrix} P_3 \\ \dot{Q}_3 \end{Bmatrix} \tag{3-34b}
$$

Eliminating the conditions at point 2, we can then write

$$[a_a]_r \begin{Bmatrix} P_1 \\ \dot{Q}_1 \end{Bmatrix} = [a_b]_f \begin{Bmatrix} P_3 \\ \dot{Q}_3 \end{Bmatrix} \tag{3-35}$$

Thus the four equations (3-34a, b) have been reduced to the pair of equations with no increase to the order of the Laplace variable. Repetition of this procedure for an N-segment line permits the elimination of every other pair of pressure-flow conditions along a line and reduces the number of equations from 2N to N (assuming that N is an even number) and the number of variables from N + 1 to (N + 2)/2 pressures and flows. This is one less equation and one less variable than for the admittance or impedance case, but this is an insignificant difference. In effect, all three of the basic matrix forms (transmission, admittance, and impedance) permit a reduction in the number of equations and number of variables by almost a factor of two for a many-segment line.

It has been noted previously that the mathematical transmission forms do not precisely obey the theorem of reciprocity; that is, the determinant of the matrix is not exactly one (ref. 16). A consequence is that some difference is obtained by use of the rearward versus the forward form of the transmission matrix. Moreover, the lack of reciprocity may be the cause of a lesser accuracy for equivalent mathematical approximations for the transmission relative to the admittance form as seen in Table I. However, if the procedure indicated by equation (3-35) is employed, where segments a and b are identical, reciprocity is precisely satisfied. This is clear since if equation (3-35) is reformulated to

$$\begin{Bmatrix} P_1 \\ \dot{Q}_1 \end{Bmatrix} = [a_a]_r^{-1} [a_b]_f \begin{Bmatrix} P_3 \\ \dot{Q}_3 \end{Bmatrix} \tag{3-36}$$

then the determinant of the matrix product must of necessity be precisely one.

3.9 Comparison of Finite-Element and Modal Approaches

For the Shuttle vehicle, as was pointed out earlier, it appears that both efficiency and accuracy in feedline modeling will be quite important. Accuracy alone is not a sufficient criterion for deciding upon which model should be used. A direct measure of efficiency and accuracy is the number of equations required to remain within a specified error bound. Using the results given in Table I for finite-element models, combined with the equation minimization procedures in section 3.8, one finds that the number of equations required to remain within the ± 5-percent amplitude and frequency limits can be readily obtained as a

function of frequency (or $\omega\tau$). Figure 23 shows the number of equations required by open-open and open-closed modes.

Table III presents numbers of equations required versus $\omega\tau$ for two of the better finite-element models as well as for open-open and open-closed modes. Since the Rayleigh model is often used in practice in an impedance formulation, Table III also presents results for this formulation. Note that the Rayleigh transmission and impedance forms are perfectly equivalent; that is, the number of segments required is identical. It is, however, possible to eliminate an additional equation from the transmission formulation for the particular values of $\omega\tau$ in Table III. In order to compute the number of segments required for the finite-element models, based on Table I, a minimum value of $\omega\tau/2\pi N$ was chosen as 0.125 for the Rayleigh lumped transmission model and 0.25 for the admittance series forced to be exact at $\omega\tau = \pi/3$.

Figure 28 presents the number of equations for the best finite-element model investigated, the $\pi/3$ admittance form, as well as the commonly used Rayleigh impedance and the open-open and open-closed modes. From this figure, it can be seen that the series-exact-at $\pi/3$ admittance formulation is significantly superior to the Rayleigh formulation.

3.10 Conclusions

1. The 5-percent frequency/amplitude error criterion yields intuitively reasonable results. The frequency error is usually the controlling error; an increase in the amplitude error to 10 percent often makes no change in the frequency range of accuracy for a model.

2. The common practice of evaluating candidate models solely on the basis of errors in modal frequencies is inadequate to satisfy the requirements for pogo modeling. Examination of Table I reveals that those finite-element models developed to minimize frequency errors were not as successful in matching the desired functions as were other models. Also, for the open-open modal model, the within-bounds frequency range is governed by amplitude error.

3. It is not possible to establish the relative accuracies of various finite-element models based on one particular number of segments. Table I shows that some models have erratic behavior from the standpoint of rate of convergence; the product-series admittance model is a notable example.

4. Among the transmission models studied, the Rayleigh lumped-parameter model has a superior behavior for regularity in matching the admittance functions over the largest frequency range. The product-series is outstanding for y_{11}, but poor for y_{12} or y_{21} (see Table I).

5. Admittance representations (equivalently, impedance ones) tend to be superior to transmission representations in matching y_{12} and y_{21}.

Table III. Number of equations required for selected models.

$\omega\tau$	Rayleigh[1] Transmission		Rayleigh Impedance		$\pi/3$ Series[2] Admittance		Open-Open Modes Eq.	Open-Closed Modes (No y_{22}) Eq.	Open-Closed Modes Eq.	Collocation Eq.
	Seg.	Eq.	Seg.	Eq.	Seg.	Eq.				
$\pi/2$	(2)	2	(2)	3	(1)	2	6	2	6	3
π	(4)	4	(4)	5	(2)	3	6	3	6	
$3\pi/2$	(6)	6	(6)	7	(3)	4	6	3	6	
2π	(8)	8	(8)	9	(4)	5	6	4	6	
$5\pi/2$	(10)	10	(10)	11	(5)	6	6	4	7	
3π					(6)	7	6	5	7	6
$7\pi/2$					(7)	8	7	5	7	
4π					(8)	9	7	6	7	
$9\pi/2$					(9)	10	8	6	7	
5π					(10)	11	8	7	8	
$11\pi/2$							9	7	8	
6π							9	8	9	
$13\pi/2$							10	8	9	
7π							10	9	10	
$15\pi/2$							11	9	10	
8π							11	10	11	

[1] Based on a minimum $\omega_o\tau/2\pi N = 0.125$ from Table I.

[2] Based on a minimum $\omega_o\tau/2\pi N = 0.25$ from Table I.

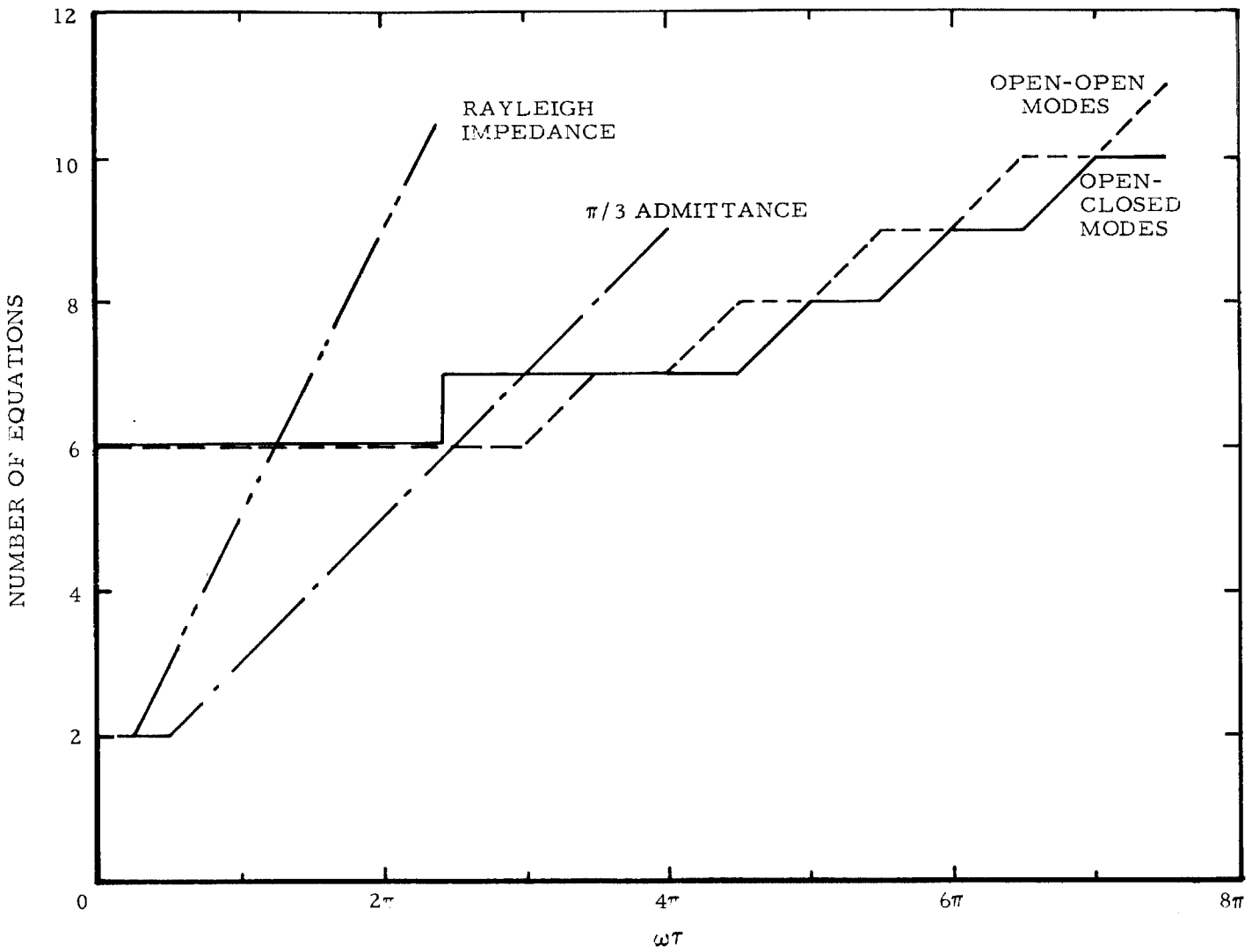

Figure 28. Number of equations vs. $\omega\tau$ for selected models.

The exact-at-$\pi/3$ is the best of the admittance representations studied (see Table I).

6. Straightforward methods can be applied to minimize the number of equations for admittance, impedance, and transmission formulations. The consequence for admittance models is the elimination of interior flow variables along a segmented line; for impedance models, interior pressures are eliminated; and for transmission models, pressure and flow at alternate interior positions are eliminated. For a many-segment line, the result for any of the finite-element models is almost a halving of the number of equations.

7. Of all the models investigated using the 5-percent error criterion, the exact-at-$\pi/3$ admittance model provides the most efficient means (i.e., minimum number of equations) for modeling lines when $\omega\tau < 2.5\pi$ (corresponding to the third open-closed mode). The Rayleigh lumped-parameter model is superior to a modal model for $\omega\tau < 1.2\pi$ (somewhat above the first open-open mode).

8. For open-open modes (N flexible plus one rigid body):

   a. The error in y_{22} (= y_{11}) is primarily a frequency error which can be measured by determining open-closed modal frequencies. Figure 16 shows that, at any N, the error falls within a relatively narrow band up to and including the Nth open-open modal frequency.

   b. The error in y_{12} (= y_{21}) is primarily an amplitude error which can be measured by determining amplitudes at the open-closed modal frequencies. This error, shown in figure 17, is a strong function of both N and frequency range $\omega\tau$.

   c. If the 5-percent accuracy criterion is used, figure 23 shows that the addition of a mode extends the frequency range of validity in $\omega\tau$ by π.

9. For open-closed modes (N flexible plus one rigid body):

   a. The functions y_{22} and y_{21} (= y_{12}) are within acceptable accuracy bands (< 2 percent error) up to the last open-closed modal frequency.

   b. The error associated with the function y_{11} dictates the accuracy of the open-closed modal representation; a lack of symmetry is the cause. The error associated with this function is a frequency error which can be measured by determining the closed-open modal frequencies from the open-closed modes. As shown in figure 22, the error at any N again falls within a relatively narrow band up to and including the (N-1)st closed-open modal frequency.

10. As illustrated in figure 23, no significant advantage exists for the use of open-closed modes over open-open modes when account is taken of the errors in y_{11} resulting from the lack of symmetry of the open-closed modes. The function y_{11} represents the flow at the open end due to a pressure at the open end. The importance of tank outflow in determining vehicle stability (discussed in section 2) requires accurate determination of the flow when the open end for the modes is assumed at the tank-bottom/line interfere.

11. The collocation method using polynomial interpolation functions produced results comparable to those of the normal-mode methods for the particular case investigated (using six collocation points).

3.11 Recommendations

1. For general use in pogo analysis, an approximate representation of a uniform section of line should be evaluated in terms of the accuracy with which all four functions in its admittance (impedance) matrix approximate the exact transmissionline functions.

2. A criterion involving both amplitude and frequency errors is required. The 5-percent tolerances used herein seem reasonable and are recommended. (The 5-percent frequency tolerance is consistent with the recommended practice in ref. 1 for achieving an acceptable structural model.)

3. In formulating a model of a particular feedsystem, the following procedure is recommended for achieving a model using a minimum number of equations: (a) the system should be divided into sections established by natural "break points" such as branch points, area changes, bends, local resistances, or corrective device locations; (b) for each of the resultant two-terminal sections, the maximum value of $\omega\tau$ should be computed (where τ is the travel time for the particular section); (c) those sections for which $\omega\tau \leq 2.5\pi$ should be represented by the exact-at-$\pi/3$ admittance model; (d) those elements for which $\omega\tau > 2.5\pi$ should be represented by modes (open-open modes are recommended because of their inherent symmetry).

4. The resulting model for the feedsystem should be evaluated for accuracy by first determining the overall admittance matrix (involving all points where significant inputs may exist, such as line terminations or bends). Then the admittance elements of this matrix should be compared with the corresponding elements in an "exact" admittance matrix using amplitude and frequency error bounds. This "exact" matrix can be based on use of transcendental functions or on use of a model having considerably more refinement.

5. If factors other than minimizing the number of equations suggest the use of some other modeling approach, the accuracy evaluation in item (4) above should be employed.

6. Future efforts in feedline modeling should include (1) an evaluation of the influence of distributed dissipation on the modeling, (2) consideration of closed-closed modes, and (3) further exploration of the collocation method.

4. ENGINE ANALYSIS AND TESTING

4.1 Objective

The ideal objective for the mathematical modeling of an engine for pogo analysis is to develop a linearized model of its pertinent physical properties. For Saturn vehicles, however, the practice has been to provide only a transfer-function description of the engine as if it were a "black box." Transfer functions can be beneficial if, because of complexity of a physical model, their use materially aids the ease or cost of computations. However, the need for a physical model still exists; since it provides a basis for: (a) studies of the effects of uncertainty in any physical parameters, (b) correlation with test data for pressures and flows throughout the engine, (c) visibility over the consequences of thrust variation, off-nominal conditions, or malfunctions, and (d) maintaining cognizance over the assumptions made in deriving transfer functions. It is the very complexity of the Shuttle engine (brought about by such things as variable thrust operation, multiple flow paths, the presence of two-phase hydrogen flow, multiple pumps for each propellant, and the presence of a preburner) that makes it essential that a physical model be available.

4.2 Analytical Estimation of Pump Dynamics

Pumps are quite important contributors to the dynamic behavior of engines. The two most significant characteristics of pumps are the compliance[1] due to cavitation at the pump inlet and the pump dynamic gain[2]. At present we have no theoretical basis for coping with either of these characteristics. This situation is not likely to change for at least the next several years. A recently completed attempt to develop a theoretical analysis for cavitation compliance has produced a completely negative outcome (ref. 19 under contract NAS 8-26266). Other theoretical studies recently begun at the California Institute of Technology, if continued in association with experimental studies, give hope of eventually providing a theoretical basis for pump dynamics, most optimistically some several years hence (ref. 20 and 21, under contract NAS 8-28046).

Another recent study of cavitation compliance has yielded an empirical method of estimation for the cavitation compliance of pumps within the Rocketdyne family of designs (ref. 22, under contract NAS 8-27731). The basis of the method was a correlation of the measured cavitation compliance for the H-1, F-1, and J-2 fuel and oxidizer pumps with pump design and performance information. A key factor in the success of the method is the substantial correlation of the data achieved by normalizing the parameter expressing the pump suction operating condition (i.e., cavitation number, suction specific speed, or NPSH)

---

[1] Compliance is a measure of the volume change of the collection of bubbles per unit of pressure change of the liquid surrounding the bubbles under dynamic conditions.

[2] Dynamic gain is the partial derivative of pressure rise across the pump with respect to inlet pressure under dynamic conditions.

with respect to the value of that parameter at head breakdown as shown in figure 29. Reference 22 provides the best available basis for estimating cavitation compliance in advance of experimental determination of pump dynamics. An initial prediction for the Shuttle pumps is presented in section 5.

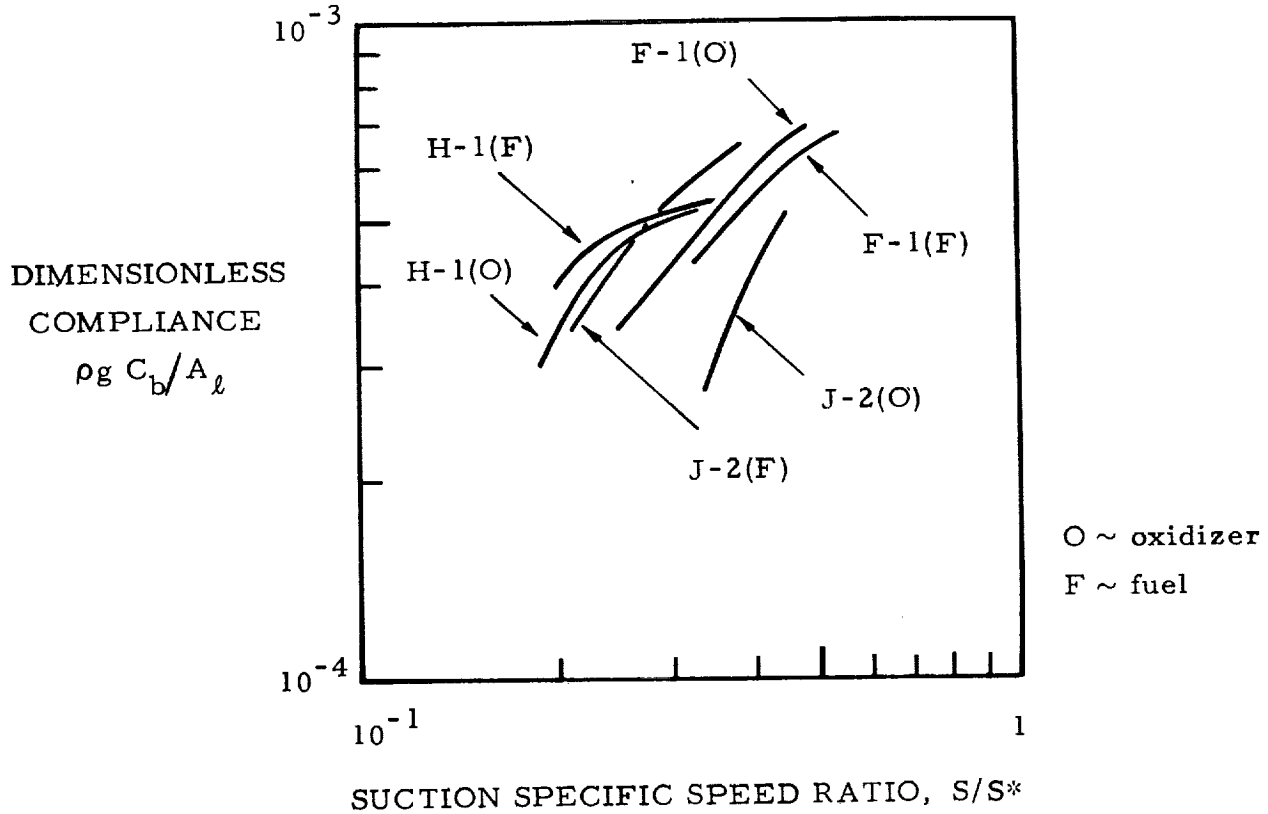

Figure 29. Correlation of compliance data for Rocketdyne pumps.

There is no body of experimental data for the dynamic gain of the Rocketdyne pumps, such as exists for the cavitation compliance. The Rocketdyne pumps operate in a regime which is essentially free of cavitation head loss. In other words the static gain, which defined to be the slope of the steady-state head-rise characteristic, is essentially unity. Data on Titan pumps (fig. 6 of ref. 1) would suggest that the dynamic gain of the Rocketdyne pumps should be about unity if the static gain is unity. However, there have been sporadic indications from Saturn V and Thor testing that dynamic gains may be of the order of two. In our opinion, about all that can be done in advance of experimental determination of pump gain for the Shuttle pumps is to assume that the gain values can lie between one and two.

4.3 Past Test Practice

Past practices of pump or engine testing have produced some results of rather poor quality. Most obviously, there has been considerable uncertainty in the determination of pump cavitation compliance. The basic approach to the determination of cavitation compliance has been to locate a fundamental hydraulic resonance of the test system by sinusoidal hydraulic excitation, and then to infer the value of pump-inlet compliance assuming that all other parameters of the test system are known. For example, this approach has led to the following degrees of uncertainty in compliance values (based on results in ref. 19):

1. For the F-1 lox pump, up to a factor of three due primarily to uncertainty in the mechanical compliance of a pressure-volume compensator device in the feedline.

2. For the F-1 fuel pump, up to a factor of five between results from a cold-flow pump test (referred to as a "bobtail test") using excitation near the pump discharge and results from a single-engine test using excitation near the pump inlet.

3. For the J-2 lox pump, up to a factor of two due to the use of two types of mathematical models of the pump (that is, a single - vs. a double-compliance model).

As mentioned earlier, pump dynamic gain has received rather little attention in testing. What has perhaps not been recognized is the possibility that the value of pump dynamic gain may have a significant influence on the location of a resonant frequency and thus, on the inference of cavitation compliance. Our own recent experience shows that this is so for the Thor fuel system. Figure 30 shows, for the short-tank configuration of the Thor, how a cavitation compliance inferred from an observed resonant frequency depends on whether the pump gain is assumed to be one or two. Thus, it may be necessary to first infer pump dynamic gain from the test data in order to be able to then infer cavitation compliance. It is not clear to what extent this matter has been considered in the testing of Saturn pumps.

To gain additional insight into causes of past difficulties, consider the application of past test practices to a two-pump configuration representative of the Shuttle engine. Figure 31 is a schematic of the setup. The sinusoidal input flow Q_{in} is produced by an exciter near the pump inlet, and pressure measurements $P_{\ell 1} \ldots P_{\ell n}$, P_2, P_3 and P_4 are recorded. The object is to determine the following frequency-response relationships vs. frequency: input impedance to boost pump (P_1/Q_1), input impedance to main pump (P_3/Q_3), and pressure ratio across the two pumps (P_4/P_1). These relationships will be employed to determine parameters of an analytical model of the system.

A major detriment to the accuracy of the results of this test is that meters for measurement of dynamic flow are absent from the test. For example, Q_1 will be determined from the difference $Q_{in} - Q_\ell$, where Q_{in} is known from measurement of motion of the mechanical piston relative to the feedline pipe assuming no cavitation at the piston; Q_ℓ is based on "calibration" of the feedline in

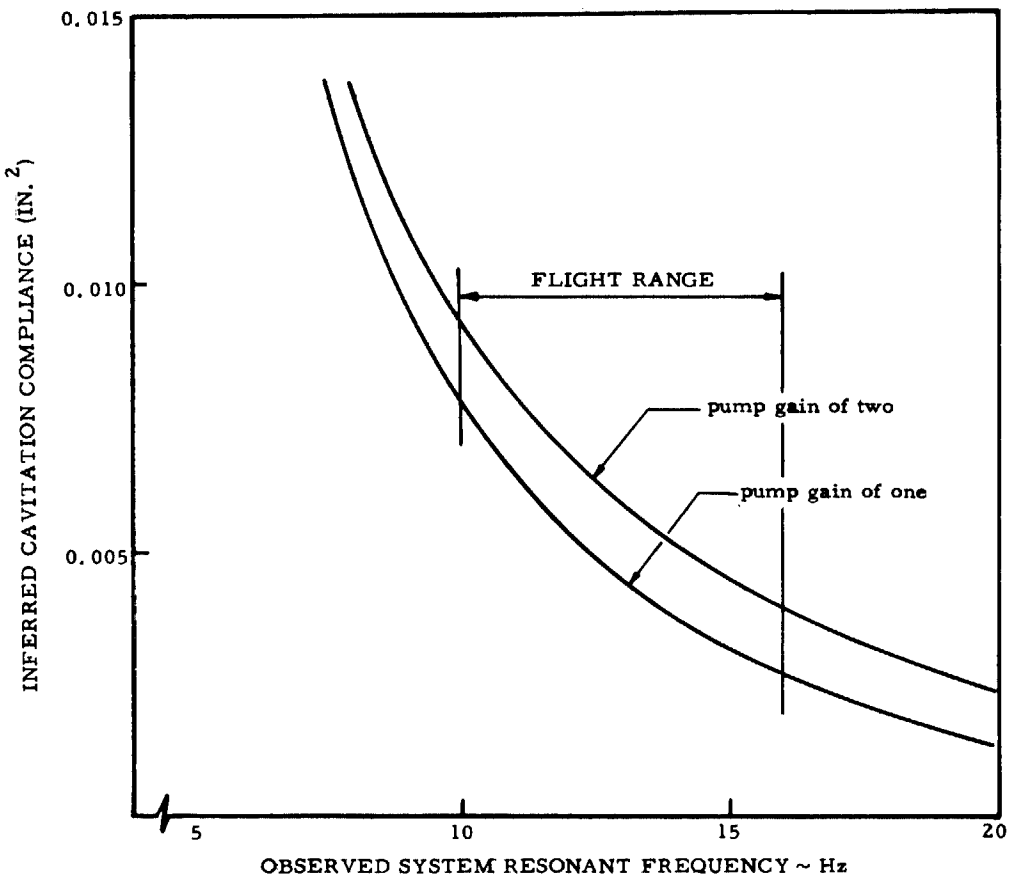

Figure 30. Importance of pump gain on the inference of compliance for the Thor short-tank fuel system.

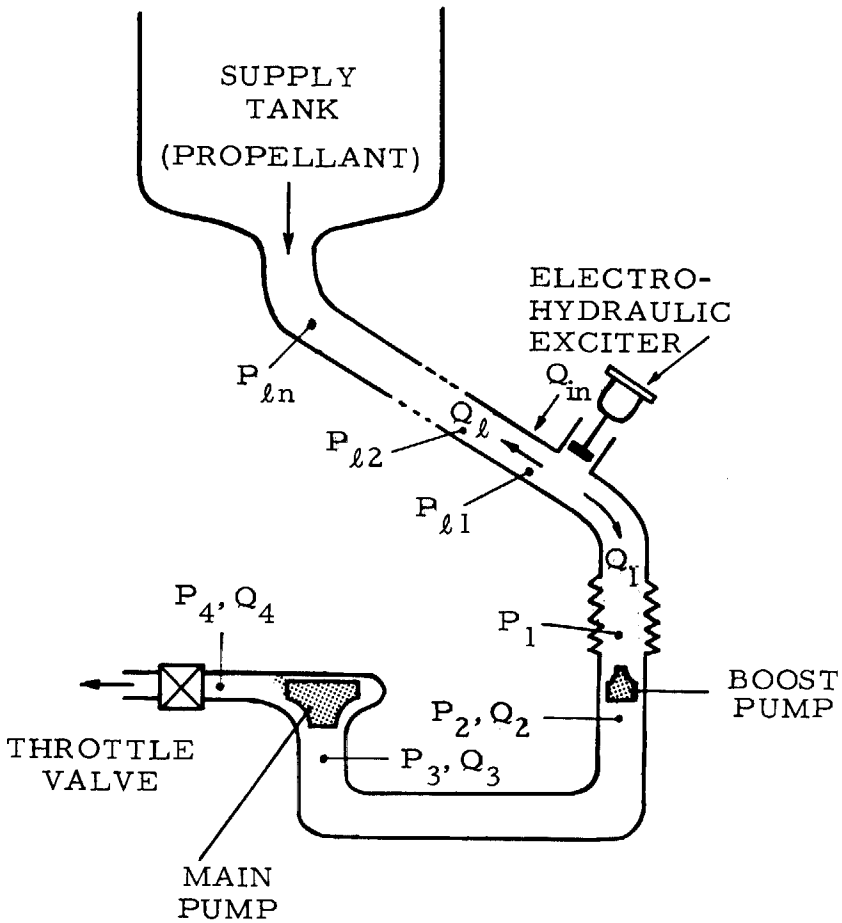

Figure 31. Schematic of a setup for dynamic testing of Shuttle pumps.

terms of $P_{\ell 1} \cdots P_{\ell n}$ at a condition of no steady flow (line blocked immediately downstream of the exciter). The splitting of the exciter flow Q_{in} according to the upstream and downstream impedances, Z_ℓ and Z_1 respectively, is expressed by

$$Q_1 = \frac{Z_\ell}{Z_1 + Z_\ell} Q_{in} \qquad (4\text{-}1)$$

Clearly, if $Z_\ell \ll Z_1$ nearly all the exciter dynamic flow will go upstream; that is, $Q_\ell \simeq Q_{in}$. Therefore the substraction $Q_{in} - Q_\ell$ to obtain the desired Q_1 will tend to be highly inaccurate, since a difference of two, nearly equal, numbers is involved. Figure 32 shows the results of an estimation of the impedance magnitudes $|Z_1|$ and $|Z_\ell|$ vs. frequency for a typical setup. It is seen that this type of inaccuracy in inlet flow to the boost pump will become increasingly important as the frequency falls below 10 Hz.

The other needed dynamic flow Q_3, at low frequencies, is inferred from the pressure difference from P_2 to P_3 and the assumption of an incompressible line between the pumps on the basis that P_3 is upstream of any cavitation of the second pump. Again, because the flow impedance of that line will be small, a difference of nearly equal quantities will be involved and the inferred flow will tend to be inaccurate.

Another type of deficiency of this testing practice is that insufficient data is obtained for independent determination of the pump parameters. Neglecting rotational speed fluctuation, a pump requires four frequency-response functions for a complete description of its dynamics. These functions appear, for example, in the two equations which interrelate the pressures and flows at the inlet and discharge of the pump. A test conducted with one position of excitation and under one set of boundary conditions can only yield two relations among the four unknown functions. So the pump dynamics cannot be completely determined.

Summarizing, much of the poor quality of pump parameters stems from two deficiencies. The first is a lack of dynamic flowmeters. The process of inferring the flow lends to inaccuracy because of inherent numerical difficulties and because the characteristics of other parts of the test system are employed. The second fundamental deficiency stems from a lack of sufficient data to determine fully the pump characteristics. The flowmeter deficiency can be corrected by development of suitable measurement devices, and such development has been initiated by contract NAS 1-11756. The second deficiency can be rectified by adopting a new test philosophy and this is discussed in the next section.

4.4 New Test Philosophy

A generalized representation of a turbopump is shown in figure 33. The turbopump is imagined to be endowed with input-output state variables of inlet

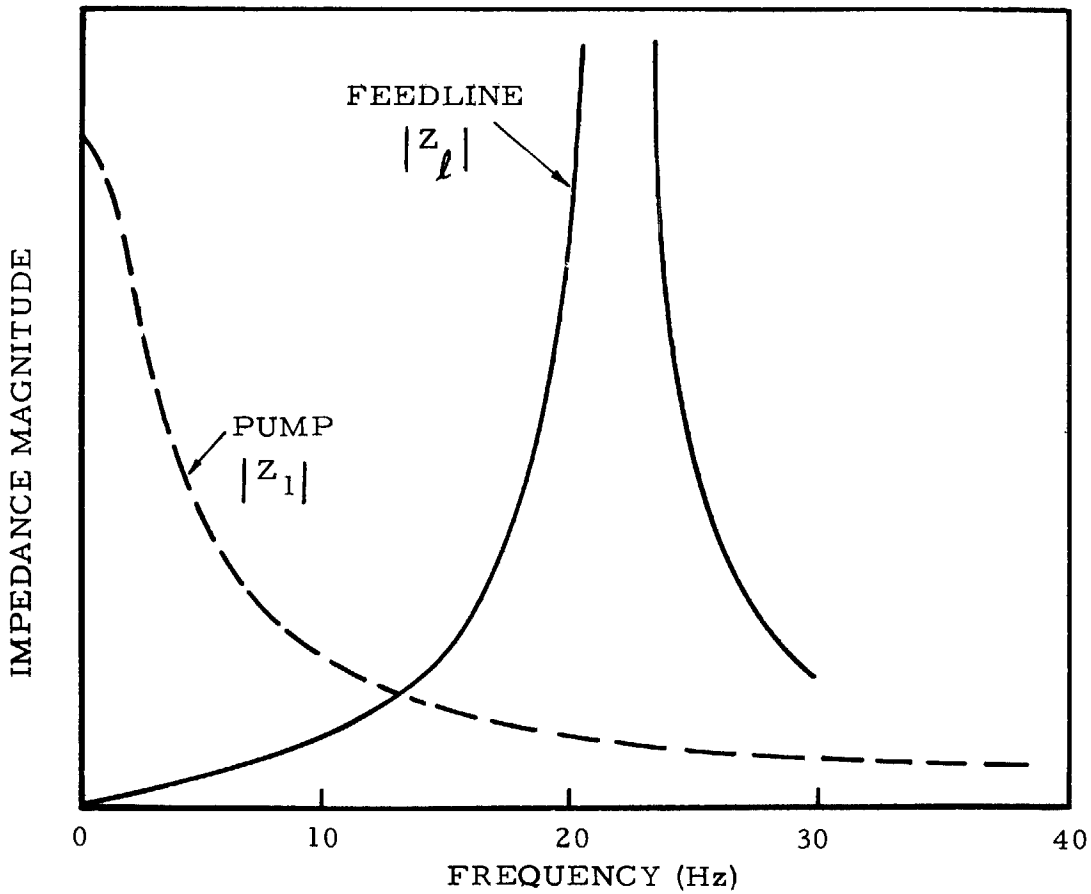

ASSUMPTIONS:

FEEDLINE LENGTH, 12.2 m

CAVITATION COMPLIANCE, 6×10^{-9} m^5/N

Figure 32. Example of test feedline vs. pump input impedance.

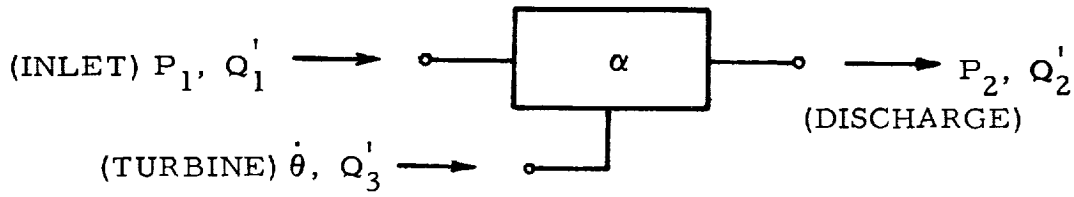

Figure 33. Generalized view of a turbopump.

pressure and flow, discharge pressure and flow, and turbine speed and flow. A full description of the dynamics is provided by a matrix relationship among these variables. For example, the form of the relationship might be

$$\begin{Bmatrix} P_1 \\ P_2 \\ \dot{\theta} \end{Bmatrix} = \begin{bmatrix} \alpha_{11} & \alpha_{12} & \alpha_{13} \\ \alpha_{21} & \alpha_{22} & \alpha_{23} \\ \alpha_{31} & \alpha_{32} & \alpha_{33} \end{bmatrix} \begin{Bmatrix} Q_1' \\ Q_2' \\ Q_3' \end{Bmatrix} \tag{4-2}$$

where the Q_i' are flows relative to the pump structure. Our goal should be to determine these nine functions of frequency $\alpha_{ij}(\omega)$ from test data and to then correlate these functions with a physical model of the turbopump. For example, for the usual simple model of the pump, we find that the cavitation compliance C_b and the dynamic gain (m + 1) are given by

$$C_b = \frac{1}{i\omega\alpha_{11}} = -\frac{1}{i\omega\alpha_{12}}$$

$$m + 1 = \alpha_{21}/\alpha_{11} \tag{4-3}$$

In general, what is required to determine the nine α_{ij}'s is to measure the six external state variables under three independent states of excitation. Recognize that this requires the measurement of three flow variables. If the three states are denoted by the subscripts a, b, c all the α_{ij}'s can be determined from the equation

$$\begin{bmatrix} \alpha_{11} & \alpha_{12} & \alpha_{13} \\ \alpha_{21} & \alpha_{22} & \alpha_{23} \\ \alpha_{31} & \alpha_{32} & \alpha_{33} \end{bmatrix} = \begin{bmatrix} P_{1a} & P_{1b} & P_{1c} \\ P_{2a} & P_{2b} & P_{2c} \\ \dot{\theta}_a & \dot{\theta}_b & \dot{\theta}_c \end{bmatrix} \begin{bmatrix} Q_{1a}' & Q_{1b}' & Q_{1c}' \\ Q_{2a}' & Q_{2b}' & Q_{2c}' \\ Q_{3a}' & Q_{3b}' & Q_{3c}' \end{bmatrix}^{-1} \tag{4-4}$$

States a and b might be achieved by using inlet excitation for two different boundary conditions at the pump discharge. One boundary condition might be the normal one which is essentially resistive; the other might be an essentially compliant one achieved by introducing a large accumulator immediately downstream of the pump. Another possibility would be the use of inlet excitation for state a and discharge excitation for state b. The turbine characteristics would logically be expected to be determined best by use of turbine flow excitation thus achieving state c.

The importance of the turbine loop to system pogo stability should be studied when a reasonably valid system mathematical model is available. The turbine loop may be shown to be unimportant for the Shuttle vehicle, as it has been for past vehicles. If so, the turbopump representation can be simplified from a nine- to a four-parameter one ($a_{11} \ldots a_{22}$) and the associated testing considerably reduced.

An overall program for determination of turbopump dynamics would be conducted in three phases. The first phase would consist of analytical studies of alternative test procedures by means of simulation studies on an analog or digital computer. The simulation would include nonlinear behavior of the turbopump and the presence of noise on the data.

Excitation techniques for collection of the greatest amount of useful data in a limited test time is a most important area for study. One of the major limitations for turbopump testing stems from the facility limitation on the duration of a single test and the budget limitation on the number of tests. Possible sinusoidal excitation techniques are (a) step changes in frequency, (b) a prescribed sweep of frequency, and (c) a closed-loop control of the sweep of frequency (ref. 23). This latter approach provides for a relatively slower sweeprate during passage through resonances to yield significant reduction in the time of the sweep for a prescribed accuracy of the derived system frequency response. An intriguing possibility for substantially increasing the information obtained during a test of limited duration is to apply several sinusoids simultaneously, using any of the aforementioned techniques of frequency change. At any instant of time the response to an individual sinusoid could be separated from the total response by means of bandpass filtering. For example, the range from 0.5 to 62.5 Hz could be covered by use of three simultaneously applied sinusoids: the first varies in frequency from 0.5 to 2.5 Hz, the second from 2.5 to 12.5 Hz, and the third from 12.5 to 62.5 Hz. The spread of the three frequencies at any instant of time should be adequate for effective bandpass filtering; care would have to be exercised that this were true in the case that closed-loop frequency control is employed since the ratio of the frequencies would then be time dependent.

The simulation studies would also encompass the following matters:

1. Independent states of excitation

2. Data reduction techniques (PSD and cross PSD; Fourier components; band-pass filtering)

3. Exciter requirements (power and stroke for electrohydraulic or electromagnetic machines, turbine supply oscillation)

4. Methods for evaluation of linearity

5. Accuracy of a_{ij} based on expected data accuracy

On the basis of these simulation studies, test requirements and optimum procedures would be developed.

The second phase in the program would consist of dynamic tests of any subscale pumps which are available after design development. Such pumps would be electric-motor driven and would use water. As concluded in reference 22, it is anticipated that the cavitation compliance would be applicable to the full-scale pump. This conclusion is based on the remarkable correlation shown in figure 29 in view of the following differences among the pumps: (a) inducer diameters from 0.15 m (6 in.) for the H-1 fuel pump to 0.41 m (16 in.) for the F-1 oxidizer pump; (b) propellants from RP-1 to liquid hydrogen for the J-2 fuel pump to liquid oxygen; and (c) from single-stage centrifugal pumps to an axial pump for the J-2 fuel. It is expected that the other pump parameters could also be adjusted for scale and propellant effects. Rotational speed oscillations could be studied to provide partial information on the effect of the turbine loop. Moreover, these tests would also provide a proving ground for the test and data-analysis procedures prior to full-scale testing.

The final phase, assuming subscale tests are conducted, would consist of verification tests on full-scale pumps to selectively evaluate propellant, scale, and perhaps turbine effects. If scale testing is not done on a pump, the full-scale testing would have to be much more thorough. Such a three-phase program provides considerable benefit relative to the past practice of solely testing full-scale pumps. First, the simulation studies, in conjunction with the availability of flowmeters and the generalized view of the turbopump, should produce improved test procedures. The result will be that the testing will be more efficient, yield more reliable results, and provide a more comprehensive evaluation of the dynamic properties of the pumps. Second, there will be a much improved utilization of manpower and facilities by testing of subscale pumps well in advance of the availability of full-scale pumps. Considerably more time is available for subscale tests, and test-facility requirements are less severe and are less likely to conflict with the needs for pump development. Finally, the possibility of surprises and the resulting upheavel late in the development program will be minimized. Visualizing that the three-phase program will involve less full-scale testing than called for by past practices, and that this will compensate for the much less expensive simulation studies and scale tests, all these benefits should be possible at no increase in overall cost.

4.5 Conclusions

1. A linearized mathematical model of the physical elements of the Shuttle liquid engine is needed for studies of pogo.

2. The best available basis for early estimates of the cavitation compliance of the Shuttle pumps is the empirical method recommended in reference 22. There is no proven basis for estimating the dynamic gain of the pumps.

3. Practices used in the past for pump testing will be inadequate for the Shuttle pumps. Major deficiencies of the past practices are the absence of dynamic flowmeters and the lack of independent determination of the turbopump parameters.

4. Simulation studies on a computer to optimize dynamic test procedures will more than pay for themselves by increasing the effectiveness of later testing.

5. Dynamic testing of subscale model pumps flowing water is likely to produce data which is applicable to the full-scale pumps flowing propellant. The subscale testing will also provide a proving ground for increasing the efficiency of test procedures to be used later for full-scale testing. The subscale tests will permit an earlier availability of test-derived pump parameters for Shuttle stability studies.

6. Reduced requirements and improved efficiency for testing of full-scale pumps should compensate for the subscale testing.

4.6 Recommendations

1. A requirement should be established for a linearized mathematical model of the physical elements of the Shuttle liquid engine. The model should be continually refined through analysis and experiment and made available to everyone conducting pogo studies.

2. The empirical method of reference 22 should be employed to provide an early estimate for the cavitation compliance of the pumps. Until test data indicates otherwise, the dynamic gains for the pumps should be assumed to lie anywhere between one and two.

3. A three-phase program for turbopump testing should be instituted for Shuttle development: (a) computer simulation studies of test procedures, (b) comprehensive dynamic tests of available subscale pumps based on independent determination of the turbopump frequency-response functions, and (c) verification tests on full-scale turbopumps.

4. Flowmeters for measuring dynamic flow should be developed for use in the pump and engine dynamic tests.

5. Results of the Rocketdyne pump dynamic tests reported in reference 19 should be re-examined to investigate the role of pump gain.

5. VEHICLE STUDIES

5.1 Introduction

Numerical studies of the vehicle were conducted using the method of approximate analysis identified in section 2. The studies which were conducted on the early configuration were directed towards the booster lox system, which was believed to be potentially the most troublesome portion of the Shuttle propulsion systems for pogo. Even though the current vehicle configuration is quite different, it is believed that the conclusions of this numerical study are meaningful for the current orbiter lox system.

An objective of the studies was to identify and investigate the critical conditions for stability. No previous vehicle has faced the situation where the first organ-pipe frequency (one-quarter wave in feedline) has been equal to or below the frequency of the fundamental longitudinal structural mode. While the standard approach of placing an accumulator at the engine inlet can readily reduce the frequency of the first feedline mode to a point where it is no longer a danger to stability, there will still be numerous coincidences of higher organ-pipe modes with high-gain structural modes. It followed that damping of the higher feedline modes may be quite important to stability. This suggested (1) an investigation of the importance of the small distributed flow resistance of the feedline for the damping in higher feedline modes, and (2) consideration of corrective devices that serve to introduce increased damping in higher feedline modes. Both these matters were dealt with in a study of alternative placements of an accumulator to positions within the engine itself. The placement concept is to allow oscillatory flow going into the accumulator to first pass through upstream engine resistance and thereby dissipate energy.

A most valuable outcome of the accumulator-placement study was the finding that the mathematical model being employed was somewhat inadequate. In an analysis conducted after the accumulator-placement study reported here, it was discovered that use of the model predicted instability in a situation for which the system was essentially passive. This recognition led to the addition of tank-outflow effects to the mathematical model, as discussed in section 1, and the identification of important consequences for stability, as discussed in section 2.

The accumulator-placement study, conducted prior to the discovery of the deficiency in the mathematical model, is reported in the next section. Even though the accumulator sizes resulting from the study are incorrect, the results may well be correct in a qualitative sense. Moreover, various intermediate findings of the study are believed to be valid. We first show the values employed for the system parameters and identify their origin. Included is the stability criterion adopted for this study. Next we show the key results.

In section 5.3, we present the results of an estimated cavitation compliance of the pumps based on the recommendations of reference 22.

5.2 Lox Study for Early Configuration

5.2.1 Parameters. - Structural modes were obtained from two vehicle contractors. Evaluation of that data to obtain conservative estimates for stability analysis led to the results shown on figure 34. High-gain structural modes can occur within the shaded bands of natural frequency versus percent of burn time shown in figure 34a. Associated with each of the frequency bands is an upper bound for the structural gain (fig. 34b) and for the tank-bottom pressure per unit engine acceleration (fig. 34c). The structural gain is to be multiplied by 12 to account for that number of engines.

Both modal analyses were based on the use of single-mode representations of the hydroelastic tanks. Experience on Titan programs has shown that higher-order tank modes significantly influence the dynamic characteristics of the vehicle. The effect of these modes is not local and their influence has been noted strongly in response analyses and in flight data from both payload and the booster systems. As a result of this lack in modeling, structural modes above region II in figure 34a are likely to be erroneous.

A simple physical model (see fig. 2) for the engine was constructed using information available from contractor reports. The results are summarized in Table IVa. Configurations and pressure drops for the tank-to-engine lox feedlines were obtained from the vehicle contractors. The parameters appear in Table IVb. The positions of feedline modes relative to the structural modes are shown in figure 34a.

An analysis of the feedlines as uniform continuous transmission lines including frictional resistance [see eq. (2-3)] yields the following damping ratio ζ for open-closed modes:

$$\zeta = R_\ell / 2\omega L_\ell \tag{5-1}$$

where ω is the natural frequency of the mode and R_ℓ and L_ℓ are the total resistance and inertance of the line, respectively. Note that the damping is inversely proportional to frequency. This is contrary to behavior which is often arbitrarily assumed (constant modal damping or even increasing damping in higher modes). Dampings obtained using equation (5-1) are shown at the bottom of Table IVb.

5.2.2 Accumulator placement study. - The closed-loop damping of the coupled structure/propulsion system was evaluated by use of equation (2-1) in the form:

$$\zeta_N = - (12G_e)(\bar{H}_{eI} + \bar{H}_{tI})/2 \tag{5-2}$$

where $12G_e$ is the structural gain for the twelve engines, and $\bar{H}_{eI}$ and $\bar{H}_{tI}$ are the individual contributions to $\bar{H}_I$ due to engine acceleration and tank pressure, respectively. For purposes of this study, a minimum value for ζ_N was set at 0.002. Experience with structural damping indicates that 0.008 is a reasonable

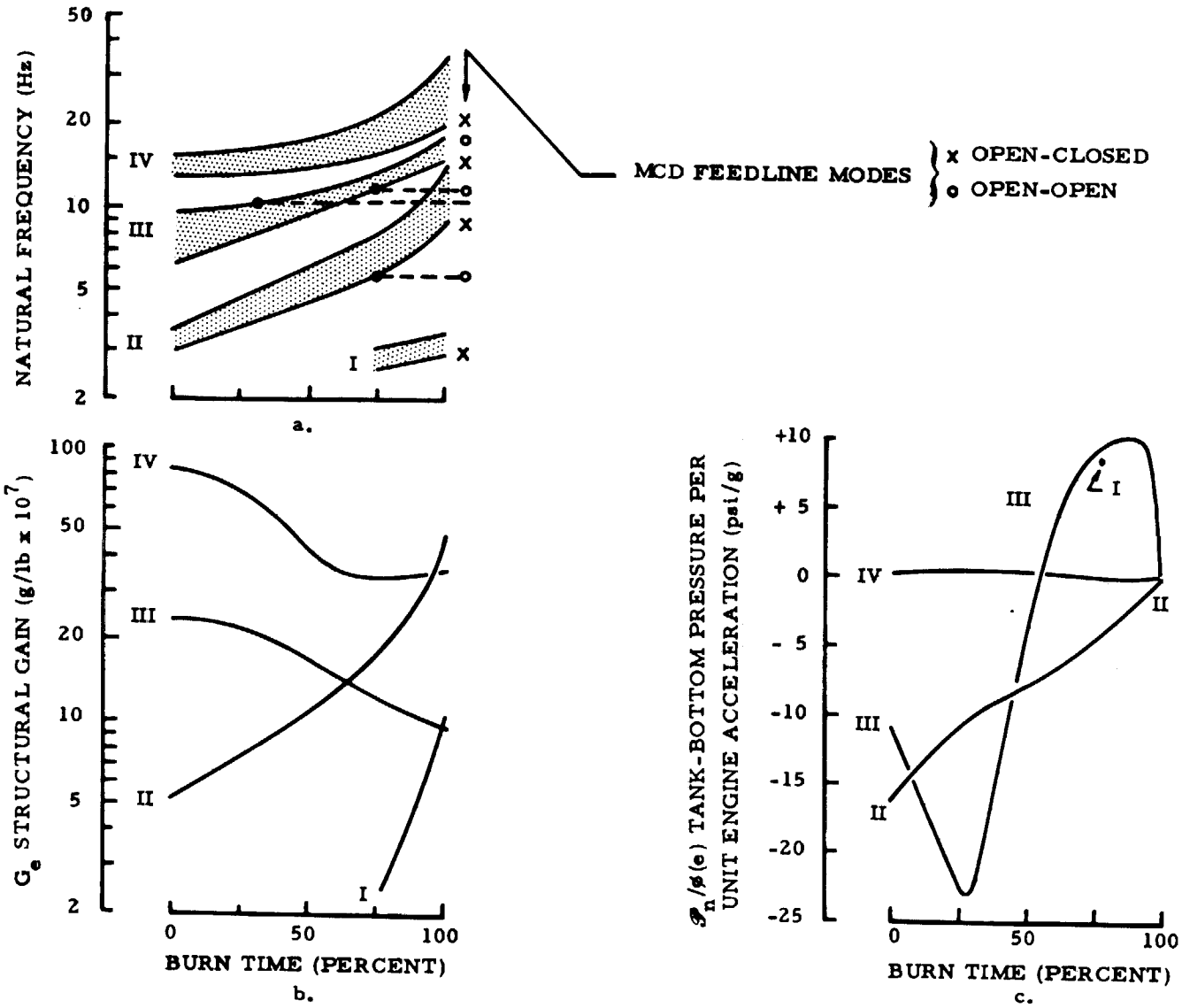

Figure 34. Structural parameters and organ-pipe frequencies for study of early configuration.

lower bound. (This may not be correct for modes which are local in nature; for example, the Saturn V, S-II engine/cross beam/lox tank modes.) Placing ζ_N at 1/4 of this value implies a "damping gain margin" (ref. 1) of 12 dB.

The accumulator locations selected for the study were at the engine inlet, at the discharge of the boost pump, and at the discharge of the first-stage of the main pump. The engine-inlet location has been employed on all past vehicles. The main-pump-discharge location was recommended for study by an engine contractor as a means of reducing peaks in propulsion frequency response and to permit use of available gox within a heat exchanger for the accumulator pressurant. The boost-discharge location was conceived as a possibly effective means of increasing the damping in engine feedline modes by forcing oscillatory flow entering the accumulator to pass through the resistance of the boost pump. The boost pump resistance is considerable relative to the distributed resistance in the engine feedline (see Table IVa). For example, an introduction into the feedline of a resistance equal to that of the boost pump would produce a pressure drop of about 1.6 MN/m^2 (230 psi) which is an order-of-magnitude higher than the pressure drop in the feedline itself (refer to Table IVb).

For a given volume of pressurant gas in the accumulator, the compliance is inversely proportional to the steady pressure. For example, during the latter portion of the booster burn period we find that equal accumulator volumes yield compliances in the ratio of 1:0.39:0.04 for the engine-inlet, boost-discharge, and main-discharge locations, respectively. The question is whether the lower compliances at the downstream locations for the accumulator can be overcome by the effect of the associated higher upstream resistances.

An initial analysis was performed at burnout, assuming no cavitation of the pumps and a gain of 2 for each pump. Since the vehicle tank is empty, there is no contribution to propulsion feedback from tank oscillatory pressure (that is, $\overline{H}_{tI} = 0$). The imaginary part of the feedback due to engine acceleration $\overline{H}_{eI}$ is plotted vs. frequency on figure 35 for four conditions: no accumulator, and 0.057 m^3 (2 ft^3) accumulators at each of the three locations. From equation (5-2), $\zeta_N \leq 0.002$ and the G_e from figure 34b were employed to obtain upper bounds on $\overline{H}_{Ie}$; these bounds are shown on the figure for modes I, II, III over the corresponding bands of frequency shown in figure 34a at burnout. An exceedance of these bounds indicates that the stability goal for ζ_N is not met. For reference the frequency of various feedline modes is indicated by the arrows at the upper right of figure 35.

Review the matters of interest on figure 35: (1) the no-accumulator case is up to 32 dB beyond the bounds for modes I and II and 17 dB for mode III. Note that the first peak occurs at 1/4 wavelength in the feedline and the higher modes at 3/4 and 5/4 wavelengths, as expected. (2) The engine-inlet accumulator only exceeds the mode II bound by about 1 dB. The strong second peak at about 6 Hz (about 1/2 wavelength) and the third peak at about 12 Hz (about 1 wavelength) are located as expected (for example, see fig. 10 of ref. 24). Relative to the effectiveness of feedline resistance, an analysis at the 6-Hz peak showed that a removal of feedline resistance would increase the peak value by 21 dB! (3) The boost-discharge accumulator does not exceed any bound. The first resonance at about 1 Hz has a somewhat lower peak value and higher frequency than the first peak for the engine-inlet accumulator; the two higher peaks occur at about the same frequencies as for the engine-inlet case, but at greatly reduced

Table IV. Propulsion-system parameters for study of early configuration.

a. Engine parameters for lox (nominal power level, mixture ratio of 6)

Boost pump resistance[1]	8.8 MN s/m^5	(0.52 sec/in.^{2})
Boost pump pressure rise	2.39 MN/m^2	(345 psi)
Resistance of first stage of main pump	44.6 MN s/m^5	(2.64 sec/in.^{2})
Discharge-line resistance	60.8 MN s/m^5	(3.64 sec/in.^{2})
Discharge-line inertance[2]	0.08 MN s^2/m^5	(0.005 sec^2/in.^{2})
Combustion-chamber resistance	36.8 MN s/m^5	(2.18 sec/in.^{2})

b. Feedline parameters

Elevation change	40.6 m	(1600 in.)
Effective area	0.0409 m^2	(63.4 in.^{2})
Inertance	1.4 MN s^2/m^5	(0.081 sec^2/in.^{2})
Quarter-wave frequency	2.9 Hz	
Static pressure drop	0.176 MN/m^2	(25.5 psi)
Resistance	0.733 MN s/m^5	(0.0434 sec/in.^{2})
Damping ratios		
Quarter wave	0.015	
Three-quarter wave	0.005	

[1] resistance in SI units is based on pressure divided by volume flow; in engineering units, weight flow is employed.

[2] the flow difference in (1) also applies to inertance.

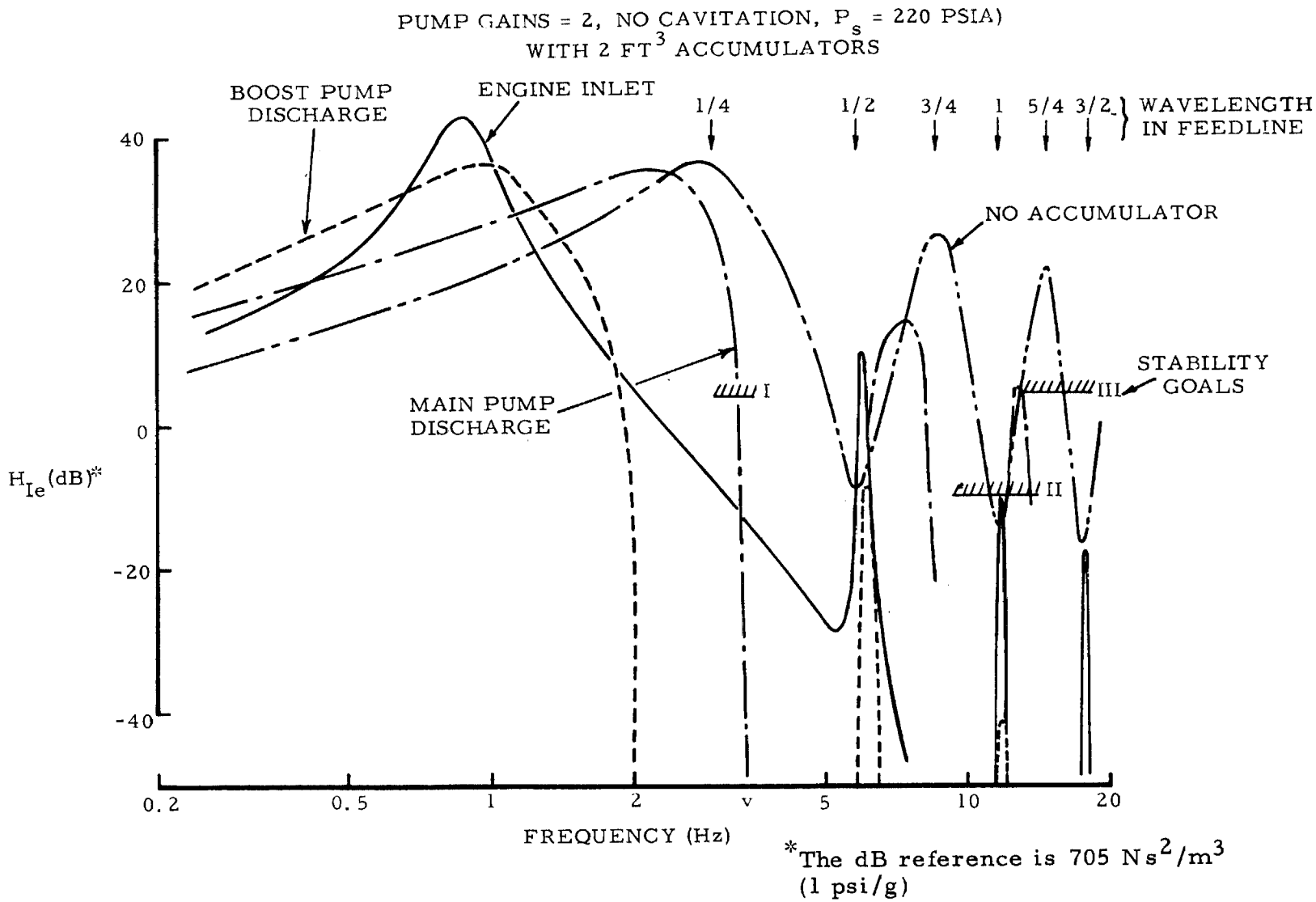

Figure 35. Propulsion feedback at burnout.

peak values (about 18 dB lower at 6 Hz and 34 dB lower at 12 Hz). The strong reductions in the higher peaks give promise of the potential effectiveness of the boost-discharge accumulator. Again looking at the importance of feedline resistance, the resistance was removed and only a 3-dB increase was observed at 6 Hz, a much lower sensitivity than for the engine-inlet accumulator. (4) The main-pump-discharge location exceeds the bound for mode II and touches the bound for mode III. The very low accumulator compliance results in peaks which are intermediate in frequency to those for no accumulator and those for the other accumulators. They are also intermediate in peak values.

On the basis of these results the main-pump-discharge accumulator was dropped from further consideration.

Worst-case stability situations were identified as coincidence of mode II with the 1/2-wave feedline mode, and mode III with the full-wave mode, at 75-percent burn time (see fig. 34a). Since the higher peaks in $\overline{H}_I$ are quite narrow band (see fig. 35), it was decided to plot transfer functions as amplitude-phase plots to assure that the definition of the peaks was complete. Figure 36 shows the result for the function $H_e(i\omega)$, the propulsion feedback due to engine acceleration, for the engine-inlet and boost-discharge accumulators. The rapid phase shifting is clearly evident at the higher resonances. When the phase is between 0 and -180 degrees the feedback is stabilizing. This plot shows that it is largely the increased phase lag in H_e that produces a lower peak value of its imaginary part for the boost-discharge accumulator.

Figure 37 shows the result for the function $H_{to}(i\omega)$, the propulsion feedback due to a unit amplitude of tank pressure. By definition the total tank-pressure effect H_t is the product of the tank pressure per unit engine acceleration, $\mathscr{P}_n/\phi_n(e)$, and H_{to}:

$$H_t(i\omega) \equiv \frac{\mathscr{P}_n}{\phi_n(e)} H_{to}(i\omega) \tag{5-3}$$

Results for all four accumulator cases are shown. Note that this function has a much different character than does $H_e(i\omega)$. The amplitude of H_{to} tends to remain relatively high at the higher frequencies. In fact, notice that the value at the second peak (at 5.9 Hz) for the engine-inlet accumulator is higher than the second peak (at 8.5 Hz) for no accumulator. We see from figure 34 that for mode II at 75-percent burn time, $\mathscr{P}_n/\phi_n(e)$ is negative and so a negative imaginary part for H_t (destabilizing) requires that H_{to} be in the first or second quadrants (between -180 deg and -360 deg on fig. 37). The situation is the reverse for mode III: positive $\mathscr{P}_n/\phi_n(e)$ and H_{to} destabilizing in third and fourth quadrants (between 0 and -180 deg or beyond -360 deg on fig. 37). For the 75-percent burn time conditions, it was found that the tank-pressure contribution dominated over the engine-acceleration contribution. Conditions of minimum stability are located on figure 37 by the X marks for the mode II and III coincidences and the boost-discharge accumulator is seen to be superior for both conditions.

The functions $H_e(i\omega)$ and $H_{to}(i\omega)$ were computed for a sequence of engine-inlet and boost-discharge accumulator volumes, and ζ_N evaluated using equations (5-3) and (5-2). Main-pump dynamic gains of 1 and 2 were employed;

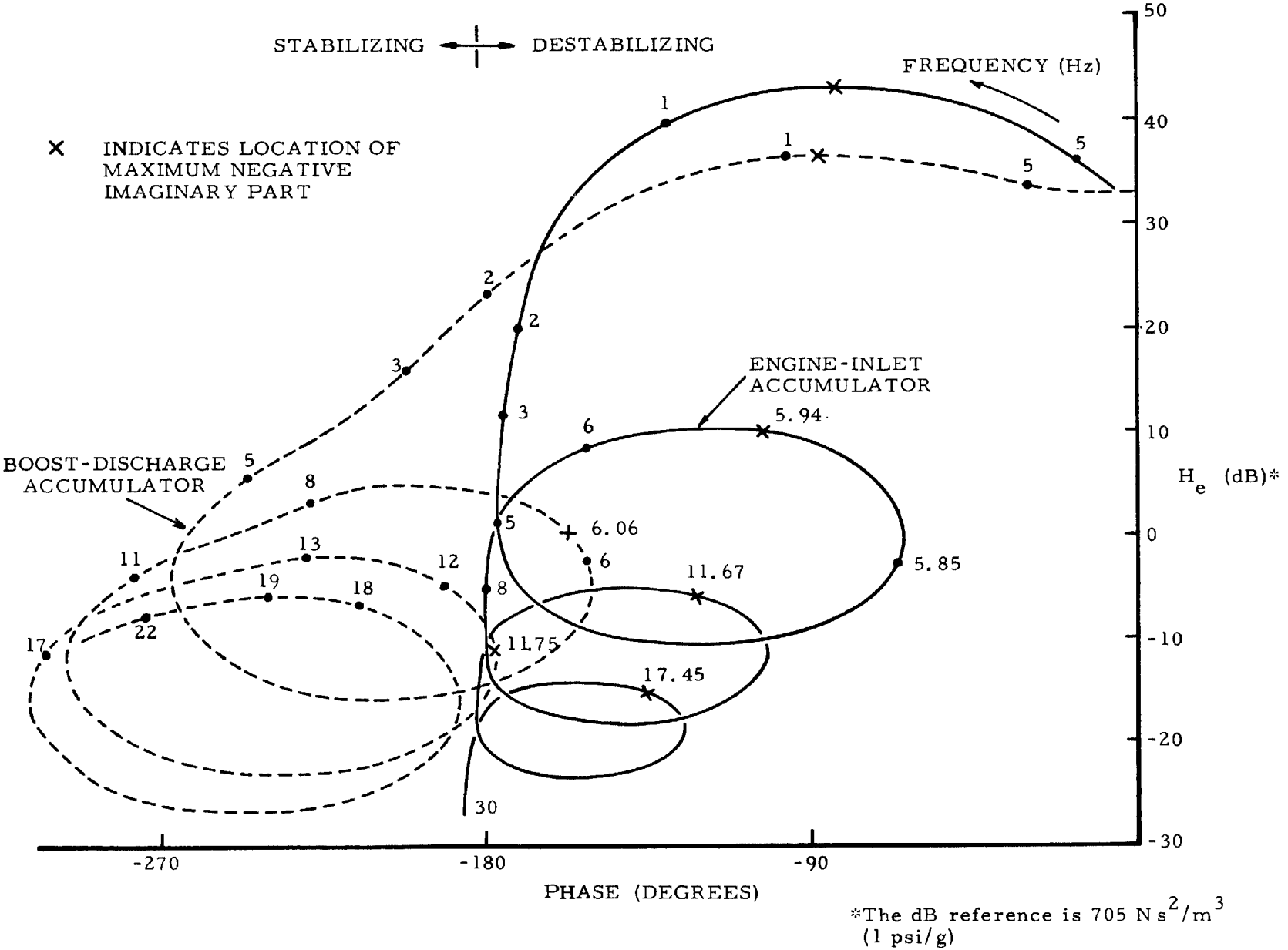

Figure 36. Amplitude-phase plot for feedback due to engine acceleration.

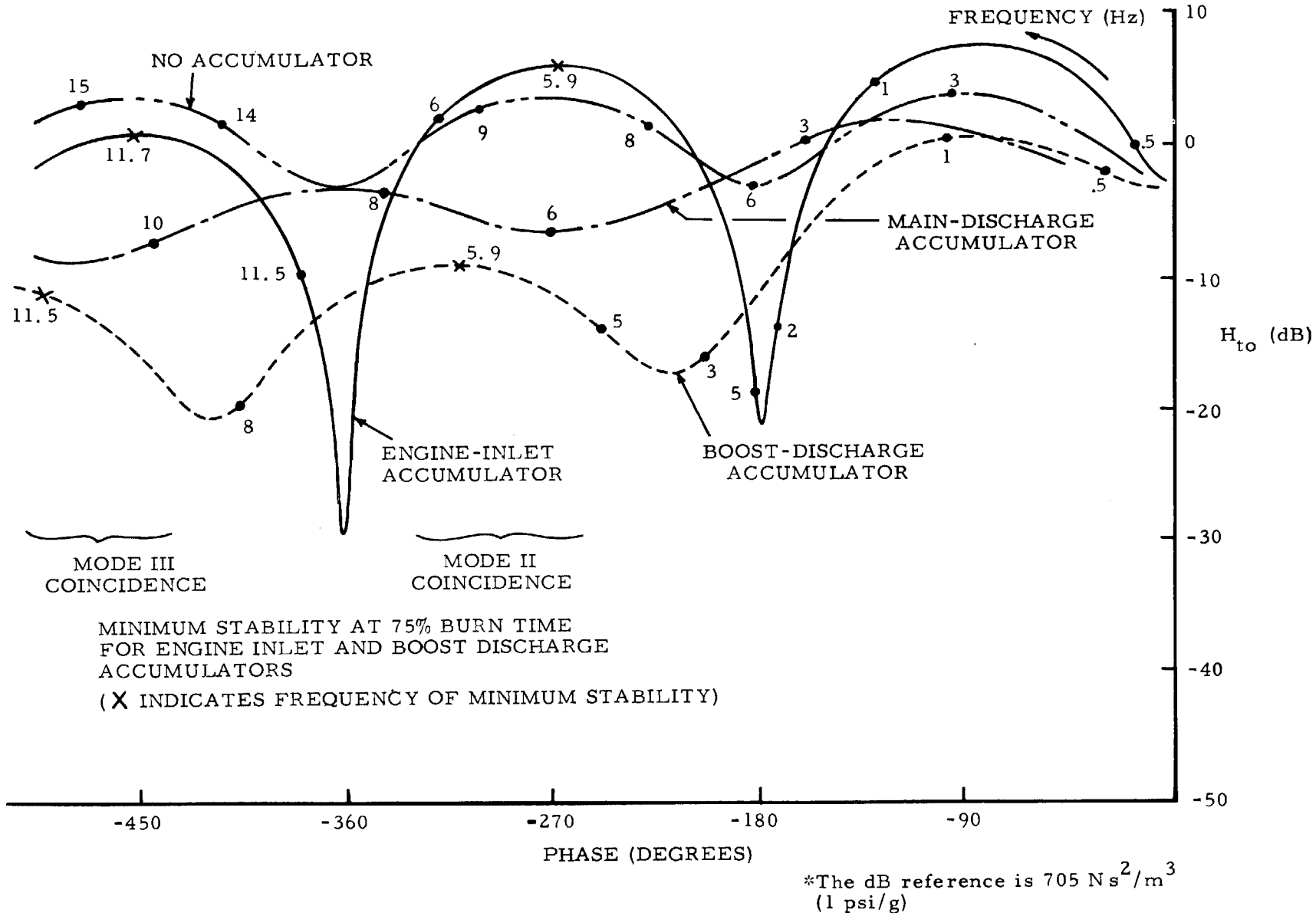

Figure 37. Amplitude-phase plot for feedback due to tank pressure.

the boost pump gain was maintained at 2. The results are shown on figure 38. A substantial size advantage for the boost-discharge location is seen. For a main-pump gain of 1, the stability goal is met with an accumulator volume of 0.048 m^3 (1.7 ft^3) at the boost discharge and 0.18 m^3 (6.3 ft^3) at the engine inlet; for a gain of 2, the corresponding volumes are 0.081 m^3 (3.2 ft^3) and 0.68 m^3 (24 ft^3). Thus we see that pump gain is quite an important parameter.

5.3 Prediction of Cavitation Compliance

The empirical method recommended in reference 22 was employed to estimate pump cavitation compliance vs. net positive suction head (NPSH). This was done for the fuel and oxidizer boost pumps and the first stage of the main pumps, for operation at a nominal power level and a mixture ratio of 6. The data employed were obtained from the engine contractor and the resulting values of parameters used for the prediction are given in Table V. The predicted values of a dimensionless compliance $\rho g C_b / A_1$ vs. NPSH are given on figure 39, where ρ is the propellant density, A_1 is the flow area at the pump inlet, and C_b is the compliance in terms of volume per unit pressure. Two curves are shown for each pump, one derived using the stay-time basis and the other the curve-fit basis of reference 22; these two bases gave an equally good correlation with test-derived compliance data for the Saturn pumps. The difference in the two curves for each Shuttle pump on figure 39 is indicative of the uncertainty of the estimation process. The regions plotted are an engineering estimate of overall uncertainty, namely from half of the lower of the two estimates up to twice the higher of the two.

5.4 Conclusions

1. The studies of the early configuration showed that the method of approximate analysis can be employed to obtain useful results.

2. An accumulator between the boost and main pump offers promise of higher effectiveness than one at the engine inlet. An accumulator downstream of the first stage of the main pump is relatively ineffective.

3. The small distributed resistance of feedlines can make a large difference in the value at high-frequency peaks in propulsion frequency response.

4. The necessary pump design information is available to apply the method of empirical estimation of pump cavitation compliance of reference 22.

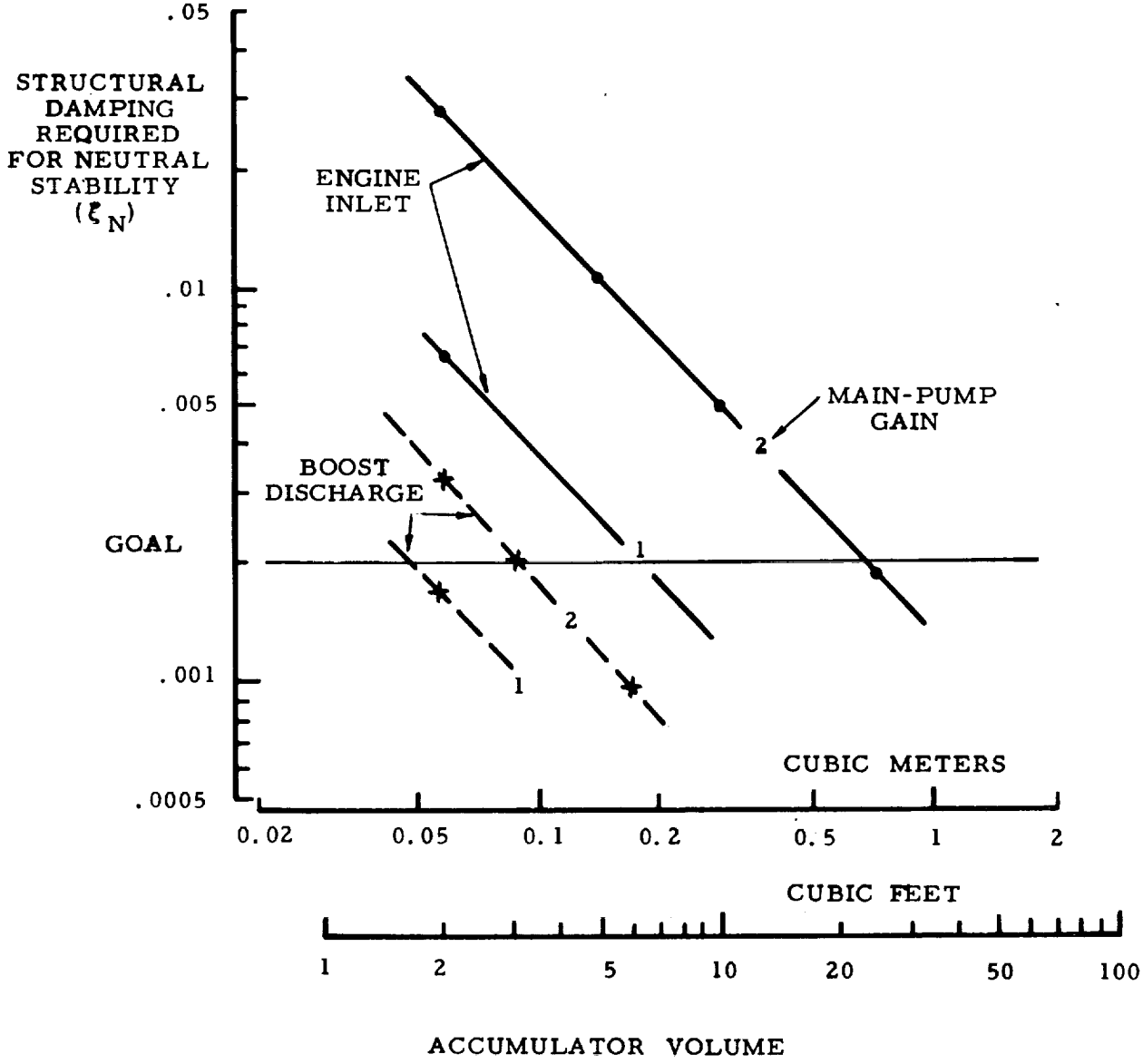

Figure 38. Structural damping required vs. accumulator volume

Table V. Values used for pump cavitation compliance estimates (nominal power level, mixture ratio of 6)

	Oxidizer boost		Fuel boost		Oxidizer first-stage main		Fuel first-stage main	
Propellant density, kg/m^3 ($lb/in.^3$)	1.13×10^3	(0.041)	70.6	(0.00255)	1.13×10^3	(0.0407)	70.0	(0.00253)
Flow area at inlet[1], m^2 ($in.^2$)	0.063	(97.8)	0.0515	(79.9)	0.0091	(14.1)	0.0117	(18.1)
Rotational speed, rev/s (rpm)	85.9	5.16×10^3	242	1.45×10^4	488	2.93×10^4	587	3.52×10^4
NPSH at head breakdown, m (ft)	3.3	(10.8)	19.0	(62.3)	62.5	(205)	1347	(4420)
Blade angle, inducer tip, deg[2]	7.2		6.5		10.8		22	
Flow coefficient at inlet	0.07		0.08		0.2		0.8	
Inducer tip radius, m (in.)	0.148	(5.85)	0.152	(6.00)	0.635	(2.50)	0.079	(3.13)

Notes:

(1) Area between inducer tip radius and inducer hub radius

(2) The leading-edge blade angle (β) is assumed to vary with the radial distance from the axis of rotation (r) according to the relation: $r \tan \beta = \text{constant}$.

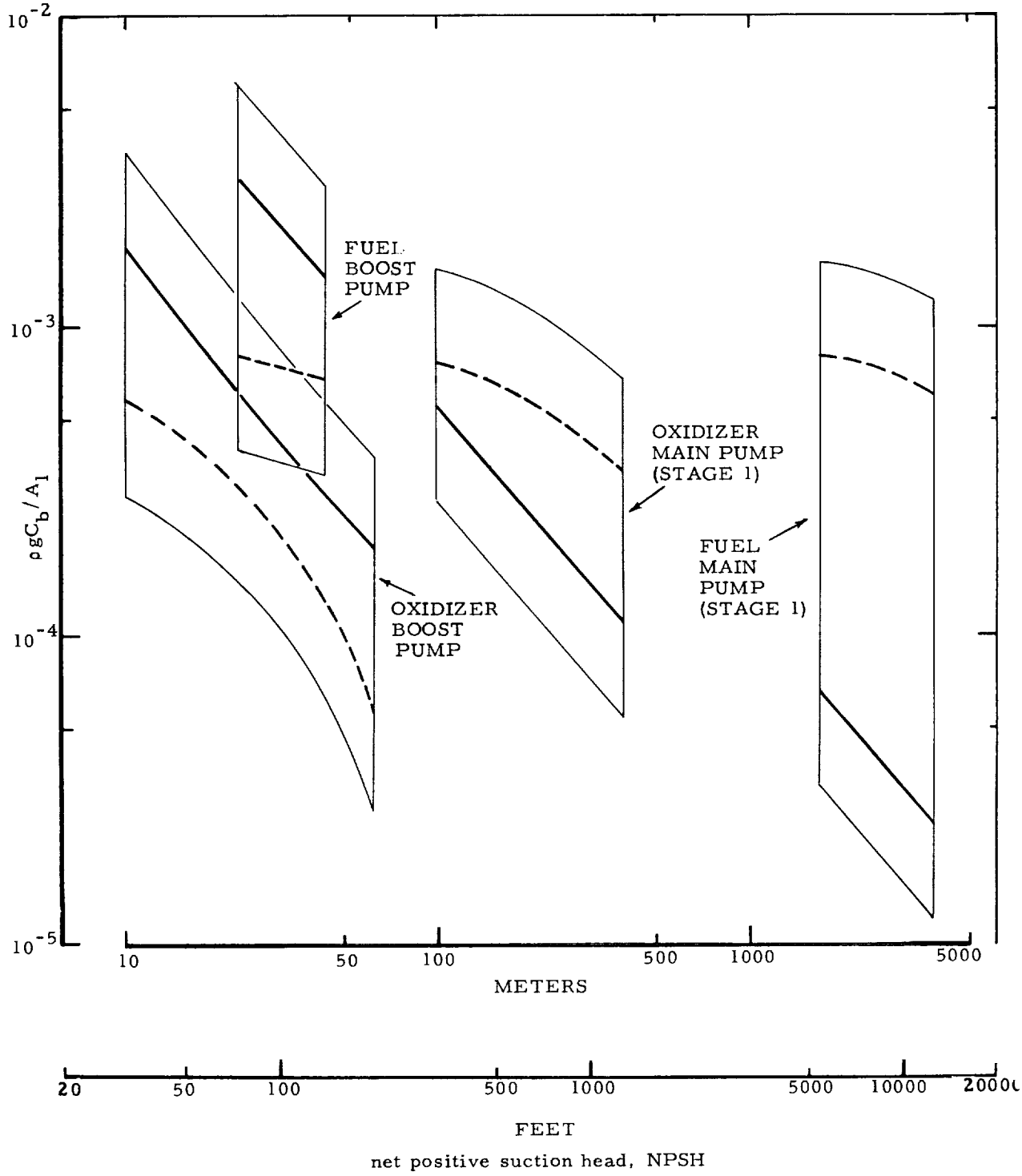

Figure 39. Estimated cavitation compliance of Shuttle pumps.

5.5 Recommendations

1. A structural damping ratio required for neutral stability of 0.002 should be employed for initial studies of stability during Shuttle development.

2. The modeling of the external oxygen-hydrogen tank for the Shuttle vehicle must be sufficiently detailed to determine accurately the first several modes of vibration of its longitudinal hydroelastic behavior.

3. Distributed feedline resistance should be included appropriately in the mathematical model for pogo stability studies.

4. Accumulators at either the engine-inlet or between the boost and main pumps should be studied early in Shuttle development.

5. Propulsion frequency response should be plotted in terms of amplitude vs. phase to assure complete definition at higher feedline resonances.

6. The method given in reference 22 is recommended for estimation of pump cavitation compliance in advance of experimental data. The estimates should be refined as improved information becomes available.

APPENDIX A

STRUCTURAL-MODE EXCITATION FROM TANK DYNAMIC OUTFLOW

A. 1 Formulation of Equations of Motion

Consider the structural/propulsion system shown in figure 1a, and assume the system is to be separated into structural and propulsion-system elements as shown in figures 1b, c. (Only a single fluid/tank system is considered.) The basic objective of this analysis is to define the necessary equations for coupling the feedline system to the tank in such a way that the effects of flow across the tank/feedline interface are properly taken into account. Of importance in figure 1 is the tank plus the boundary conditions at its exit; the particular propulsion system shown, together with the corresponding reactive forces $\vec{F}_1$, $\vec{F}_2$ are incidental to the analysis and are carried along only as an aid to the discussion. Hamilton's Principle is used to define the system equations (ref. 3 or 4).

A. 1. 1 Hamilton's Principle. - Considering the structural system of figure 1b, noting that $P_t A$ and $\vec{F}_i$ can be viewed as external forces independent of the motions and acting through the associated displacements $x_f(tb)$ and $\vec{x}_i$. The associated variational integral I, over the time interval t_1, t_2 is defined as

$$I = \int_{t_1}^{t_2} \left[\mathscr{L} + P_t A_\ell \, x_f(tb) + \sum_i \vec{F}_i \cdot \vec{x}_i \right] dt \qquad \text{(A-1)}$$

where $\mathscr{L}$ is the Lagrangian for the structural system, defined as kinetic energy T minus potential energy V. $P_t A_\ell$ and $\vec{F}_i$ are the tank-bottom pressure force and propulsive system reaction forces, respectively; $x_f(tb)$ and $\vec{x}_i$ are the corresponding absolute displacements of the applied forces.

A form of Hamilton's Principle states that an admissible motion of the system between specified states of motion at times t_1 and t_2 is the "actual" motion if and only if the variation of the integral I vanishes for arbitrary admissible variations. That is

$$\delta I = \int_{t_1}^{t_2} \left[\delta \mathscr{L} + P_t A_\ell \, \delta x_f(tb) + \sum_i \vec{F}_i \cdot \vec{x}_i \right] dt = 0 \qquad \text{(A-2)}$$

Typically, the Lagrangian $\mathscr{L}$ and the coordinates $x_f(tb)$, $\vec{x}_i$ will be expressed in terms of a selected set of generalized coordinates. The equations of motion result from expressing the integrand of equation (A-2) in terms of variations of these generalized coordinates.

A. 1. 2 The structural-system Lagrangian. - The Lagrangian of a system is defined by its potential and kinetic energy. The potential energy for the structural system is contained entirely within the structure proper since sources of fluid potential energy, such as surface waves and fluid compressibility, are neglected. Let V_s denote the stored structural energy. Then

$$V = V_s \tag{A-3}$$

Contributions to the kinetic energy, however, arise from both the structure and the fluid in the tanks. Let T_f denote the kinetic energy arising from fluid motions relative to the centroid of the vehicle, including the fluid in the tanks. Let T_s be the remaining kinetic energy, associated both with structural motion and with motion of the fluid as if it were located at the centroid of the system. The fluid motion relative to the vehicle center of gravity is defined in terms of a scalar velocity potential function Φ whose gradient defines the fluid velocity $\vec{v}_f$ at a point in the fluid denoted by the position vector $\vec{r}_f$

$$v_f(r_f, t) = -\nabla\Phi(\vec{r}_f, t) \tag{A-4}$$

The function Φ satisfies Laplace's equation

$$\nabla^2\Phi = 0 \tag{A-5}$$

which is the fluid continuity equation for an incompressible fluid, together with appropriate boundary conditions at fluid surfaces.

The motion of the fluid can be viewed as a superposition of two mutually exclusive types. The first type is fluid motion within a flexible tank structure, requiring compatibility of fluid and structural motions at their interfaces; the remaining fluid boundary conditions at the upper fluid surface and at the tank-bottom fluid surface are the same as those used for the structural-system modal analysis. Fluid motions of this type are characterized by the potential function Φ_1 and, by definition, are contained in the modal description of the structural system. Fluid motion of the second type, characterized by the potential function Φ_0, is that within a rigid, motionless tank structure; fluid boundary conditions at the upper surface and tank-bottom fluid surfaces are chosen so that the potential function $\Phi = \Phi_0 + \Phi_1$ satisfies the fluid boundary conditions of the actual system. In effect Φ_0 "corrects" for the fluid boundary conditions of the modal analysis. Thus, over the structure/fluid interfaces

$$\left.\begin{aligned} \vec{n} \cdot \nabla\Phi_1 &= \frac{\partial w_N}{\partial t} \\ \vec{n} \cdot \nabla\Phi_0 &= 0 \end{aligned}\right\} \tag{A-6a}$$

where $\vec{n}$ is a unit normal vector directed into the fluid and w_N is the normal component of the tank-wall deflection.

For simplicity surface waves and ullage-space dynamics are neglected, resulting in a zero-pressure condition at the upper fluid surface. Since oscillatory motions only are considered, the free-surface condition becomes

$$\Phi_0 = \Phi_1 = 0 \tag{A-6b}$$

In terms of the potential functions Φ_0, Φ_1, the fluid kinetic energy can be found by integration over the fluid volume V as

$$\left.\begin{aligned} T_f &= \frac{1}{2}\int_V \rho|\vec{v}_f|^2\,dV = T_{f1} + T_{f0} + \int_V \rho\nabla\Phi_1 \cdot \nabla\Phi_0\,dV \\ &\text{where} \\ T_{fi} &= \frac{1}{2}\int_V \rho(-\nabla\Phi_i)\cdot(-\nabla\Phi_i)\,dV, \qquad i = 0, 1 \end{aligned}\right\} \tag{A-7}$$

The Divergence Theorem can be used to convert a volume integral into a surface integral for a suitable vector $\vec{v}$ as follows:

$$\int_V \nabla\cdot\vec{v}\,dV = -\int_S \vec{n}\cdot\vec{v}\,dS$$

where $\vec{n}$ is the unit normal directed into the volume V, and S is the surface of V. Applying the theorem to the cross-term integral of equation (A-7), and using the boundary conditions of equations (A-6) and the fluid incompressibility requirement $\nabla^2\Phi_i = 0$, yields

$$T_f = T_{f1} + T_{f0} - \int_{A_\ell} \rho\Phi_1\vec{n}\cdot\nabla\Phi_0\,dS$$

where A_ℓ = tank-bottom/feedline interface area. Neglecting any variability of parameters across A_ℓ, the above can be written simply as

$$T_f = T_{f1} + T_{f0} + \rho\Phi_1(tb)\,A_\ell\,\dot{x}_{f0}(tb) \tag{A-8}$$

where $x_{f0}(tb)$ is fluid velocity at the tank bottom corresponding to Φ_0, and $\Phi_1(tb)$ is the velocity potential function Φ_1 evaluated at the tank bottom.

The Lagrangian function is now formed, using equations (A-3) and (A-8) as

$$\mathscr{L} = T_s + T_{f1} + T_{f0} + \rho\Phi_1(tb)\, A_\ell \dot{x}_{f0}(tb) - V_s \tag{A-9}$$

Noting that the Lagrangian corresponding to the structural-mode analysis, $\mathscr{L}_m$, includes the potential energy V_s, and the kinetic energy terms T_s and T_{f1} (arising from structural motions and from fluid motions corresponding to the potential Φ_1, respectively), $\mathscr{L}$ can also be written more simply as

$$\mathscr{L} = \mathscr{L}_m + T_{f0} + \rho\Phi_1(tb) A_\ell \dot{x}_{f0}(tb) \tag{A-10}$$

where $\mathscr{L}_m = (T_s + T_{f1} - V_s)$ is the Lagrangian of the modal analysis.

Substitution of equation (A-10) into equation (A-2) then yields the variational equation

$$\delta I = \int_{t_1}^{t_2} \left\{ \delta\mathscr{L}_m + \delta(T_{f0} + \rho\Phi_1(tb) A_\ell \dot{x}_{f0}) + P_t A_\ell \delta x_f(tb) + \sum_i \vec{F}_i \cdot \delta\vec{x}_i \right\} dt = 0 \tag{A-11}$$

A.1.3 Generalized coordinates. - By introducing the generalized coordinates from the structural analysis, $\mathscr{L}_m$ and $\Phi_1(tb)$ can be written as

$$\left.\begin{aligned} \mathscr{L}_m &= \frac{1}{2}\sum_n M_n\left(\dot{q}_n^2 - \omega_n^2 q_n^2\right) \\ \Phi_1(tb) &= \sum_n \frac{\mathscr{P}_{1n}(tb)}{\rho}\, \dot{q}_n(t) \end{aligned}\right\} \tag{A-12}$$

where M_n, ω_n are modal masses and frequencies, respectively, and $\mathscr{P}_{1n}(tb)$ is the modal pressure at the tank-bottom/feedline interface per unit modal acceleration. The equation for $\mathscr{L}_m$ is standard; the relationship between modal pressure and potential function Φ_1 is obtained from Bernoulli's equation, assuming small motions. Bernoulli's equation determines pressure at any point in the fluid as

$$\mathscr{P}_1(\vec{r}_f, t) = \rho \frac{\partial \Phi_1}{\partial t}(\vec{r}_f, t) \tag{A-13}$$

Φ_1 and $\mathscr{P}_1$ can be expanded in terms of the modal coordinates as

$$\Phi_1(\vec{r}_f, t) = \sum_n \Phi_{1n}(\vec{r}_f)\dot{q}_n(t)$$

$$\mathscr{P}_1(\vec{r}_f, t) = \sum_n \mathscr{P}_{1n}(r_f)\ddot{q}_n(t) \tag{A-14}$$

Substituting equations (A-14) into equation (A-13), equating like coefficients, and evaluating at the tank bottom yields the indicated expansion of $\Phi_1(tb)$ in equations (A-12).

Generalized coordinates can also be introduced for motions described by the potential function Φ_0. Physically, this represents the case of fluid motion in a rigid tank arising from oscillatory pressure or flow perturbations at the tank bottom. Since the fluid is incompressible, only a single coordinate is required. Define the variable $\dot{x}_{f0}(t)$ such that

$$\Phi_o(\vec{r}_f, t) = \tilde{\Phi}_0(\vec{r}_f)\dot{x}_{f0}(t) \tag{A-15}$$

where $\nabla\Phi_o(tb) = -1$. Then $\dot{x}_{f0}$ represents fluid velocity into the tank. Define an effective inertance of the fluid in the tank L_t as the ratio of pressure to the time derivative of the volumetric flow rate,

$$\mathscr{P}_0(tb) = L_t\dot{Q}_0(t) \tag{A-16}$$

where $Q_0 = A_\ell \dot{x}_{f0}(t)$. Then application of Bernoulli's equation for the potential Φ_0 [similar to equation (A-14) for Φ_1] and comparison with equation (12) yields

$$\Phi_0(tb) = \left(\frac{L_t}{\rho}\right) A_\ell \dot{x}_{f0} \tag{A-17}$$

For a given tank configuration, L_t can be determined approximately by assuming one-dimensional flow in the tank as

$$L_t = \int_0^h \frac{\rho\, d\xi}{A_t(\xi)}$$

where h is the height of fluid above the tank bottom and $A_t(\xi)$ denotes variation of tank area as a function of distance ξ above the tank bottom. Alternatively, a three-dimensional analysis may be performed, the potential function Φ_0 defined exactly, and L_t defined from considerations of pressure and flow conditions at the tank bottom as indicated above.

The kinetic energy function T_{f0} can also be expressed in terms of the "generalized" coordinate x_{f0}. Applying the Divergence Theorem to the definition of T_{f0} [equation (A-7)], noting the boundary conditions of equations (A-6) and the result of equation (A-17), leads to an expression for T_{f0} as

$$T_{f0} = \frac{1}{2} L_t (A_\ell \dot{x}_{f0})^2 \tag{A-18}$$

Substitution of equations (A-12), (A-17), and (A-18) into equation (A-11) produces the variational equation in terms of generalized modal coordinates as

$$\begin{aligned} \delta I = \int_{t_1}^{t_2} \Bigg\{ & \delta\left[\frac{1}{2}\sum_n M_n\left(\dot{q}_n^2 - \omega_n^2 q_n^2\right)\right] \\ & + \delta\left[\frac{1}{2} L_t A_\ell^2 \dot{x}_{f0}^2 + \sum_n \mathscr{P}_{1n}(tb)\dot{q}_n A_\ell \dot{x}_{f0}\right] \\ & + P_t A_\ell \, \delta x_f(tb) + \sum_i \vec{F}_i \cdot \delta\left(\sum_n \vec{\phi}_{in} q_n\right)\Bigg\} dt = 0 \end{aligned} \tag{A-19}$$

Note that aside from definition of the absolute fluid displacement at the tank bottom [that is, $x_f(tb)$ in terms of x_{f0}, q_n], the above equation is independent of the specific boundary conditions assumed at the tank-bottom/feedline fluid interface. The final equations of motion are derived below for modal analyses assuming several particular choices of this boundary condition.

A.2 Case 1: Zero Absolute Flow

The simplest case results when one assumes that the absolute motion of the fluid is zero at the tank-bottom opening. The tank-bottom structure is unconstrained, so that outflow from the tank is permissible in the structural system modes. This is equivalent to having a piston in the tank-bottom opening, fixed in inertial space. Then, at the tank bottom,

$$x_{f1}(tb) = 0$$

By definition of Φ, Φ_0, Φ_1, the absolute velocity of the fluid at the tank bottom $\dot{x}_f(tb)$ is given by

$$\dot{x}_f(tb) = \dot{x}_{f1}(tb) + \dot{x}_{f0}(tb)$$

Accounting for the tank-bottom boundary condition, the absolute motion of the fluid at the tank-bottom/feedline interface is defined solely by Φ_0 and we can write

$$x_f(tb) = x_{f0}(tb) \tag{A-20}$$

Substituting equation (A-20) into equation (A-19), performing the indicated variations and integrating by parts those terms containing variations of velocities $\delta\dot{q}_n$ and $\delta\dot{x}_{f0}$, noting that the operations of variation and time differentiation are commutative and that δq_n, δx_{f0} are zero when evaluated at t_1 and t_2, yields

$$\delta I = \int_{t_1}^{t_2} \left\{ \frac{1}{2} \sum_n \left[-M_n \left(\ddot{q}_n + \omega_n^2 q_n \right) - \mathscr{P}_{1n}(tb) A_\ell \ddot{x}_{f0} + \sum_i \vec{F}_i \cdot \vec{\phi}_{in} \right] \delta q_n \right.$$

$$\left. + \left[-L_t A_\ell \ddot{x}_{f0} - \sum_n \mathscr{P}_{1n}(tb) \ddot{q}_n + P_t \right] A_\ell \, \delta x_{f0} \right\} dt$$

Setting $\delta I = 0$ for arbitrary variations, so that the required equations of motion are

$$\left.\begin{aligned} \ddot{q}_n + \omega_n^2 q_n &= \frac{\mathscr{P}_{1n}(tb)}{M_n} \dot{Q} + \sum_i \frac{\vec{F}_i \cdot \vec{\phi}_{in}}{M_n} \\ P_t &= -L_t \dot{Q} + \sum_n \mathscr{P}_{1n}(tb) \ddot{q}_n \end{aligned}\right\} \tag{A-21}$$

The absolute volumetric flow at the tank-bottom/feedline interface, $Q = -A_\ell \dot{x}_{f0}$, has been introduced (positive direction downward in fig. 1) for compatibility with the usual formulation of the propulsion-system equations.

A.3 Case 2: Zero Relative Flow (Closed-Bottom Tank)

In the usual approach to computing structural modes, the tank bottom is assumed to be closed, that is, the fluid and structure at the tank bottom have the same motion. Equivalently, a piston in the tank-bottom opening is fixed to the tank-bottom structure. Therefore,

$$x_{f1}(tb) = x(tb)$$

where x(tb) is the tank-bottom structural motion. For this case the potential function Φ_0 represents flow across the tank bottom. Accordingly, absolute fluid velocity is given by

$$\dot{x}_f(tb) = \dot{x}_{f0} + \dot{x}(tb)$$

or, we can write

$$x_f(tb) = x_{f0}(tb) + x(tb) \tag{A-22}$$

Noting that the tank-bottom displacement can be written in terms of the structural modal coordinates as

$$x(tb) = \sum_n \phi_n(tb) q_n$$

Substitution of equation (A-22) into the variational equation (A-19) yields

$$\delta I = \int_{t_1}^{t_2} \left\{ \delta\left[\frac{1}{2}\sum_n M_n\left(\dot{q}_n^2 - \omega_n^2 q_n^2\right)\right] + \delta\left[\frac{1}{2} L_t A_\ell^2 \dot{x}_{f0}^2 + \sum_n \mathscr{P}_{1n}(tb)\dot{q}_n A_\ell \dot{x}_{f0}\right] \right.$$
$$\left. + P_t A_\ell \, \delta\left[x_{f0}(tb) + \sum_n \phi_n(tb) q_n\right] + \sum_i \vec{F}_i \cdot \delta\left(\sum_n \vec{\phi}_{in} q_n\right) \right\} dt = 0$$

Performing the indicated variations, integrating variations of velocity terms by parts, and requiring the variational equation $\delta I = 0$ to be satisfied for arbitrary variations produces the following equations of motion:

$$\left.\begin{aligned} \ddot{q}_n + \omega_n^2 q_n &= \frac{\mathscr{P}_{1n}(tb)}{M_n}\,\dot{Q}_R + \frac{P_t A_\ell}{M_n}\,\phi_n(tb) + \sum_i \frac{\vec{F}_i \cdot \vec{\phi}_{in}}{M_n} \\ P_t &= -L_t \dot{Q}_R + \sum_n \mathscr{P}_{1n}(tb)\ddot{q}_n \end{aligned}\right\} \qquad \text{(A-23)}$$

where $Q_R = -A_\ell \dot{x}_{f0}$ is the outflow from the tank. By continuity the absolute volumetric flow Q (positive downward) is given by

$$Q = Q_R - A_\ell \dot{x}(tb)$$

or, introducing modal coordinates,

$$Q = Q_R - A_\ell \sum_n \phi_n(tb)\dot{q}_n \qquad \text{(A-24)}$$

Eliminating the relative flow term Q_R from equation (A-23) by use of equation (A-24) produces the following equations in terms of absolute volumetric flow Q:

$$\left.\begin{aligned} \ddot{q}_n + \omega_n^2 q_n - \frac{\mathscr{P}_{1n}(tb)}{M_n}\left(\sum_k A_\ell\,\phi_k(tb)\ddot{q}_k\right) &= \frac{\mathscr{P}_{1n}(tb)}{M_n}\,\dot{Q} + \frac{P_t A_\ell\,\phi_n(tb)}{M_n} + \sum_i \vec{F}_i \cdot \vec{\phi}_{in} \\ P_t &= -L_t \dot{Q} + \sum_k [\mathscr{P}_{1k}(tb) - A_\ell L_t \phi_k(tb)]\ddot{q}_k \end{aligned}\right\} \qquad \text{(A-25)}$$

Unfortunately, the modal coordinates for this system are coupled. The coupling coefficients, however, can be shown to be a function of the ratio of feedline area divided by tank area and are therefore small (see sec. 1.5).

A.4 Case 3: Free Flow

The final case to be considered is that of free or unrestrained flow at the tank bottom. For this case a zero-pressure condition exists at the tank-bottom

opening in the modal analysis, implying

$$\Phi_1(tb) = 0$$

The variational equation becomes

$$\delta I = \int_{t_1}^{t_2} \left\{ \delta\left[\frac{1}{2}\sum_n M_n\left(\dot{q}_n^2 - \omega_n^2 q_n^2\right)\right] + P_t A_\ell\, \delta\left[\sum_n \phi_{fn}(tb) q_n\right] + \vec{F}_i \cdot \sum_i \vec{\phi}_{in}\, \delta q_n \right\} dt \tag{A-26}$$

and yields the structural-system equation

$$\ddot{q}_n + \omega_n^2 q_n = \frac{P_t A_\ell}{M_n}\, \phi_{fn}(tb) + \sum_i \vec{F}_i \cdot \vec{\phi}_{in} \tag{A-27a}$$

Absolute fluid volumetric flow at the line/tank interface is defined by

$$Q = - A_\ell \sum_n \phi_{fn}(tb)\dot{q}_n \tag{A-27b}$$

A.5 A Reciprocity Relationship

An interesting reciprocity relationship evolves from the symmetry of the cross-term integral containing Φ_1, Φ_0 in equation (A-7). An interchange of the roles of Φ_1 and Φ_0 in the application of the Divergence Theorem produces the equality:

$$\int_{A_\ell} \rho\Phi_1 \vec{n} \cdot \nabla\Phi_0\, dS = \int_{S'} \rho\Phi_0 \vec{n} \cdot \nabla\Phi_1\, dS$$

where S' is the surface area not in contact with the ullage. This can also be written as

$$\int_{A_\ell} \rho\Phi_1 \dot{x}_{f0}\, dS = \int_{S'} \rho\Phi_0 |\dot{w}_N|\, dS \qquad \text{(A-28)}$$

Disregarding time derivatives, equation (A-28) can be interpreted as stating a reciprocity relationship between pressures and motions in the flexible- and rigid-tank systems (corresponding to the fluid potentials Φ_1 and Φ_0, respectively). From Bernoulli's equation [see equation (A-13)] the terms $\rho\Phi_1$ can be seen to represent fluid pressures. The left side of equation (A-13) can therefore be viewed as expressing the work done over the tank-bottom area A_ℓ, by the pressure at the tank-bottom in the flexible-tank system acting through the tank-bottom fluid displacement x_{f0} in the rigid-tank system. Considering Case 1, where Φ_1 is zero over the tank bottom, S' becomes the wetted area of the tank. The right side of equation (A-28) can be interpreted as the converse of the left side, namely the work done, over the tank wetted surface, by the tank-wall pressures in the rigid-tank system acting through the normal dispacements of the tank wall in the flexible-tank system. For Case 2, the right side also contains terms from integration over the tank-bottom area A_ℓ.

A.6 Summary

The equations of motion for the structural-system modal coordinates have been modified to account for the effects of tank dynamic outflow. The equations are presented for three cases, based on different boundary conditions for the fluid at the tank-bottom/feedline interface in the structural-system modal analysis. For ease in coupling with the propulsive-system equations, the system equations are defined in terms of the pressure P_t and absolute volumetric flow Q at the tank-bottom/feedline interface, propulsion-system reactive forces F_i, and structural-system modal coordinates q_n.

The fluid boundary conditions considered were (1) zero absolute flow, with the resulting equations of motion given by equations (A-20); (2) zero relative flow (closed-bottom tank), with the equations of motion being given by equations (A-25); and (3) free flow (free surface), with the equations of motion being given by equations (A-27).

APPENDIX B

MINIMUM-FREQUENCY ERROR MODELS

Our goal is to derive models which minimize the error in modal frequencies. Consider a transmission matrix $[a]$ representing one of N segments of a uniform line. The transmission matrix for the entire line is then $[\tilde{a}] = [a]^N$. Following the work of reference 15, when $a_{11} = a_{22}$

$$\tilde{a}_{11} = \tilde{a}_{22} = \tilde{\lambda}^N \cos N\theta \tag{B-1a}$$

$$\tilde{a}_{12} = \tilde{\lambda}^N \sqrt{\frac{-a_{12}}{a_{21}}} \sin N\theta \tag{B-1b}$$

$$\tilde{a}_{21} = \tilde{\lambda}^N \quad \frac{-a_{21}}{a_{12}} \sin N\theta \tag{B-1c}$$

where

$$\tilde{\lambda}^2 = |a|$$

and

$$\theta = \sin^{-1}\left[\sqrt{\frac{-a_{12}\,a_{21}}{\tilde{\lambda}}}\right] \tag{B-1d}$$

For a spring-mass system of N segments with the input end fixed and the output end free, corresponding to open-closed boundary conditions for a fluid, we have

$$\begin{Bmatrix} F_1 \\ 0 \end{Bmatrix} = \begin{bmatrix} \tilde{\alpha}_{11} & \tilde{\alpha}_{12} \\ \tilde{\alpha}_{21} & \tilde{\alpha}_{22} \end{bmatrix} \begin{Bmatrix} 0 \\ \ddot{x}_N \end{Bmatrix}$$

or

$$a_{22}\ddot{x}_N = 0$$

which is only true for the non-trivial case if

$$\tilde{\alpha}_{22} = 0 \tag{B-2}$$

Using equation (B-1a), the open-closed characteristic equation is then

$$\cos N\theta = 0 \quad \text{or} \quad N\theta = \frac{2\nu - 1}{2}\pi \tag{B-3}$$

where $\nu = 1, 2, \ldots, \infty$. Similarly, the zeros of $\tilde{\alpha}_{12}$ and $\tilde{\alpha}_{21}$ are the eigenvalues for the free-free and fixed-fixed boundary conditions. For either case

$$\sin N\theta = 0 \quad \text{or} \quad N\theta = \nu\pi \tag{B-4}$$

where $\nu = 1, 2, \ldots \infty$.

Consider a transmission matrix with an undetermined coefficient "a" as follows:

$$[\alpha] = \begin{bmatrix} 1 - \frac{(\omega\tau')^2}{2} & -L\left[1 - a(\omega\tau')^2\right] \\ \frac{1}{L}(\omega\tau')^2 & 1 - \frac{(\omega\tau')^2}{2} \end{bmatrix} \tag{B-5}$$

where $\tau' = \tau/N$ is the travel time for one segment. From equation (B-1d),

$$\tilde{\lambda}^2 = 1 + (1/4 - a)(\omega\tau')^4$$

Letting

$$u = \sin\theta = \frac{(\omega\tau')\sqrt{1 - a(\omega\tau')^2}}{1 + (1/4 - a)(\omega\tau')^4}$$

we obtain

$$u = (\omega\tau')\left[1 - \frac{a}{2}(\omega\tau')^2 - \left(\frac{a^2}{8} - a + \frac{1}{4}\right)(\omega\tau')^4 + \ldots\right]$$

However

$$\theta = u + u^3/6 + 3u^5/40 + \ldots$$

and hence

$$\theta = (\omega\tau') \left[1 + \left(\frac{1}{6} - \frac{a}{2} \right) (\omega\tau')^2 + \ldots \right] \tag{B-6}$$

Retaining only lower order terms, this series can be reverted to yield,

$$(\omega\tau') = \theta \left[1 - \left(\frac{1}{6} - \frac{a}{2} \right) \theta^2 + \ldots \right] \tag{B-7}$$

Combining equation (B-7) with (B-5) for a fixed-fixed or free-free condition yields

$$N\omega\tau' = \omega\tau = (\nu\pi) \left[1 - \left(\frac{1}{6} - \frac{a}{2} \right) \frac{\nu^2\pi^2}{N^2} + \ldots \right] \tag{B-8}$$

The exact solution is, of course, from

$$\sin(\omega\tau) = 0 \quad \text{or} \quad \omega\tau = \nu\pi \tag{B-9}$$

To eliminate the $1/N^2$ term in equation (B-8), we employ the value a = 1/3. Thus the transmission matrix

$$[\alpha] = \begin{bmatrix} 1 - \frac{(\omega\tau)^2}{2} & -L\left(1 - \frac{(\omega\tau)^2}{3}\right) \\ \frac{1}{L}(\omega\tau)^2 & 1 - \frac{(\omega\tau)^2}{2} \end{bmatrix} \tag{B-10}$$

will have an error proportional to $1/N^4$.

Similarly, starting from the more general transmission matrix

$$[\alpha] = \begin{bmatrix} 1 - a(\omega\tau)^2 & -L\left[1 - b(\omega\tau)^2\right] \\ \frac{1}{L}(\omega\tau)^2 & 1 - a(\omega\tau)^2 \end{bmatrix}$$

it is possible to show that the pairs of roots of the following two equations

$$270\, a^2 - 480\, a + 167 = 0$$

$$b = 4\, a - 5/3$$

will result in a frequency error proportional to $1/N^6$. The pairs of roots are

$$a = 0.4746, \qquad b = 0.2317...$$

and

$$a = 1.303, \qquad b = 3.545...$$

The first pair of roots corresponds to coefficients similar to previous models and yields reasonable results, while the second pair yields results quite removed from others. Thus the transmission matrix

$$[\alpha] = \begin{bmatrix} 1 - 0.4746(\omega\tau)^2 & -L\left[1 - 0.2317(\omega\tau)^2\right] \\ \frac{1}{L}(\omega\tau)^2 & 1 - 0.4746(\omega\tau)^2 \end{bmatrix} \tag{B-12}$$

is used as having a frequency error proportional to $1/N^6$.

REFERENCES

1. Anon.: Prevention of Coupled Structure-Propulsion Instability (POGO). NASA Space Vehicle Design Criteria (Structures), SP-8055, 1970.

2. Lewis, W.: Simplified Analytical Model for Use in Design of Pump-Inlet Accumulators for the Prevention of Liquid-rocket Longitudinal Oscillation (POGO). NASA TN D-5394, 1969.

3. Crandall, H.; Karnopp, D. C.; Kurtz, F. K., Jr.; and Pridmore-Brown, D. C.: Dynamics of Mechanical and Electromechanical Systems. McGraw-Hill Book Co., 1968.

4. Fung, Y. C.: Foundations of Solid Mechanics. Prentice-Hall, Inc., New Jersey, 1965.

5. Franklin, J. N.: Matrix Theory. Prentice-Hall, Inc., New Jersey, 1968.

6. Rubin, S.: Longitudinal Instability of Liquid Rockets Due to Propulsion Feedback (POGO). J. Spacecraft Rockets, vol. 3, no. 8, August 1966, pp. 1188-1195.

7. Wenzel, L. M.; and Szuch, J. R.: Analysis of Chugging in Liquid-Bipropellant Rocket Engines Using Propellants with Different Vaporization Rates, NASA TN D-3080, October 1965.

8. Payne, J. G.: POGO Stability Analysis Program. TOR-0172(2122)-10, The Aerospace Corporation, 1972.

9. Rich, R. L.: Saturn V POGO and a Solution. Presented at AIAA Structural Dynamics and Aeroelasticity Conference (New Orleans), April 16-17, 1969.

10. DiMaggio, O. D.; and Nishimoto, T.: Feedline Dynamic Effects on Shuttle POGO Stability. NASA CR112068, 1972.

11. Rose, R. F.; Staley, J. A.; and Simson, A. K.: A Study of System-Coupled Longitudinal Instabilities in Liquid Rockets. AFRPL-TR-65-163, pt. 1, Air Force Rocket Propulsion Lab., September, 1965.

12. Vaage, R. D.; and Zehnle, R. A.: Linear Equation Development, System Coupled Longitudinal Oscillation (POGO). TM 0472/20-4-68, Martin Marietta Corp., 1968.

13. Astleford, W. J.; Holster, J. L.; and Gerlach, C. R.: Analysis of Propellant Feedline Dynamics. Interim Technical Report No. 1, Contract NAS8-25919, Southwest Research Institute, August 1972.

14. Caughey, T. K.; and O'Kelly, M. E. J.: Classical Normal Modes in Damped Linear Dynamic Systems. Journal of Applied Mechanics, Trans. ASME, Series E, Vol. 87, 1965.

15. Rocke, R. D.: Evaluation of Models for One-Dimensional Vibration Systems. The Shock and Vibration Bulletin, December 1970.

16. Rubin, S.: Mechanical Immittance- and Transmission-Matrix Concepts. Journal of the Acoustical Society of America, Vol. 41, No. 5, May 1967.

17. Bisplinghoff, R. L.; Ashley, H.; and Halfman, R. L.: Aeroelasticity. Addison-Wesley Publishing Co., Inc., 1955.

18. Jacobsen, L. S.; and Ayre, R. S.: Engineering Vibrations. McGraw-Hill Book Co., Inc., 1958.

19. Vaage, R. D.; Fidler, L. E.; and Zehnle, R. A.: Investigation of Characteristics of Feed System Instabilities. Report MCR-72-107, Martin Marietta Corp., May 1972.

20. Brennan, C.; and Acosta, A. J.: A Note on Turbopump Blade Cavitation Compliance for the POGO Instability. ASME 1972 Polyphase Flow Forum (San Francisco), ASME (New York), March 1972, pp. 23-24.

21. Kim, J. H.: Analysis of Unsteady Cavity in Internal Flows. Ibid., pp. 25-26.

22. Ghahremani, F. G.; and Rubin, S.: Empirical Evaluation of Pump Inlet Compliance. Report ATR-73(7257)-1, The Aerospace Corporation, August 1972.

23. Lorenzo, C. F.: Variable-Sweep-Rate Testing: A Technique to Improve the Quality and Acquisition of Frequency Response and Vibration Data. NASA TN D-7022, 1970.

24. Rubin, S.: Instability Model of Missile Longitudinal Oscillation Due to Propulsion Feedback. Report TOR-269(4126)-28, The Aerospace Corporation, September 1964. (Available from DDC as AD 458 211.)